ERNST-MORITZ-ARNDT-UNIVERSITÄT
GREIFSWALD

Mass measurements on short-lived Cd and Ag nuclides at the online mass spectrometer ISOLTRAP

I n a u g u r a l d i s s e r t a t i o n

zur
Erlangung des akademischen Grades
doctor rerum naturalium (Dr. rer. nat.)
an der Mathematisch-Naturwissenschaftlichen Fakultät
der
Ernst-Moritz-Arndt-Universität Greifswald

vorgelegt von: Martin Breitenfeldt
                  geboren am 15. Dezember 1980
                  in Berlin

Greifswald, 03. Juli 2009

Dekan	Prof. Dr. Klaus Fesser
Betreuer und erster Gutachter:	Prof. Dr. Lutz Schweikhard
Zweiter Gutachter:	Prof. Dr. Jens Dilling

CONTENTS

LIST OF FIGURES

LIST OF TABLES

LIST OF PARAMETERS

A .... mass number
a .... surface thickness
A_z .... axial amplitude
B .... binding energy
C_4 .... octupole fraction of electric field imperfection
C_6 .... dodecapole fraction of electric field imperfection
d .... trap parameter
E .... energy
E .... quasi particle energy
e .... elementary charge
E_{kin} .... kinetic energy
g^δ .... statistical weight
I .... asymmetry parameter
I .... current
I_{pb} .... proton beam intensity
I_{RIB} .... Intensity of radioactive beam
J .... total angular momentum for more than one particle
j .... total angular momentum for one particle
K .... ion mobility
k_B .... Boltzmann constant
l .... orbital angular momentum
m .... mass
$M_\odot$ .... solar mass
ME .... mass excess
N .... number of neutrons
n .... neutron
n .... principle quantum number
N_A .... Avogadro number
n_i .... number density of a nuclide
N_{tar} .... target thickness
O .... Overlap
O .... overlap of states
p .... pressure
p .... proton
p_0 .... pressure at normal conditions
q .... charge
R .... resolving power
r_0 .... nuclear radius
s .... intrinsic spin
S_n .... neutron separation energy
S_p .... proton separation energy
S_{2n} .... two neutron separation energy
S_{2p} .... two proton separation energy
T .... temperature
t .... time
T_0 .... temperature at normal conditions
T_z .... isospin

U .... emptiness factor
V .... fullness factor
V_d .... amplitude dipolar excitation
V_q .... amplitude quadrupolar excitation
X_i .... mass fraction of a nuclide
Y_i .... abundance of a nuclide
Z .... number of protons
z_0 .... minimal distance trap center endcap electrode

1. INTRODUCTION

Penning ion traps are versatile tools used in many areas in atomic and nuclear physics [Gho95, MGW04]. One application is high precision mass spectrometry of atomic nuclei which leads to important input data for, e.g., nuclear structure studies [Bla06, SB06]. Uncertainties down to a few electron volts have been obtained for mass measurements on stable nuclides [BPR$^+$99, RTP04, RWMM07]. For short-lived radionuclides the achieved precision is currently in the ppb-range as reported by a number of facilities around the world (ISOLTRAP [MBB$^+$08b], CPT [CBB$^+$03], JYFLTRAP [JEH$^+$06], LEBIT [SBL$^+$03], SHIPTRAP [BAB$^+$05], and TITAN [DBB$^+$06]) covering the whole chart of nuclides. These precise data allow to test various nuclear models [LPT03], which employ different approaches, and incorporate different physical data and to improve mass predictions for exotic nuclides which have not been addressed experimentally so far. In the present work some of the models as used in the on-line database *nuclearmasses.org* [Smi] are compared and discussed.

In nuclear astrophysics mass differences, i.e., Q-values of nuclear decays, and thus nuclear masses are essential for the modeling of many nucleosynthesis processes, which occur in different astrophysical sites. A current goal is to extend high-precision mass measurements to nuclei very far from stability, in particular towards the very neutron-deficient nuclei in the rapid proton-capture process (rp process) and towards the very neutron-rich nuclei, which are important in the the rapid neutron-capture process (r process). In addition to Penning trap experiments, this goal is also addressed by storage ring mass spectrometry at the ESR facility at GSI [FGM08]. ISOLTRAP has recently contributed a number of precision mass measurements to this area such as ^{22}Mg improving the knowledge of the NeNa cycle in super novae [MKB$^+$04, MBB$^+$08a], ^{72}Kr for the rp-process path [RKA$^+$04, RKA$^+$05], and ^{80,81}Zn [BAB$^+$08], ^{95}Kr [DAB$^+$06] as well as ^{132,134}Sn [SAB$^+$05, SAB$^+$06, DAB$^+$08] on the neutron-rich side determining input parameters for the r-process path.

In this work Penning trap mass measurements of neutron-deficient Cd isotopes down to ^{99}Cd are presented that are important for modeling the isotopic abundances produced by the astrophysical rp process [WW81, SAG98, FMPL$^+$06, PHW$^+$06]. The rp process is a sequence of rapid proton captures and β^+ decays, often close to the proton drip line. For the $A \approx 99$ mass region, the rp process has been suggested [WW81, SAG98] and discussed [FCS$^+$08] as a candidate to resolve the long-standing puzzle of the origin of the relatively large amounts of ^{92,94}Mo and ^{96,98}Ru in the solar system [Lod03]. This is a lower-abundance group of so-called "p nuclei" that are shielded from the slow and rapid neutron-capture process, the s and r process, respectively, which synthesize the rest of the heavy elements. While standard p-process scenarios based on photodisintegration processes produce most other p-nuclei, they severely underproduce ^{92,94}Mo and ^{96,98}Ru [RGW$^+$06, AG03].

The rp process is the main energy source of type I X-ray bursts on the surface of accreting neutron stars [Sch06]. In some bursts, characterized by long timescales of the order of 100 s, the rp process can reach the Cd region [SAB$^+$01]. A reliable estimate of the produced composition is needed to model neutron star crust processes that are related to a number of observables such as the rare superbursts or the cooling of transiently accreting neutron stars [GBS$^+$07]. In addition, it has been shown that a small fraction of the processed matter could be ejected during X-ray bursts, renewing interest in these scenarios in terms of producing the Mo and Ru p-isotopes [WBS06].

The rp process is also thought to occur in proton-rich neutrino-driven outflows in core collapse supernovae [FMPL$^+$06, PHW$^+$06]. Because of the prominent role that neutrinos play in this nucleosynthesis it is referred to as "νp process". It has been shown that for certain model parameters the process can synthesize the Mo and Ru p-isotopes and that it passes through the ^{99}Cd region investigated in this work [PHW$^+$06]. For both scenarios the importance of accurate nuclear masses has been discussed before [PHW$^+$06, FCS$^+$08, SR06, FHP09, WEF$^+$08, WBS08]. For the present work network calculations describing the rp process were performed by H. Schatz using the mass values of the atomic-mass evaluation AME2003 [AWT03] updated with the most recent results in the vicinity of ^{99}Cd [FCS$^+$08, WEF$^+$08, MAA$^+$07, KEB$^+$08, HEE$^+$07].

Furthermore data from the most recent AME [LA09]. The importance of such an evaluation will be demonstrated for solving conflicts between data from different experiments, such the influence of less precise known reference masses can be reduced.

In addition, mass values of exotic nuclide, especially if measured for the first time, allow systematic studies of nuclear structure in that mass region. The two neutron separation energy as a mass difference is a good indicator for major changes and is used to discuss shell and sub-shell closures. For examples, mass values determined recently at ISOLTRAP provided important information for the discussion of, e.g., the subshell closure at $N = 32$ in the Cr, Mn -region [GAB$^+$05] and the reincarnation of the neutron shell closure at $N = 82$ for tin region [DAB$^+$08]. The required accuracy for these investigations is in the order of $100\,$keV.

Whereas the study of local phenomena, such as the interaction between the last (two) proton(s) with the last (two) neutron(s) δV_{pn} [ZWYG88, ZCB89], needs mass values with an accuracy of about a few $10\,$keV. Recent surveys using the AME2003 [AWT03] led to fascinating results [CBCM05, BCC06] as the influences of the orbits of the valence nucleons on the interaction strength in the ^{208}Pb mass region and characteristic patterns could be observed for approaching and crossing magic neutron and proton numbers. More detailed investigations by new mass measurements has been suggested by Brenner *et al.* [BCC06], and some of those masses could already be determined, like the mass of ^{208}Hg, measured recently [CLP$^+$09] at the ESR-facility [FGM08]. At ISOLTRAP the proposed studies of the trends in δV_{pn} in the vicinity of the neutron-rich Rn nuclides have been performed. The deviation from the expect trends has been interpreted as a hint for octupolar deformation [NAB$^+$09]. Furthermore the masses of ^{122,124,126,128}Cd have been requested, which are presented and discussed among others in the present work.

The irregularities of trends in the δV_{pn}-values are compared with trends as obtained from the S_{2n} and the Garvey-Kelson relations [GK66, GGJ$^+$69]. All three quantities indicate an unexpected behavior and thus suggest remeasurements of the nuclear masses in the vicinity of the investigated region on the nuclear chart, which could not be addressed during the runs described in the present work.

2. THEORY

2.1 Nucleosynthesis of the elements

On earth 272 stable and 55 natural radioactive nuclides have been found [BBFH57]. One of the most important questions to nuclear astrophysics is the explanation of the relative abundance of the different elements and their isotopes as listed, e.g., in [AG89]. For the creation of elements beyond iron various scenarios and astrophysical sites are proposed. The paths of some of the most important scenarios, such as the s, r, p, and rp process are given schematically in Fig. 2.1 [Bla06].

For the investigation of the different scenarios various nuclear physical input parameters are needed. The most important ones are the β-decay half-lives, branching ratios, the level density, and the neutron- or proton-separation energies $S_n(Z, N)$ and $S_p(Z, N)$, where the separation energies are
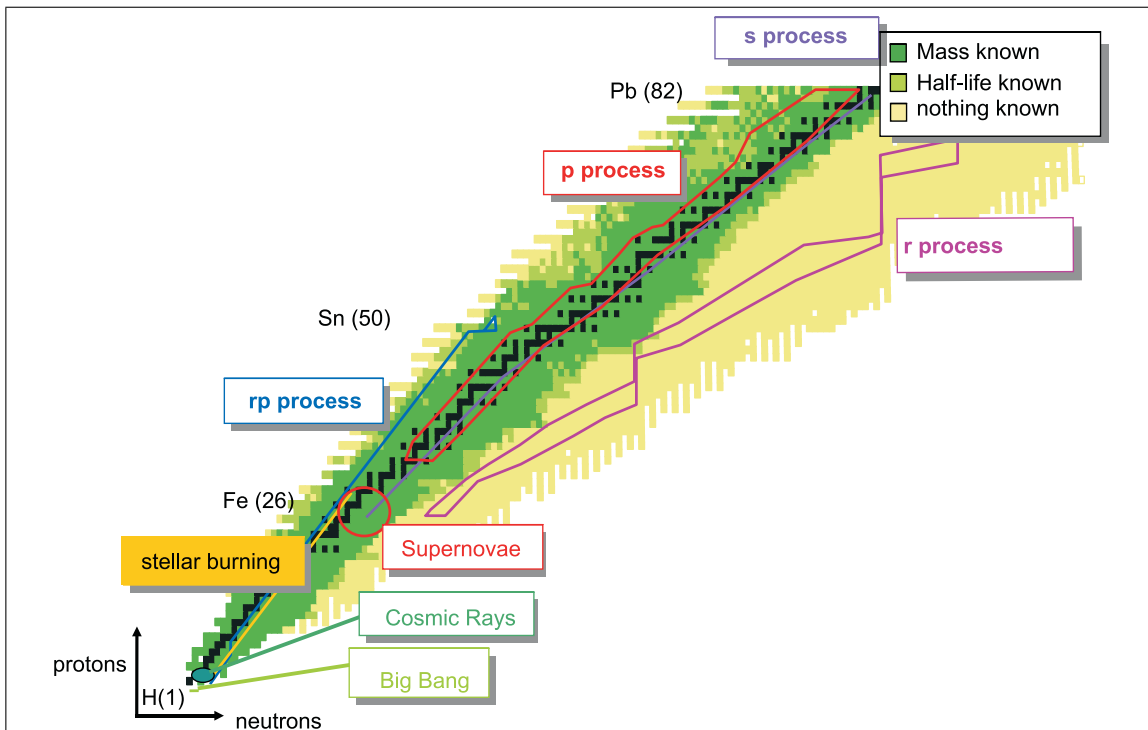
Fig. 2.1: Paths of several nucleosynthesis scenarios in the (N, Z) plane. The s process follows the valley of β-stability on the neutron-rich side, the r process is passing far out from stability on the neutron-rich side and the rp process is creating nuclides close to the proton drip line. Color-coded are the availability of experimental data for half-lives and masses as given in the AME2003 [AWT03]. The plot is taken from [Bla06].

Fig. 2.2: The main path of the s-process plotted in the region of $Z = 44-51$ in the (N, Z) plane as given in [BBFH57]. The neutrons are captured by stable nuclides (light gray boxes) and unstable nuclides (white boxes) are β^--decaying, indicated by horizontal and diagonal arrows, respectively. Note, in the case of ^{107}Pd the half-life is $6.5 \cdot 10^6$ years. Stable nuclides, which are not created by the s-process are called r-nuclides neutron-rich side and p-nuclides on the neutron-deficient side. The rp-process path in the vicinity of ^{99}Cd (dark grey box) and the creation of ^{98,99}Ru are indicated by arrows.

given by the mass differences

$$S_n(Z, N) = [-m(Z, N) + m(Z, N-1) + m(n)] \cdot c^2,$$
$$S_p(Z, N) = [-m(Z, N) + m(Z-1, N) + m(^1H)] \cdot c^2, \qquad (2.1)$$

with c as the speed of light in vacuum. Therefore, the masse values m of the mother and the daughter nuclide have to be determined with a relative uncertainty of less than $\delta m/m = 1 \cdot 10^{-7}$. Figure 2.1 displays a status of the available data for the half-lives and masses in the vicinity of the astrophysical pathes on the nuclide chart as given in the last atomic-mass evaluation [AWT03]. The s-process path can be considered as completely discovered as nuclear physics is concerned and already lots of masses and half-lives are available for the rp-process. Nevertheless, close to its predicted end in the SnSbTe cycle [SAB$^+$01] there are experimental data missing. On the neutron-rich side where the r-process is passing, hardly anything is known since the r-process is approaching the presently unreachable neutron drip-line. Only in the cases for which the path is blocked by neutron-shell closures as in the $N = 82$ region, where the nucleosynthesis has to pass the neutron shell $N = 82$, there are some experimental data available, e.g. for the nuclide ^{132}Sn.

Using the available nuclear data, conclusions can be drawn from model calculations and compared with astronomical observations such as luminosities of stars, the wavelength spectra of emitted light, and rotation frequencies. The majority of the nuclides heavier than ^{56}Fe in the universe are created in the s-process, which is taking place in stars where only a low abundance of neutrons is given. Those are generated by (α,n) reactions of the relatively rare nuclides ^{13}C and ^{22}Ne. Therefore, the

capture of neutrons is happening at timescales which are long as compared with the β-decay half-lives. Figure 2.2 shows the s-process path in the region of $Z = 44 - 51$. The stable nuclides (grey boxes) are catching a neutron until the resulting daughter nuclide is unstable against β^--decay (white boxes), which leads to a movement upwards in the nuclide chart. Note, in the case of ^{107}Pd the half-live of the ground state is $6.5 \cdot 10^6$ years, which can be considered sufficiently long for the neutron capture [BBFH57]. The nuclides, which are not touched by the s-process path, need a different scenarios in order to be created. On the neutron-rich side the r-process is suggested, while on the proton-rich side the p-process is a possible scenario and those nuclides are referred to as r- and p-nuclides, respectively.

The aim of the first part of the investigation presented in this work is to contribute to the explanation, why the p-process underproduces the abundances of the p-nuclides ^{92,94}Mo and ^{96,98}Ru compared to the natural abundance as observed in the our solar system [AG03]. As a candidate to answer this question the rp-process has been suggested. Its predicted path in the vicinity of ^{99}Cd is shown in Fig. 2.2 as well as the β^+ decays towards ^{98,99}Ru. To discuss a possible contribution from the rp process, it has to be shown that nuclides, which are sufficiently produced by the s and the p process, are not created in large amounts by the rp process.

In the following an overview of the rp-process site, namely the X-ray binary, and the rp-process itself is given. The importance of proton-separation energies, and thus nuclear masses, for the rate calculations as performed by H. Schatz for the present work will be discussed. Furthermore a short summary of the r-process will be presented and the measurement of very neutron rich silver and cadmium, such as ^{129}Ag and ^{130}Cd, will be motivated.

2.1.1 rp-process

A scenario for explaining the underproduction of the p-nuclides ^{92,94}Mo and ^{96,98}Ru is the rp-process, which is taking place during type I X-ray burst of a neutron star of so called X-ray binaries [Psa04]. In Fig. 2.3 such a system consisting of a neutron star and the companion star (typically a red giant) is given in a schematic way. The marked gravitational equipotential surface is the Roche lobe, where the material such as the hydrogen/helium atmosphere is still bound by gravitation. Typically the neutron star has a mass of about $1.4M_\odot$ (solar masses) and a radius of about $10\,\mathrm{km}$ [Wal05], while the mass of the companion of a Low-Mass X-ray Binary (LMXB) is usually less than the mass of the neutron star.

rp-process site

In this scenarios material from the Roche lobe of the companion star can pass the inner Lagrange point due to the gravitational forces from the companion towards the neutron star. Depending on the accretion rate of material onto the surface of the neutron star several processes can be observed. For type I X-ray bursts, the rp-process site, typical accretion rates of $10^{-8} - 10^{-10} M_\odot$ per year are necessary [Bil97].

On the surface the accreted hydrogen is burning four protons via $p(p, e^+\nu_e)d$, $d(p, \gamma)^3$He, and ^{3}He(^{3}He,$2p$)^{4}He to one ^{4}He. If there is some carbon in the neutron star, hydrogen is also burning to ^{4}He in the CNO cycle: ^{12}C$(p, \gamma)^{13}$N, ^{13}N$(e^+\nu_e)^{13}$C, ^{13}C$(p, \gamma)^{14}$N, ^{14}N$(p, \gamma)^{15}$O, ^{15}O$(e^+\nu_e)^{15}$N, ^{15}N$(p,^4$He$)^{12}$C. The released energy of the exothermic reaction is heating the outer layer until the ignition conditions are fulfilled [Bil97]. If the temperature is high enough $3\alpha \rightarrow^{12}$ C, so-called triple α reactions, occur and will produce even more seeds for the CNO cycle. The temperature is rising further and in the following it is high enough for (α, p) and (p, γ) reactions beyond the CNO cycle.

Fig. 2.3: A schematic plot of an X-ray binary consisting of a neutron (black) and a companion star (dark gray). The Roche lobe (light gray) is the space, where material is still bound by gravity and at the Lagrange point the gravitational forces cancel out.
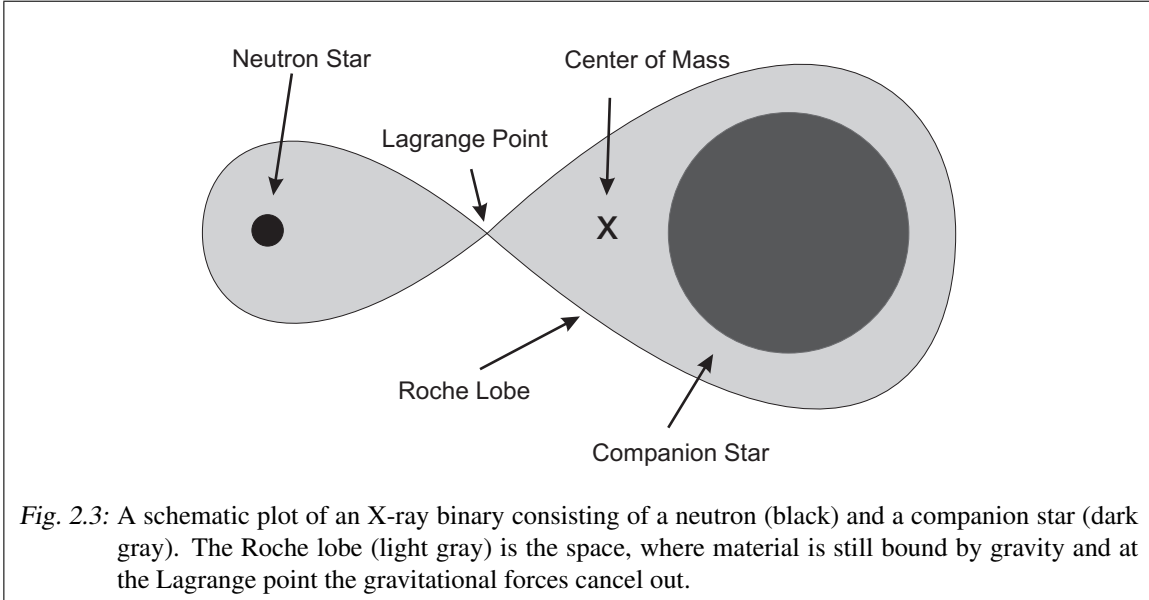
This path is referred to as the αp-process, which starts around ^{14}O and goes until approximately ^{41}Sc, where the Coulomb barrier will prevent further α-captures.

For the case that enough hydrogen is available the actual rp-process starts, the processing towards heavier nuclei continues via (p, γ) reactions until a low proton-separation energy prevents the attachment of more protons. The path is hindered at a (p, γ)-(γ, p) equilibrium between mother and daughter nuclide until β^+-decays occur to bring the path closer to stability and it can be further processed by (p, γ) reactions. This reaction path is called the rp-process, which continues until it reaches the SnSbTe cycle as described by Schatz *et al.* [SAB$^+$01].

The reaction is sensitive to the temperature, which is decreased when the process path is at the so called waiting-point nuclides due to uncompensated radiative losses. These are nuclides with low proton-separation energy, so the (p, γ)-(γ, p) will occur, and they have long β-decay half-lives. Thus the β-decay half-lives and the proton-separation energies are important input parameters for network calculations.

The reactions for the rp-process are coming to an end, when all hydrogen fuel is consumed. The temperature decreases dramatically due to the radiation and the current status of the rp-process is freezing out, namely no further (p, γ) reactions occur and the particles are converted to stable nuclides by β-decays. For this reason the produced abundances are usually given as a function of mass units, e.g. mass $A = 99$ coming from the precursor ^{99}Cd represents the nuclide ^{99}Ru in the case of the rp-process products.

rp-process calculations

In order to understand the rp-process, a network of reactions is build up. In the following, the rate calculations are described in the cgs system as the majority of the astrophysical literature is using these units (e.g. [FCZ75, Bil97, SAG98, SR06]). Note that the calculations were performed by H. Schatz. For the understanding of the importance of the masses, the principle of reaction network calculation is given briefly in this section.

Describing the abundance Y_i of a nuclide i independent of the volume or the density in the astro-
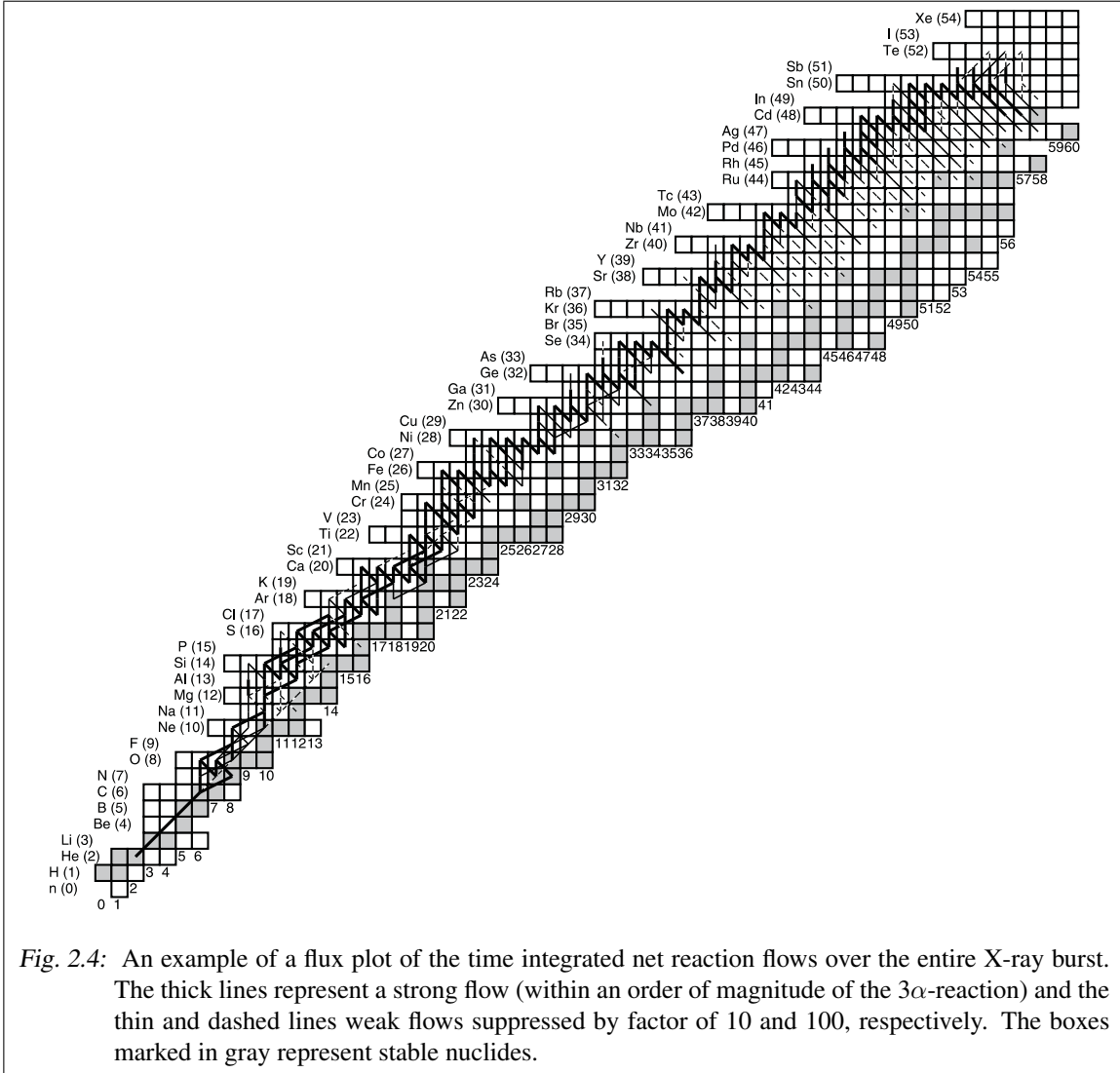
Fig. 2.4: An example of a flux plot of the time integrated net reaction flows over the entire X-ray burst. The thick lines represent a strong flow (within an order of magnitude of the 3α-reaction) and the thin and dashed lines weak flows suppressed by factor of 10 and 100, respectively. The boxes marked in gray represent stable nuclides.

physical environment using X_i as the mass fraction and A_i as the mass number results in

$$Y_i = \frac{X_i}{A_i}. \tag{2.2}$$

Then the number density is given by

$$n_i = \frac{X_i \rho_n}{m_i}, \tag{2.3}$$

with ρ_n as the density of the nuclear matter in g/cm^3 and m_i being the atomic mass of i, which can be approximated to $m_i \approx A_i \cdot m_u$. Using the atomic-mass unit m_u, which in the cgs-system is the inverse of the Avogadro number N_A, the number density can be rewritten as $n_i = Y_i \rho_n N_A$.

In the example of a single binary reaction $i + j \rightarrow k + l$ (in the following $i(j,k)l$) with $i, j \neq k, l$ the change in abundance Y_i of a nucleus i already using the substitution of n_i is

$$\frac{\mathrm{d}Y_i}{\mathrm{d}t} = -Y_i Y_j \rho_n N_A \langle \sigma\nu \rangle_{ij,kl}, \tag{2.4}$$

where $\langle \sigma \nu \rangle$ is the product of the cross section and the relative velocity, which is averaged over the Maxwell Boltzmann distribution of the astrophysical plasma. The reaction rate has a negative sign, since a nucleus i is destroyed during this process. Generalizing this approach results in a differential equation consisting of four parts:

$$
\begin{aligned}
\frac{\mathrm{d}Y_i}{\mathrm{d}t} =& \sum_{k,l} N_i \frac{Y_k^{N_k}}{N_k!} \frac{Y_l^{N_l}}{N_l!} (\rho N_A)^{N_k+N_l-1} \langle \sigma \nu \rangle_{kl,ij} \\
&- \sum_{j} N_i \frac{Y_i^{N_i}}{N_i!} \frac{Y_j^{N_j}}{N_j!} (\rho N_A)^{N_i+N_j-1} \langle \sigma \nu \rangle_{ij,kl} \\
&+ \sum_{j} Y_j \frac{\ln 2}{t_{1/2_{j \rightarrow i}}} \\
&- \sum_{i} Y_i \frac{\ln 2}{t_{1/2_{i \rightarrow j}}},
\end{aligned}
\tag{2.5}
$$

where the multiplicity of the nuclides i, j, k and l is described by N_i, N_j, N_k and N_l, respectively. The first two summands describe a change in abundance by binary reactions as well as a few possible three-body reactions, like the triple α reaction. The factorials are included to avoid double counting in the case of a reaction consisting of alike particles. The other two summands are describing the creation and destruction of a nuclide by decays with $t_{1/2}$ as the corresponding decay half-lives. The time evolution of the nuclides is critically depending on the reaction rates. A more detailed description can be found in [FCZ75].

$N_A \langle \sigma \nu \rangle_{(j,k)}$ is the rate for a nuclear reaction $i(j,k)l$, which is a function of the particle energy E, the energy dependent cross section $\sigma(E)$, and the stellar temperature T

$$
N_A \langle \sigma \nu \rangle_{(i,j)} = \left[\frac{8}{\mu \pi} \right]^{1/2} (k_B T)^{3/2} \int_0^\infty E \sigma(E) \exp(-E/k_B T) \mathrm{d}E,
\tag{2.6}
$$

where μ is the reduced mass in the target projectile system. The reaction cross section σ depends strongly on the nuclear structure of the compound nucleus and for charged particle reactions additionally on the Coulomb barrier between the two interacting particles.

The reaction rates in the case of a low level density system can be described by single resonant Breit-Wigner terms and by non-resonant contributions, where the resonant terms correspond to unbound states and the non-resonant terms to bound states in the compound nucleus.

$$
N_A \langle \sigma \nu \rangle = N_A \langle \sigma \nu \rangle_r + N_A \langle \sigma \nu \rangle_{nr}
\tag{2.7}
$$

The case of low level density is mainly given in light mass nuclides and nuclides near close shells. The network calculations and their results are discussed in Sec. 7, which are based on experimental data and on calculations of the nuclear structure [Cyb].

For nuclear reactions occurring in the rp-process for nuclides with $A \geq 40$ the level density in the compound system is generally high such that the cross section is dominated by a multitude of overlapping resonances and appears non-resonant [Sar82]. The reaction cross section σ can then be approximated by the use of the Hauser-Feschbach approach, which is widely used for the determination of thermonuclear reaction rates [HWFZ76, WFHZ78]. For a reaction $i^\delta(j,k)l^\nu$ the reaction cross

section σ can be expressed as the function of the transmission coefficients T:

$$\sigma_{jk}^{\delta\nu}(E_{ij}) = \frac{\pi\hbar^2}{2\mu_{ij}E_{ij}} \frac{1}{(2J_i^\delta + 1)(2J_j + 1)}$$
$$\times \sum_{J,\Pi}(2J+1)\frac{T_j^\delta(E, J, \Pi, E_j^\delta, J_j^\delta, \Pi_j^\delta)T_k^\nu(E, J, \Pi, E_k^\nu, J_k^\nu, \Pi_k^\nu)}{T_m(E, J, \Pi)}, \qquad (2.8)$$

where E_{ij} is the energy in the center of mass system and μ_{ij} the reduced mass in the target pro-jectile system. Note the nucleus is here described by the total angular momentum J, by the cor-responding excitation energy E, and the parity of the excited state Π. The transmission coefficient $T_k^\nu(E, J, \Pi, E_k^\nu, J_k^\nu, \Pi_k^\nu)$ describes the transition from a state (E, J, Π) in the compound nucleus into a state ν of the final nucleus under emission of a particle k. And $T_j^\delta(E, J, \Pi, E_j^\delta, J_j^\delta, \Pi_j^\delta)$ is the trans-mission coefficient of the entrance channel accordingly. The coefficient $T_m(E, J, \Pi)$ represents the total transmission summed over all channels, which can be expressed by a sum over all known experi-mental states in the final nucleus (labeled with the emitted particle m) and a part, which represents the integration over the level density $\rho(E_m, J_m, \Pi_m)$ in the final nucleus above the highest experimentally known level E_m^ω up to the maximum energy $E - S_m$:

$$T_m(E, J, \Pi) = \sum_{\lambda=0}^{\omega} T_m^\lambda(E, J, \Pi, E_m^\lambda, J_m^\lambda, \Pi_m^\lambda)$$
$$+ \int_{E_m^\omega}^{E-S_m} \sum_{J_m,\Pi_m} T_m(E, J, \Pi, E_m, J_m, \Pi_m)\rho(E_m, J_m, \Pi_m)\mathrm{d}E. \qquad (2.9)$$

S_m represents the respective channel separation energy, such as the proton separation energy. In general, along the rp-process path there is no information available on excited states in the nuclei, so the transmission coefficient is determined by transmissions to the ground state ω_0 and the integration part of Eq. 2.9.

For the calculation of the total cross section into all final states ν

$$\sigma_{jk}^\delta = \sum_\nu \sigma_{jk}^{\delta\nu} \qquad (2.10)$$

the transmission coefficient for the exit channel T_k^ν in Eq. 2.8 has to be replaced by the definition of the total transmission coefficient T_k (Eq. 2.9). To determine the cross sections σ_{jk} in an astrophysical plasma, the thermally populated states δ have to be considered:

$$\sigma_{jk} = \frac{\sum_\delta(2J_i^\delta + 1)\exp(-E_i^\delta/k_BT)\sigma_{j,k}^\delta}{\sum_\delta(2J_i^\delta + 1)\exp(-E_i^\delta/k_BT)}, \qquad (2.11)$$

where T is the temperature of the plasma.

For the determination of the cross sections for proton capture processes using the Hauser-Feshbach formalism some of the most crucial input parameters are the nuclear masses, which determine the proton separation energies, the transmission coefficients and the γ reaction channels. The cross sec-tions were determined using the SMOKER-code [RTK97]. The detailed mechanisms included in the program are explained by Rauscher *et al.* [RTK97] and also an estimate of the reliability for the cross-section predictions using the statistical model approach for n-, p- and α-target reactions is given.

Furthermore, the inverse reactions play an important role in the network calculation. For the case of the inverse reaction to the proton capture (p, γ), the photodesintegration process (γ, p), the reaction rate $\lambda_{i(\gamma,p)j}$ is given by

$$\lambda_{i(\gamma,p)j} = \frac{(2J_p + 1)G_j}{G_i} \left(\frac{\mu k_B T}{2\pi \hbar^2}\right)^{3/2} \exp\left(-\frac{Q_{j(p,\gamma)i}}{k_B T}\right) \cdot \langle \sigma \nu \rangle_{j(p,\gamma)i}, \qquad (2.12)$$

where the G_i and G_j are normalized partition functions, which describe the thermal population of the excited states of the initial i and the final nucleus j

$$G_i = \sum_{\delta}^{\omega} g_i^{\delta} \exp\left(-\frac{E_x^{\delta}}{k_B T}\right) + \int_{E_\omega} \int_{J_i,\Pi_i} \exp\left(-\frac{E}{k_B T}\right) \rho_i(E, J, \Pi) \mathrm{d}E \mathrm{d}J \mathrm{d}\Pi \qquad (2.13)$$

$g^{\delta} = 2J_{\delta} + 1$ is the statistical weight of the state δ with the spin J_{δ}. $Q_{j(p,\gamma)i}$ is the proton separation energy, a function of the masses of the mother and the daughter nuclide of the reaction. As in Eq. 2.9 the separation energy is entering exponentially in the equation and thus a strong dependence of all reaction-calculation results on the masses of the involved nuclides is given.

Calculating a burst and integrating the resulting flux as given in Eq. 2.5 between two nuclides over the entire burst

$$F_{i,j} = \int \left[\frac{\mathrm{d}Y_i}{\mathrm{d}t}_{(i \to j)} - \frac{\mathrm{d}Y_j}{\mathrm{d}t}_{(j \to i)}\right] \mathrm{d}t \qquad (2.14)$$

A diagram for all involved nuclides is plotted in Fig. 2.4. The thick lines represents a reaction flow comparable to the flow through the triple α reaction.

Nevertheless, with all understanding of the rp-process, the contribution to the nuclear abundances in the solar system is still not answered as long as no reliable scenario for the ejection of the burst ashes is existing [AG03]. In Weinberg *et al.* [WBS06] a super-Eddington luminosity driven wind is suggested as a solution. The luminosity by accretion is increased by the radiation coming from the nuclear reactions in the X-ray bursts. Network calculations have been performed to give an estimate of the released energy and thus the strength of the wind. Furthermore the composition of such ejecta is discussed, thus an ejection of material up to the mass number of $A = 60$ was predicted, which would not lead to contributions of the rp process to the production of the Mo and Ru p-nuclides. Nevertheless, an estimate for the conditions in a super-burst was given with an indication for ejection of heavier masses than $A = 60$. Thus the composition of the burst ash as discussed in Sec. 7 could contribute to solve the quest of the underproduction of ^{96,98}Ru.

2.1.2   r-process

On the neutron-rich side of the valley of stability the r-process was suggested to explain the abundances of neutron-rich nuclei, which cannot be produced by the s-process [BBFH57, CTT91]. In general, r-processes of different kinds are possible depending on the temperature and the neutron density, as explained in a recent review by Arnould *et al.* [AGT07]. As demonstrated in the previous section for the rp process and the proton-separation energy, the neutron separation-energy S_n is one of the most important input parameters for reaction-network calculations of the r-process, which determines the reaction path on the nuclide chart. Other import parameters are the β^--decay half-lives, the branching ratios, and the level densities of the nuclides involved.

A detailed understanding of the r-process, which is possible due to well determined input data, will provide a more profound knowledge about our solar system. In this context meteorites are important

Fig. 2.5: The tellurium isotopic chain and the production mechanisms of its isotopes. Stable isotopes are indicated with gray boxes and the arrows represent nuclear reactions of the r- and the s-process, as well as $\beta^{\pm}$ decays.
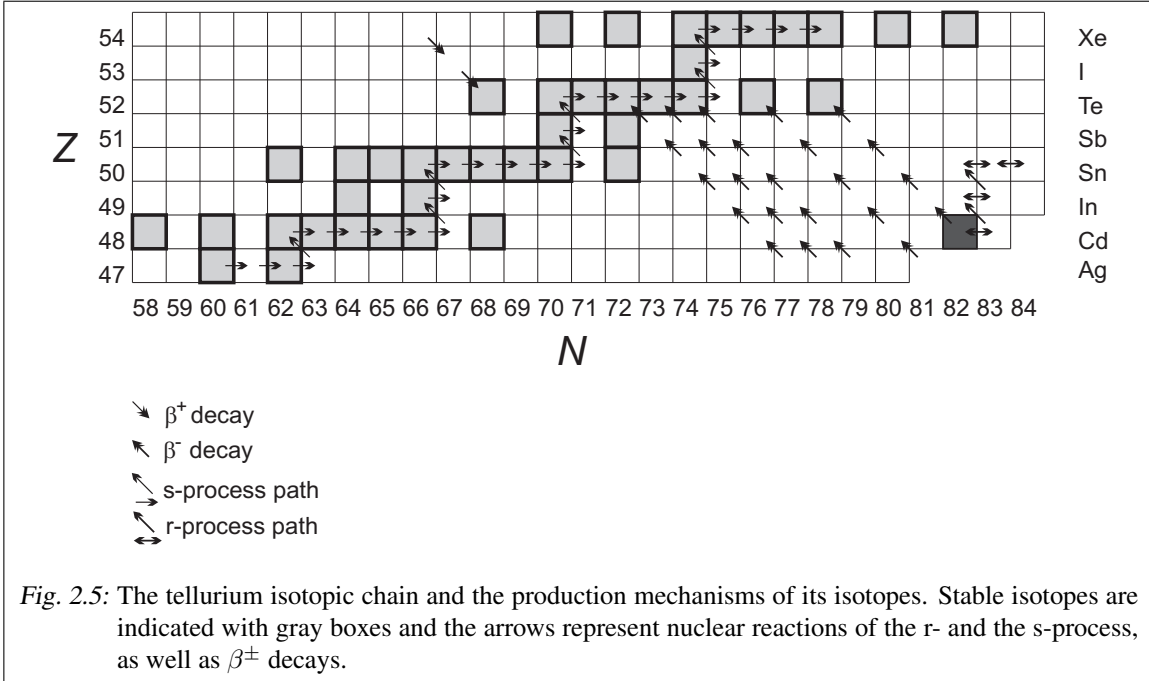
probes of nuclear abundances at different times in our solar system. Depending on the time of their creation during the evolution of the solar system they carry different nuclear abundance distributions. An interesting example is the isotopic chain of tellurium, which has three s-only isotopes $^{122-124}$Te, a p-nuclide ^{120}Te, and two r-only isotopes ^{128}Te and ^{130}Te. The other two stable tellurium nuclides ^{125}Te and ^{126}Te can be produced by both, the s-process and the r-process [SRL78, FRH$^+$05]. The relative abundances of the heavy tellurium isotopes on pre-solar meteorites are indicators for a rapid separation of supernova ejecta [ROB98]. Thus of special interest for the cadmium isotopic chain is the neutron binding energy of the $N = 83$ nuclide ^{131}Cd, which determines the waiting-point behavior of ^{130}Cd, the precursor of ^{130}Te in the r-process, which is still calculated by using masses given by mass models.

A similar quest is given for the abundance distribution in meteorites of the Xe isotopes [GT07]. The stable ^{129}Xe has its precursor along the r-process path in ^{129}Ag, one of the expected waiting points of the scenario. Thus a measurement of the masses of ^{129,130}Ag would lead to the neutron separation energy of ^{130}Ag, which determines the waiting-point behavior of ^{129}Ag.

2.2 Nuclear structure and Mass models

Since the last published AME [AWT03] lots of progress has been made as summarized by Weber *et al.* [WBS08] for the most recent mass measurements with astrophysical application. Moreover, as it will be discussed below in Sec. 5.2 and concerning our results of ^{100}Cd and ^{100}In in Sec. 6, a recompilation of the atomic mass evaluation was necessary to obtain better quality input data for the best possible calculation. This goal has been achieved in the present work.

Nevertheless, not in all regions of the nuclide chart experimental data, such as masses, half-lives, and level densities are yet available. Thus nuclear models are very important for providing input data, especially for the nucleosynthesis scenarios, which are passing far off stability. The theoretical

description experienced a strong development in the last few decades driven by the increase of computational power and, of course, by the increasing amount and the precision of available experimental data. For example in 1995 there were about 1800 masses known experimentally, while in the year 2003 this number increased to more than 2200 [AWT03].

A first very simple macroscopic approach of the nuclear binding energy of a nuclide (Z, N)

$$B = \left[Z \cdot m(^1\text{H}) + N \cdot m(n) - m(Z, N) \right] \cdot c^2 \tag{2.15}$$

has been suggested already in the 1930's by von Weizsäcker and Bethe [vW35, BB36], also known as the liquid drop model, which incorporates a volume term $\propto A$, a surface term $\propto -A^{2/3}$ and a Coulomb term $\propto -Z(Z-1)A^{-1/3}$. Additionally there are contributions from a symmetry term $\propto -a_{sym}A/I$ and a surface symmetry term $\propto A^{2/3}I^2$. This leads to an improved Weizsäcker-Bethe mass formula [MS66]:

$$B = a_{vol}A + a_{sf}A^{2/3} + \frac{3e^2}{5r_0}Z^2A^{-1/3} + \left(a_{sym}A + a_{ss}A^{2/3} \right) I^2, \tag{2.16}$$

where $I = (N - Z)/A$ is the charge-asymmetry parameter. Typical values for the parameters are $a_{vol} = -15.73\,\text{MeV}$, $a_{sf} = 26.46\,\text{MeV}$, $r_0 = 1.2185\,\text{fm}$, $a_{sym} = 17.77\,\text{MeV}$, and $a_{ss} = 17.70\,\text{MeV}$ [LPT03]. With these values the Weizsäcker-Bethe mass formula has a root mean square (rms) error

$$\sigma_{rms} = \left[\frac{1}{i} \sum_{j=1}^{i} \left(m_j^{exp} - m_j^{theo} \right)^2 \right]^{\frac{1}{2}} \tag{2.17}$$

of about 2.94 MeV to the $i = 2034$ existing mass values for $N, Z \geq 8$ as published in the AME2003 [AWT03]. This is a remarkable result of a fit to more than 2000 data using only five parameters. Nevertheless a plot of the differences between the experimental and the theoretical predicted binding energies $B_{exp} - B_{theo}$ as a function of the neutron (proton) number N (Z) reveals a striking pattern as given in Fig. 2.6: Some nuclides are particularly stable for certain neutron (proton) numbers and thus there is a big deviation between the experimental and theoretical values. These so-called magic numbers (2, 8, 20, 28, 50, 82, 126 ...) inspired the nuclear shell model, which is adopted from the atomic shell model. Nuclides with a magic number in either, protons or neutrons are referred to as magic, and nuclides being magic for protons and neutrons are called doubly-magic.

Using the single-particle approach the energies of the nucleons can be described individually. First an average nucleus is assumed, in whose potential the nucleons are propagating individually. For the determination of the energy levels the Schrödinger equation has to be solved.

The shell model describes the nucleons (fermions) filling orbits with nucleons in the potential under the application of the Pauli principle, which prohibits alike particles in the same orbit. Analogous to the atomic shell model the orbits can be described by quantum numbers, such as n, the radial quantum number, l, the orbital angular momentum, and j as the total angular momentum. The later describes the sum of intrinsic spin $s = \pm 1/2$ of a nucleus and the orbital angular momentum l and thus $j = l \pm 1/2$, except for the $l = 0$ orbits, which only exist with $j = 1/2$. Furthermore each particle with the total angular momentum j has $2J + 1$ magnetic substates and the parity of the state Π is defined by $(-1)^l$. Figure 2.7 gives an example of single particle energies for neutrons in a ^{208}Pb nuclide calculated by [Bro05] using different potentials. The harmonic oscillator potential results in equidistant levels with a degeneracy in l and J (Fig. 2.7 left). Choosing an anharmonic potential, such as the one proposed by Woods and Saxon [WS54]

$$V(r) = -\frac{V_0}{1 + \exp(\frac{r-R}{a})}, \tag{2.18}$$
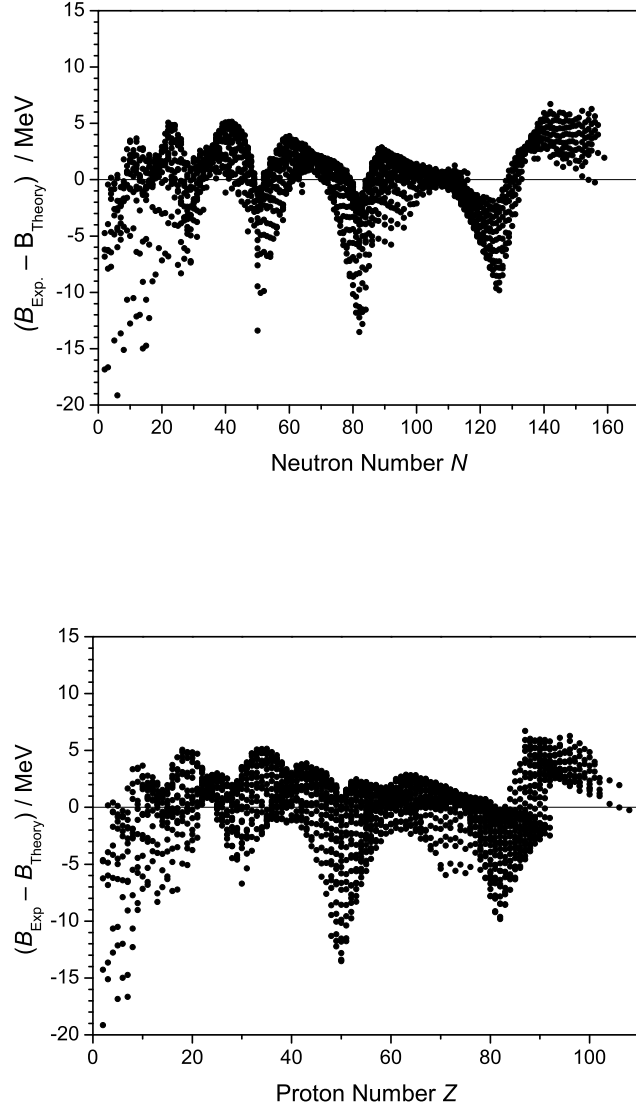
Fig. 2.6: Difference between the experimental binding energies and those predicted by the liquid droplet mass formulas as a function of neutron number N (left) and proton number Z (right). The differences were calculated using [Smi]

results in a level structure, where the l degeneracy is split (Fig. 2.7 middle). The potential is described by r as the distance from the center of the nucleus, by a as a length representing the thickness of the surface and $R = r_0 A^{1/3}$ the nuclear radius with $r_0 \approx 1.2$ fm. The deepness of the potential is given by the parameter V_0, which is normally given in the range of 50 MeV and the surface thickness is about a=0.6 fm. Introducing in addition a spin-orbit coupling also the degeneracy in j is broken (Fig. 2.7 right). For a calculation for the proton single particle energies the repulsive Coulomb force has to
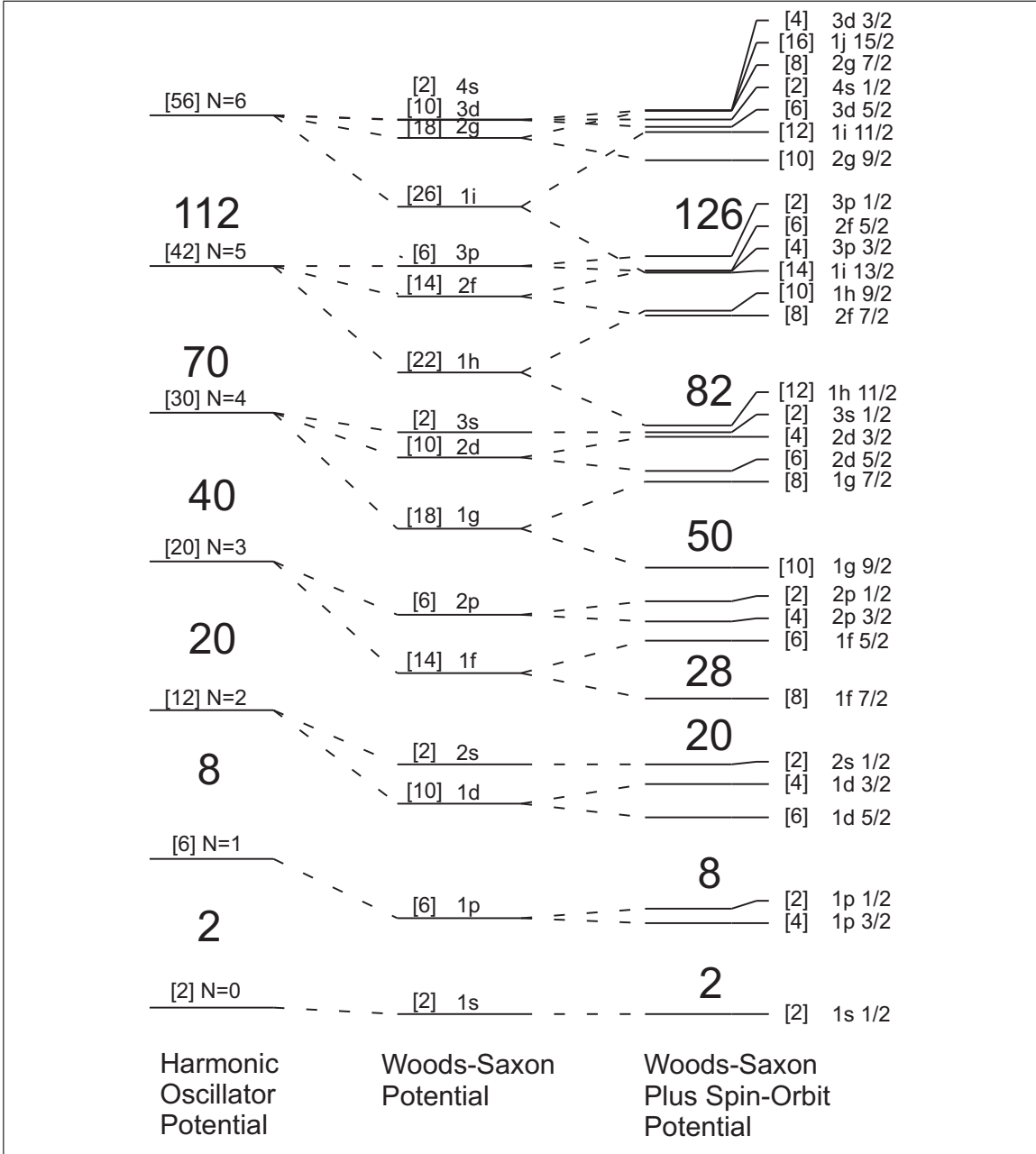
Fig. 2.7: Neutron single-particle states in ^{208}Pb with three potential models, harmonic oscillator (left), Woods-Saxon without spin-orbit (middle) and Woods-Saxon with spin orbit (right). The numbers in square brackets are the maximum number of neutrons in that each level can contain. In addition, the harmonic oscillator shell is $N = 2(n-1) + l$, the Woods Saxon is labeled by n, l and the Woods-Saxon with spin-orbit is labeled by n, l, j. The plot is taken from [Bro05] and slightly modified.

taken into account additionally.

At this point the convention for the notation of states is introduced: First, comparable to atomic physics, the different values of orbital angular momentum $l = 0, 1, 2, 3, 4, 5, 6, \ldots$ are described by
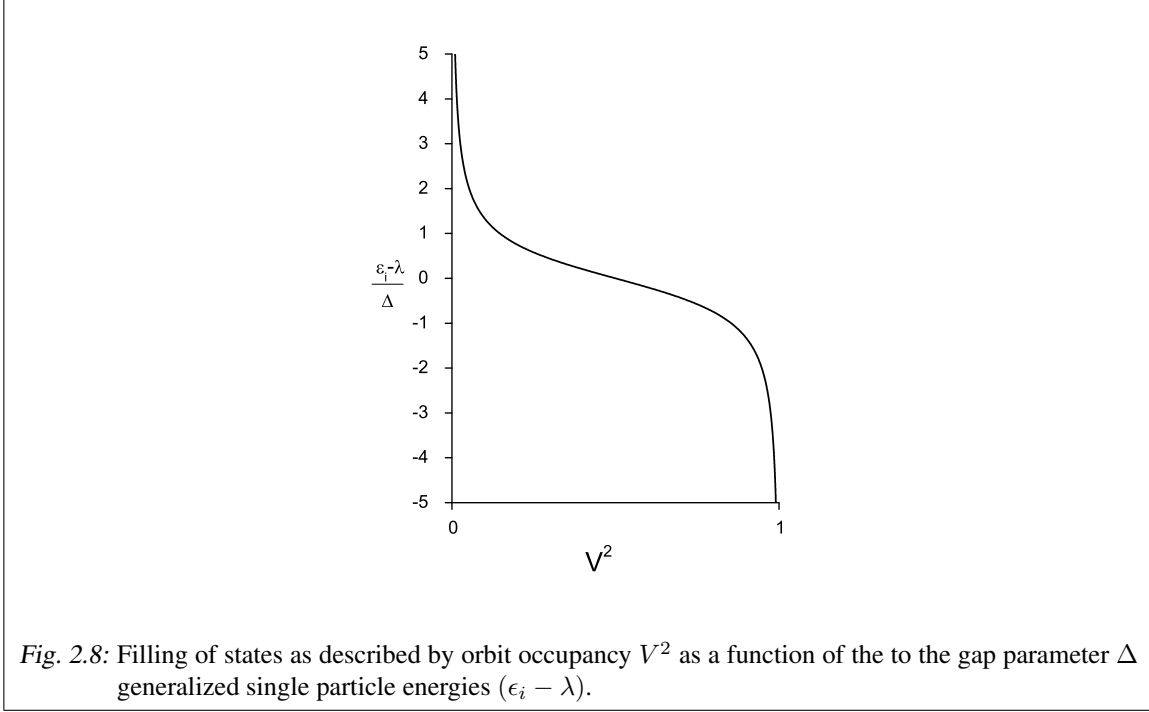
Fig. 2.8: Filling of states as described by orbit occupancy V^2 as a function of the to the gap parameter Δ generalized single particle energies $(\epsilon_i - \lambda)$.

letters of the Latin alphabet $s, p, d, f, g, h, i, \ldots$. An orbit is then described with the nl_j. The example of the $2d_{5/2}$ shell is characterized by $n = 2$, $l = 2$, $s = +1/2$, and thus $j = 5/2$. Note, for more than one particle, the total angular momenta j_i of the i nucleons couple to the total angular momentum J. The state of multi particle configurations are then described by the total angular momentum and the parity J^Π.

In the single particle approach the pairing can be describe by introducing a force V_{pair} as defined by the matrix elements

$$\langle j_1 j_2 J | V_{pair} | j_3 j_4 J\prime \rangle = -G \left(j_1 + \frac{1}{2} \right)^{1/2} \left(j_2 + \frac{1}{2} \right)^{1/2} \delta_{j_1 j_2} \delta_{j_3 j_4} \delta_{J0} \delta_{J\prime 0} \tag{2.19}$$

where the

$$G_p = \frac{17}{A} \text{ MeV} \tag{2.20}$$

and

$$G_n = \frac{23}{A} \text{ MeV} \tag{2.21}$$

denote the overall interaction strength for protons and neutrons, respectively. This attractive interaction is only effective for 0^+ states of identical nucleons in the same orbit. Without the presence of the pairing force the nucleons would fill all levels up to the Fermi energy, and the level above would stay empty. However, with pairing the occupancy of the levels changes as shown in Fig. 2.8, as described

Fig. 2.9: Left: Compression of levels near the ground state for odd nuclides due to pairing. Right: Increase
of level energies and the pairing gap in even-even nuclides. The plot is taken from [Cas00].
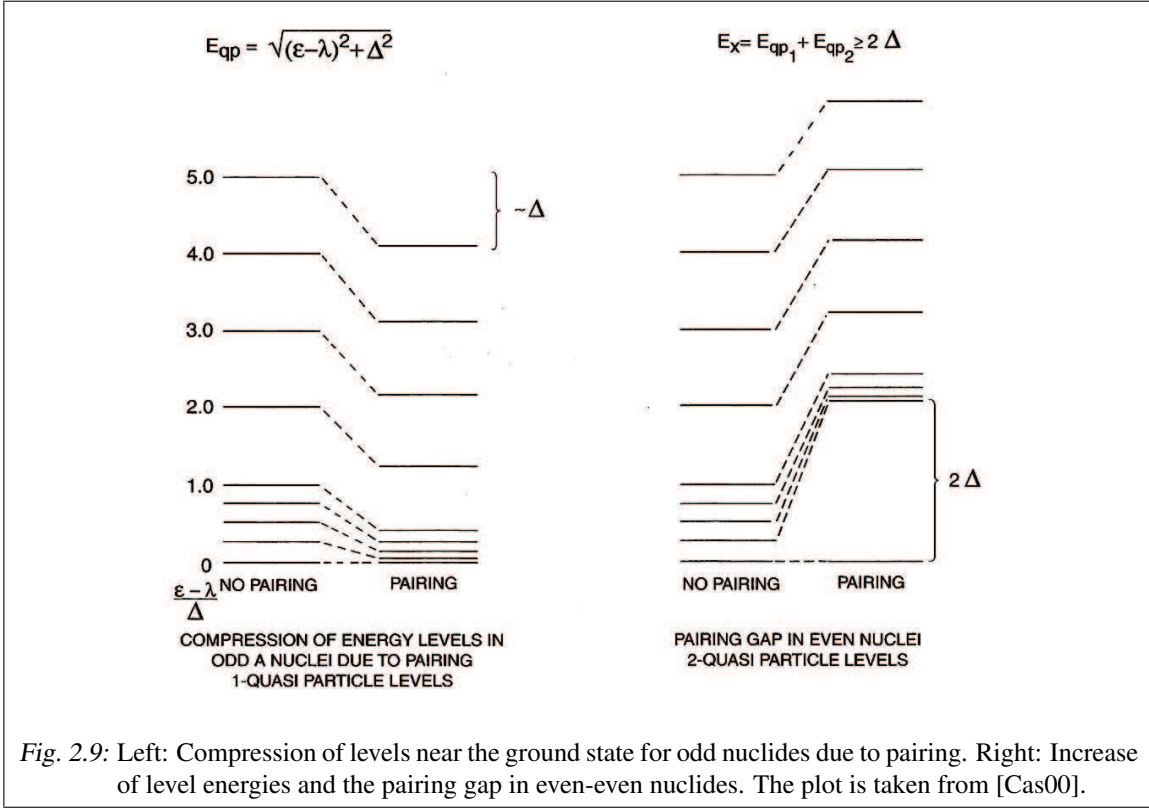
by the fullness factor V_i and the emptiness factor U_i

$$V_i = \frac{1}{\sqrt{2}} \left[1 - \frac{\epsilon_i - \lambda}{\sqrt{(\epsilon_i - \lambda)^2 + \Delta^2}} \right]^{1/2}$$

$$U_i = \frac{1}{\sqrt{2}} \left[1 + \frac{\epsilon_i - \lambda}{\sqrt{(\epsilon_i - \lambda)^2 + \Delta^2}} \right]^{1/2}. \tag{2.22}$$

Here, the pairing gap

$$\Delta = G \sum_{i,j} U_i V_j \tag{2.23}$$

is described as the as sum over the filling of the orbits. The Δ can be estimated by either the pairing
gap in even-even nuclides or from odd-even mass differences. The pairing gap and the increased level
density, which are shown in Fig. 2.9 at the right and marked with 2Δ, is characteristic for almost
any even-even nuclide. In the vicinity of the Cd nuclides it is about $2\Delta = 2\,\text{MeV}$. In odd nuclei the
pairing has the effect of level compression near the ground state and a decrease of level energy by Δ
for higher lying states (Fig. 2.9 left).

The states including the pairing are so-called quasi particle states with an energy of

$$E_i = \sqrt{(\epsilon_i - \lambda)^2 + \Delta^2}. \tag{2.24}$$

This allows one to determine the minimum energy for an excited state to:

$$E^o_{x_i} = E_i - E_0 = \sqrt{(\epsilon_i - \lambda)^2 + \Delta^2} - \sqrt{(\epsilon_0 - \lambda)^2 + \Delta^2}, \tag{2.25}$$

with E_0 as the quasi particle energy of the orbit with closest energy to the Fermi level λ and ϵ_o the single particle energy of the same orbit. More information about the pairing force can be found in textbooks as [Cas00]. Note, that for nuclides with strong collective behavior the level schemes as given in Fig. 2.9 are not applicable. A good measure for the grade of collectivity in even-even nuclides is the $R_{4/2}$, the ratio of the energy of the first 4^+ state to the energy of the first 2^+ state. For $R_{4/2}$ below 2 the single particle approach is valid.

A microscopic approach to describe the complete nucleus is the Hartree-Fock-Bogolyubov method (HFB), which unifies the self-consistent description of nuclear orbits as given in the Hartree-Fock method using an effective interaction, a phenomenological Wigner term describing the stronger binding for $N = Z$ [MS66], and the adjusted Bardeen-Cooper-Schrieffer (BCS) pairing theory into a single variational theory. Here the Wigner term describes a strong interaction in nuclides with $N = Z$, whereas the pairing force is needed to account for the odd-even staggering of the binding energy as a function of neutrons and protons. The trial variational wave function is a linear combination of independent particle states representing various possibilities of occupying nucleons of single-particle states [DFT84]. A goal is to find a description of nuclides for all different areas of the nuclide chart, e.g. the vicinity of the magic nuclides, where the nuclides are spherical, and for the regions of deformation, which are usually mid-shell.

As an example, the HFB series by a group from Brussels uses a few nuclides to fit the parameters of the Skyrme force, the Wigner term and the pairing term. Afterwards the results are tested with respect to masses and other nuclear properties, such as e.g. charge radii, for the remaining nuclides. Different nuclides were chosen for the models HFB2 [GSH$^+$02], HFB8 [SGP03, SGBP04], and HFB14 [GSP07]. The latest member of this series, HFB17 [GCP09b], was determined by fitting the 18 parameters (10 for the Skyrme force, 4 for the Wigner term, and 4 for the pairing) to all nuclear masses of the AME2003 and thus of course the agreement to those masses improved. Furthermore, this model agrees within its uncertainties to more than 400 masses recently determined by the ESR facility [LGR$^+$05].

The following approaches to predict masses are a link between the microscopic models as those based on the Hartree-Fock method and the phenomenological Weizsäcker-Bethe mass formula, which is also referred to as a macroscopic model. These formulas are designed to save computational power and thus are limited in the included physics. For this reason their prediction power is limited to masses. A few of the most advanced of these so-called microscopic-macroscopic approaches are presented here. For a more detailed discussion see [LPT03].

Dulfo-Zuker (DZ)

One of the most successful mass models in the past years is the Duflo-Zuker model concerning the rms uncertertainty as compared to experimental data. It has a Hamiltonian separated into a monopole and a multipole part, where the monopole term describes the single particle energies, while the multipole term accounts for the residual interactions, allowing configuration mixing, which includes pairing and the Wigner correlation. These monopole and multipole parts are parameterized by the application of symmetry and scaling arguments [DZ95]. Thus saturation and configuration mixing is achieved such that the magic numbers and also the regions of strong deformation are described.

Finite Range Droplet Model (FRDM)

The liquid drop model of Weizsäcker and Bethe [vW35, BB36] was extended by Myers and Swiatecki [MS69] to the droplet model, which includes the distinction of the neutron and proton densities and

Tab. 2.1: Comparison of the mass models to the AME2003 using the rms Eq. 2.17.

Mass Model	Global	Ag	Cd
Number of Isotopes Used	2034	25	31
	σ_{rms} / MeV		
DZ	0.35	0.25	0.28
WB	2.94	2.96	4.24
HFB2	0.64	0.56	0.67
HFB8	0.61	0.73	0.94
HFB14	0.69	0.44	0.72
HFB17	0.55	0.30	0.53
FRDM	0.60	0.35	0.52
ETFSI	0.74	0.72	0.41
KTUY	0.65	0.26	0.54

an introduction of the diffuseness of the surface. Furthermore the diffuse property of the surface is described by a finite range term and an exponential compressibility term was included to improve the macroscopic part of the description, from which the name is derived. In addition, the microscopic treatment of the pairing in a BCS fashion, the Strutinski shell corrections, and a Wigner term are included [MNMS95]. The 31 mass dependent parameters of this model are partly predetermined by other nuclear properties, thus only 19 parameters were included in the mass fit.

Extended Thomas-Fermi plus Strutinski Integral (ETFSI)
The Extended Thomas-Fermi plus Strutinski Integral (ETFSI) [APDT95] is a model with only nine parameters. It is based on a Hartree-Fock type Skyrme force and a pairing force. The approximation used in the ETFSI method separates the Skyrme force in two parts, a semiclassical treatment of the Hartree-Fock method by the application of the full fourth-order extended Thomas-Fermi method and the attempt to improve this by small perturbations for the shell corrections. The latter part is based on the Strutinski-integral form [BQ81] based on the Strutinski theorem [Str67, Str68]. This is an important step towards the HFB models.

Koura Tachibana Uno Yamada (KTUY05)
Koura, Tachibana, Uno and Yamada presented a method to calculate shell energies from spherical objects [KUTY00] using a term describing general trends and fluctuation term, which accounts for fluctuation as given by shell structure. This formula did not account for the odd-even staggering and thus a more thorough treatment by adding a BCS-pairing term as in HFB formalism was performed [KTUY05]. Beside the masses, also the first derivative (proton and neutron separation energies) can be reproduced nicely, which is important with respect to astrophysical applications.

In the following the results of the above mentioned approaches that predict binding energies are compared with the data as tabled in the atomic-mass evaluation 2003. The differences were calculated using tools available at the web interface *nuclearmasses.org* [Smi] using the provided models and including manually the values of HFB17 as provided online by Goriely *et al.* [GCP09a]. A measure
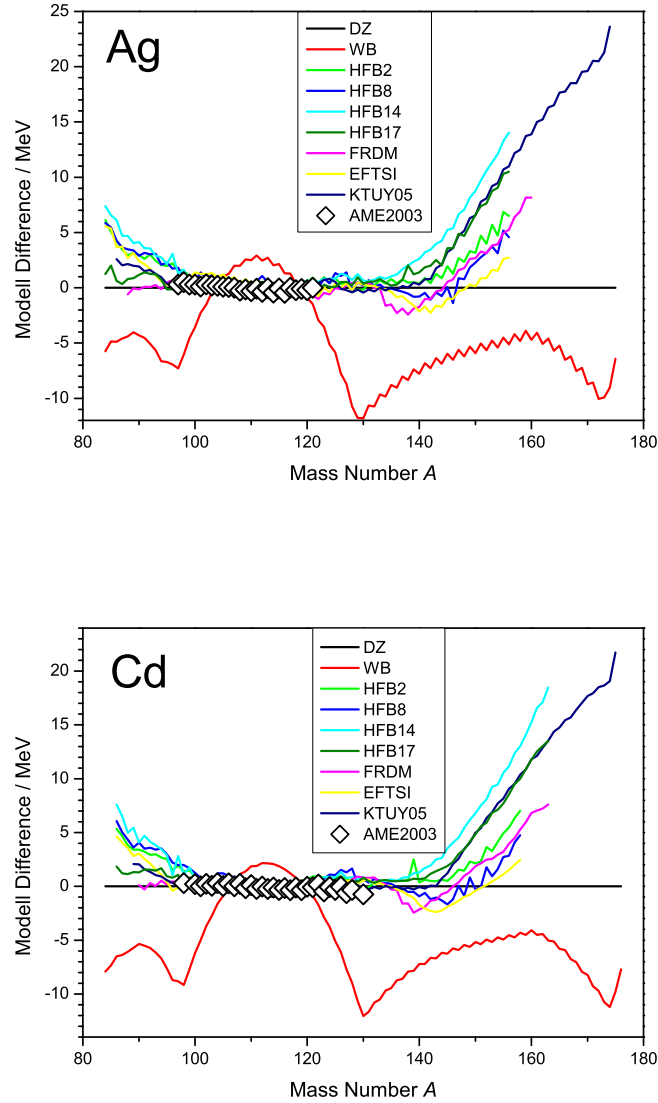
Fig. 2.10: Comparing different massmodels and experimental results for the Ag (top) and Cd nuclides (bottom). Note, the model by Duflo and Zuker (DZ) [DZ95] was chosen as a reference to allow a comparison for nuclides with no experimental data available. The models are discussed in the text.

for the quality of these mass predictions is given in the form of the rms deviation (Eq.2.17) to the AME2003 [AWT03] in Tab. 2.1, which are compared for the isotopic chains of silver and cadmium as well as for entire nuclide chart.

In addition, the agreement of the models with the available data for Ag and Cd is plotted in Fig. 2.10. For reasons of comparison for very exotic nuclides, where no experimental data are available, the plotted values are differences between the Duflo-Zucker model and the other models dis-

cussed below for the Ag and Cd nuclides. Also included are the available experimental masses as compared to the Duflo-Zuker model. The mass differences are plotted just for the expected proton drip line to the expected neutron drip line, where the proton and neutron separation energies, S_p and S_n are becoming zero. Already in this criteria the models differ by a few nuclides. In addition, towards the the drip lines the binding energies differ by up to 15 MeV. Nevertheless, close to the drip lines the slopes of the binding energy differences are comparable and thus it is expected to obtain less deviating separation energies.

2.3   Garvey-Kelson Relations

Using a local relation between masses provides a test of the smoothness of the mass surface. Amongst the most successful local algebraic mass formulas are the Garvey-Kelson relations [GK66, GGJ$^+$69]. The mass differences are combined, such that all interactions are canceled out for Garvey-Kelson 1:

$$
\begin{aligned}
0 = {} & ME(Z-1, N+1) - ME(Z+1, N-1) \\
& + ME(Z, N-1) - ME(Z, N+1) \\
& + ME(Z+1, N) - ME(Z-1, N)
\end{aligned}
\tag{2.26}
$$

and Garvey-Kelson 2

$$
\begin{aligned}
0 = {} & ME(Z+1, N+1) - ME(Z-1, N-1) \\
& + ME(Z, N-1) - ME(Z, N+1) \\
& + ME(Z-1, N) - ME(Z+1, N),
\end{aligned}
\tag{2.27}
$$

which are schematically shown in Fig. 2.11 left and center, respectively. Thus a nuclide is involved in
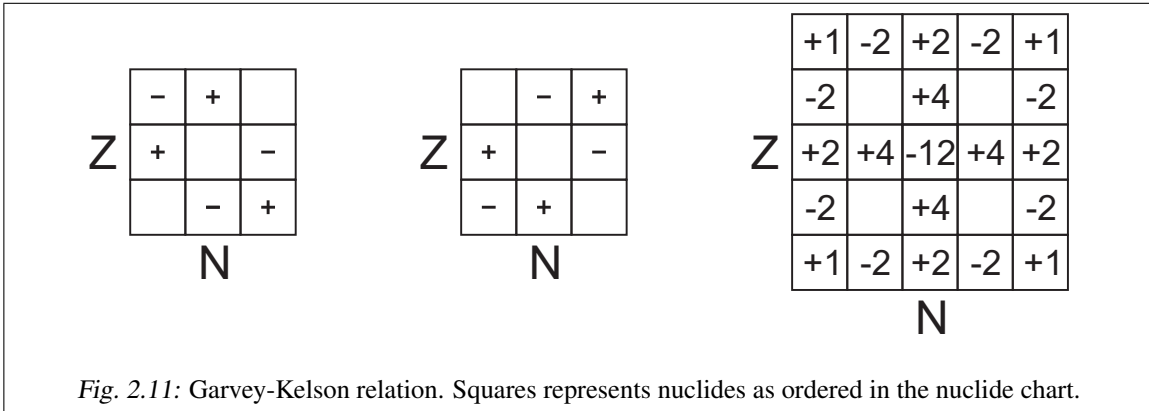
Fig. 2.11: Garvey-Kelson relation. Squares represents nuclides as ordered in the nuclide chart.

twelve Garvey-Kelson relations (Fig. 2.11 right). Writing the Eq. (2.26) and (2.27) as function of the mass number $A = Z + N$ and the isospin $T_z = 0.5(N - Z)$ results in:

$$
\begin{aligned}
0 = {} & ME(A, T_z + 1) - ME(A, T_z - 1) \\
& + ME(A-1, T_z - \tfrac{1}{2}) - ME(A-1, T_z + \tfrac{1}{2}) \\
& + ME(A+1, T_z - \tfrac{1}{2}) - ME(A+1, T_z + \tfrac{1}{2})
\end{aligned}
\tag{2.28}
$$

(a) Garvey Kelson 1

(b) Garvey Kelson 2

Fig. 2.12: Scheme of the Garvey-Kelson relations as discussed in [JM88].
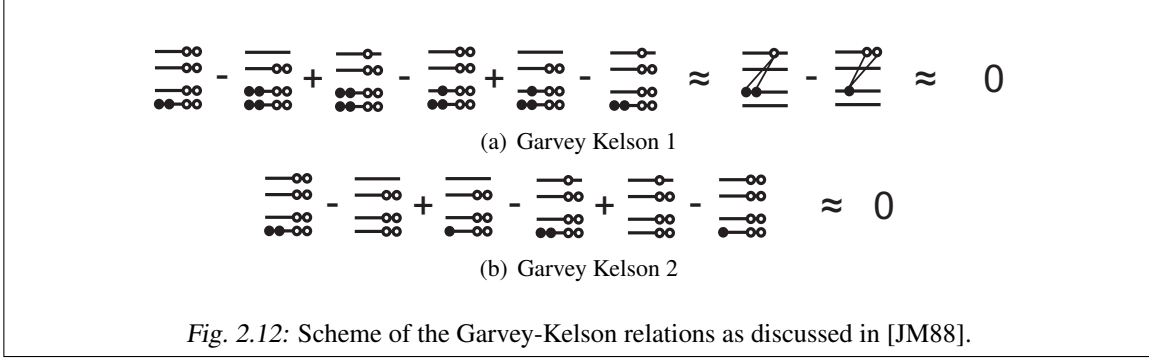
and

$$
\begin{aligned}
0 = {} & ME(A+2, T_z) - ME(A-2, T_z) \\
& + ME(A-1, T_z - \tfrac{1}{2}) - ME(A+1, T_z - \tfrac{1}{2}) \\
& + ME(A-1, T_z + \tfrac{1}{2}) - ME(A+1, T_z + \tfrac{1}{2}),
\end{aligned}
\tag{2.29}
$$

which are reordered. Thus, the first relation with Eq. 2.26 and 2.28 relates differences between three pair of masses, where the members of each pair have the same A but different T_z. In Fig. 2.12(a) a scheme is given, of how the interactions between proton-proton, neutron-neutron, and proton-neutron, as well as the single-particle energies cancel out in an independent-particle picture. The other relation as given in Eqs. 2.27 and 2.29 represents three pairs of differences with the same isospin as drawn in Fig. 2.12(b).

Thus, with the knowledge of five of the masses a prediction of the sixth is possible. In total there are twelve different possibilities to obtain the mass value of a certain nuclide from the Garvey-Kelson mass relation, which is only possible if all mass data are available and hence, they are only applicable in the vicinity of the valley of stability. In Fig. 2.11 (right) the combined relation is given for the central nuclide. Recently, a survey over the entire chart of nuclide using these mass relations was performed with the experimental data tabled in the AME2003 [AWT03] and a root mean square error as given in Eq. 2.17 of $\sigma_{rms} \approx 76\,\mathrm{keV}$ has been obtained for the mass region $A \geq 60$, if all twelve relations can be applied [BFH$^+$08].

Nevertheless, there are some simple physical arguments, that these relations should not hold exactly [GGJ$^+$69]. First: the single particle energies change for different nuclei, due to different sizes of the nuclei and different strength of the Coulomb potential, and due to the onset of deformation. Second, the ground state is not exactly described by an independent particle configuration. And finally, the assumption that a nucleus is in a parentage relationship with its neighbors is not holding in every case. In [GGJ$^+$69] some examples are given like the cases of ^{11}B and ^{47}Ti. For this reason the reliability of the Garvey-Kelson relation is not expected to be better then the currently achieved limits.

2.4 Indicator for nuclear structure: δV_{pn}

While it is useful for mass predictions, or tests of the mass surfaces to use differences between the masses of several nuclides, another application of mass differences is the application as a filter for interactions. To this end the concept of the $T_z = 0$ interaction of even-even nuclides δV_{pn} [ZWYG88,

Fig. 2.13: Schematic illustration of δV_{pn} for the case of even-even nuclide.
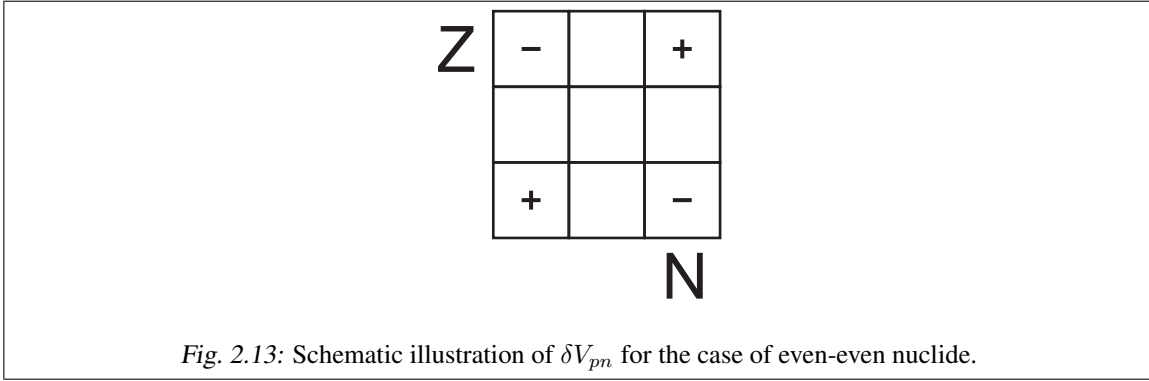
ZCB89] was introduced:

$$\delta V_{pn}^{ee}(Z, N) = -\frac{1}{4}(\{ME^{ee}(Z, N) - ME^{ee}(Z, N-2)\} \tag{2.30}$$
$$- \{ME^{ee}(Z-2, N) - ME^{ee}(Z-2, N-2)\}),$$

The intuitive understanding of this double difference is illustrated schematically in Fig. 2.14. Each component of Eq. 2.31 includes contributions from proton-proton, neutron-neutron, and proton-neutron interaction, as well as a contribution from the spherical field. The last term describes the part of the interaction, which is not driving the deformation otherwise the obtained result is adulterated with those terms as discussed by Neidherr *et al.* [NAB$^+$09]. With the first difference (as described in Eq. 2.31) the interaction of the last two neutrons with the Z protons is isolated, whereas the second difference describes the interaction of the last two neutrons with the $Z-2$ protons. Subtracting these differences results in the pure interaction between the last two protons with last two neutrons. The value is normalized to the involved nucleons $n = \Delta Z \cdot \Delta N$.

Fig. 2.14: Schematic expanation of δV_{pn} for the case of even-even nuclide. The scheme is given as plotted in [ZCB89].
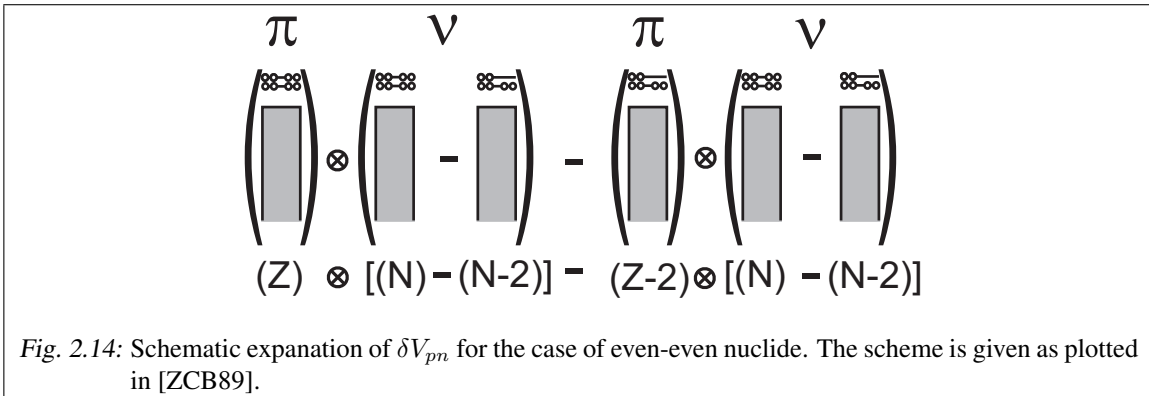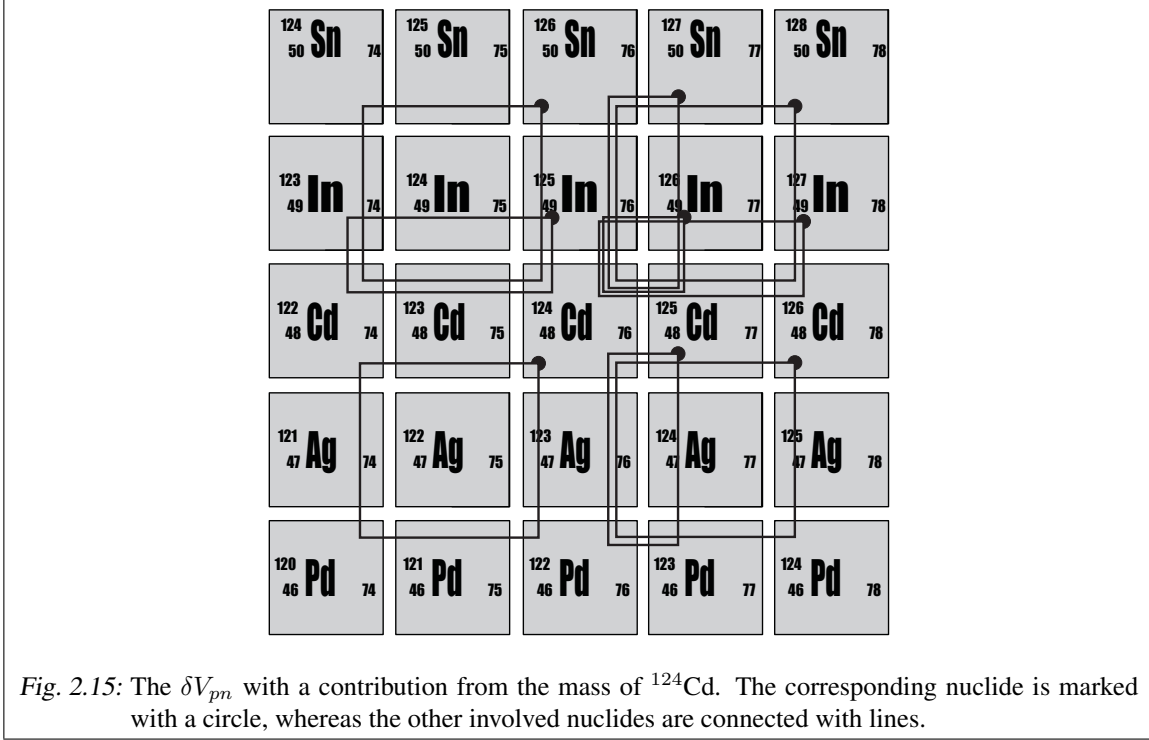
Fig. 2.15: The δV_{pn} with a contribution from the mass of ^{124}Cd. The corresponding nuclide is marked with a circle, whereas the other involved nuclides are connected with lines.

Extending this concept for even-odd, odd-even, and odd-odd nuclides leads to:

$$\delta V_{pn}^{eo}(Z, N) = -\frac{1}{2}(\{ME^{eo}(Z, N) - ME^{ee}(Z, N - 1)\} \tag{2.31}$$
$$- \{ME^{eo}(Z - 2, N) - ME^{ee}(Z - 2, N - 1)\}),$$

$$\delta V_{pn}^{oe}(Z, N) = -\frac{1}{2}(\{ME^{oe}(Z, N) - ME^{oe}(Z, N - 2)\} \tag{2.32}$$
$$- \{ME^{ee}(Z - 1, N) - ME^{ee}(Z - 1, N - 2)\}),$$

$$\delta V_{pn}^{oo}(Z, N) = -\frac{1}{1}(\{ME^{oo}(Z, N) - ME^{oe}(Z, N - 1)\} \tag{2.33}$$
$$- \{ME^{eo}(Z - 1, N) - ME^{ee}(Z - 1, N - 1)\}).$$

These values are normalized to the number n of involved nucleons. The uncertainties of the δV_{pn}-values are given by the square root of the sum of the squared uncertainties of the contributing mass-excess values

$$\sigma(\delta V_{pn}) = \frac{1}{n}\sqrt{\sum_{i=1}^{4} \sigma^2(ME_i)}. \tag{2.34}$$

Thus, the mass of an even-even nuclide contributes to nine δV_{pn} values, as shown in Fig. 2.15 for the example of ^{124}Cd, its mass is involved in the calculation of δV_{pn} values for $^{124-126}$Cd, $^{125-127}$In, and $^{126-128}$Sn.

Previous investigations led to the observation, that the interaction of the protons and neutrons is the strongest, when both fill similar orbits[CBCM05, BCC06]. The interaction represented by the δV_{pn} values is strongest for the $N = Z$ nuclei and local maxima are given when the last protons

Fig. 2.16: The δV_{pn} values are shown color-coded for nuclides in the vicinity of ^{208}Pb. The plot is taken from [CLP$^+$09].
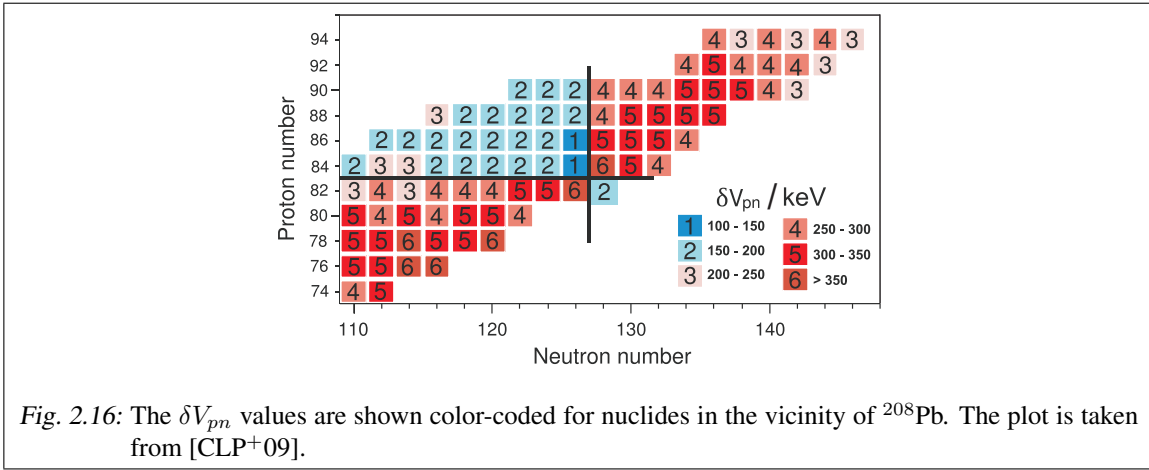
and the last neutrons in states just before or just after a shell closure. This can be seen in Fig. 2.16, where the δV_{pn} values are plotted for nuclides in the vicinity of ^{208}Pb as published in [CLP$^+$09]. Furthermore, those nuclides, for ehich one kind of the nucleons just passed the shell closure, while the other kind still stays below it, show a very low interaction strength.

3. PENNING TRAPS

The importance of nuclear masses for astrophysics and nuclear structure as discussed above stresses the requirement for data of short-lived nuclei with half-lives down to a few milliseconds. The determination of the cyclotron frequency of an ion in a magnetic field $\omega_c = qB/m$ measured with Penning traps has been established as a powerful method to reach relative mass uncertainties down to 10^{-9}. The application of this method needs a thorough understanding of the principle of Penning traps. In the following (Sec: 3.1) the eigenmotions in a Penning trap are characterized by simple equations of motions. These are still solvable for controlled perturbations, which cause a manipulation of the eigenmotions and their radii. Three different techniques are commonly used to change the radii of the radial eigenmotions: (Sec: 3.1) an azimuthal dipolar radio-frequency (rf) excitation at the eigenfrequencies ν_+ or ν_- for increasing the radii of the radial eigenmotions, (Sec: 3.1) a quadrupolar rf excitation at $\nu_c = \nu_+ + \nu_-$ for a conversion of the magnetron motion into the cyclotron motion and vice versa, and (Sec: 3.1) a quadrupolar excitation in a buffer-gas environment for a mass-selective centering of the ions.

3.1   Ideal Penning trap and the characteristic eigenmotions

In an ideal Penning trap a charged particle is confined in radial and axial direction by a homogeneous magnetic field $\vec{B} = B\vec{e}_z$ and a quadrupolar electrostatic field $\vec{E} = -\vec{\nabla}\Phi$, respectively. The surfaces of the electrodes can be described by $2z^2 - x^2 - y^2 = -\rho_0^2$ for the ring electrode and by $2z^2 - x^2 - y^2 = 2z_0^2$ for the two-piece endcap electrode. The potential Φ is then given in cylindrical coordinates to

$$\Phi = \frac{U_0}{2d^2}\left(z^2 - \frac{\rho^2}{2}\right), \tag{3.1}$$

by applying a voltage U_0 between the ring electrodes and the endcaps, where

$$d^2 = \frac{1}{2}\sqrt{\frac{\rho_0^2}{2} + z_0^2} \tag{3.2}$$

is the trap parameter with ρ_0 as the ring-electrode radius and z_0 as half the distance between the endcaps. A particle of the charge q and the mass m in such a trap experiences the Lorentz force

$$\vec{F}_{Lorentz} = q\left(\dot{y}B\vec{e}_x - \dot{x}B\vec{e}_y\right) \tag{3.3}$$

and the electrostatic force

$$\vec{F}_{Coulomb} = \frac{qU_0}{d^2}\left(\frac{x}{2}\vec{e}_x + \frac{y}{2}\vec{e}_y - z\vec{e}_z\right). \tag{3.4}$$

Solving the equations of motion [BG86] results in the eigenmotions of a charged particle in Penning
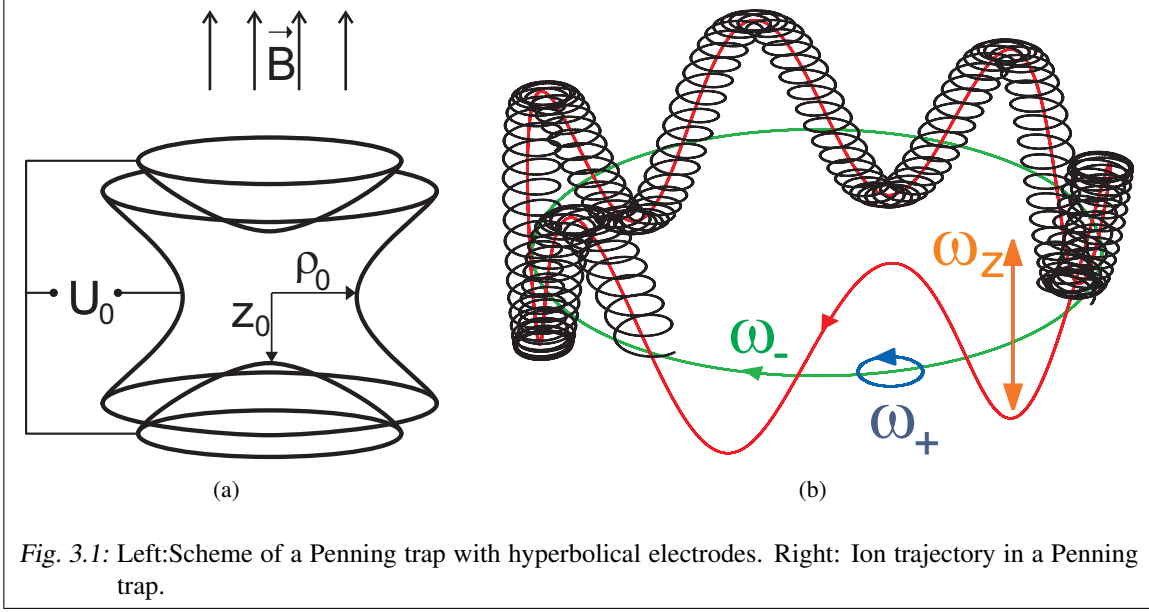
Fig. 3.1: Left:Scheme of a Penning trap with hyperbolical electrodes. Right: Ion trajectory in a Penning trap.

trap:

$$x(t) = \rho_{-,0} \cos(\omega_- t - \varphi_-) + \rho_{+,0} \cos(\omega_+ t - \varphi_+),$$
$$y(t) = \rho_{-,0} \sin(\omega_- t - \varphi_-) - \rho_{+,0} \sin(\omega_+ t - \varphi_+),$$
$$z(t) = A_z \sin(\omega_z t - \varphi_z). \tag{3.5}$$

with an axial oscillation of the eigenfrequency

$$\omega_z = \sqrt{\frac{qU_0}{md^2}} \tag{3.6}$$

and two radial motions, the magnetron motion and the cyclotron motion, with the magnetron ω_- and the reduced cyclotron frequency ω_+, respectively,

$$\omega_\pm = \frac{\omega_c}{2} \pm \sqrt{\left(\frac{\omega_c}{2}\right)^2 - \frac{\omega_z^2}{2}} \tag{3.7}$$

where

$$\omega_c = \frac{q}{m} B \tag{3.8}$$

is the cyclotron frequency of a charged particle in a homogeneous magnetic field. Typical frequency values at ISOLTRAP for example of ^{85}Rb, ^{99}Cd, and ^{133}Cs, are given in Tab. 3.1.

From these formulas one can derive three important relations between the eigenfrequencies and ω_c:

$$\omega_c = \omega_+ + \omega_-, \tag{3.9}$$
$$2\omega_+\omega_- = \omega_z^2, \tag{3.10}$$
$$\omega_c^2 = \omega_+^2 + \omega_-^2 + \omega_z^2. \tag{3.11}$$

Tab. 3.1: Eigenfrequencies and ω_c for ^{85}Rb, ^{99}Cd, and ^{133}Cs in the ISOLTRAP Penning traps.

Nuclide	$\omega_-/(2\pi)$ /kHz	$\omega_z/(2\pi)$ /kHz	$\omega_+/(2\pi)$ /kHz	$\omega_c/(2\pi)$ /kHz
Preparation Penning trap				
^{85}Rb	0.3	22.7	857.1	857.4
^{99}Cd	0.3	21.0	735.6	735.9
^{133}Cs	0.3	18.1	547.5	547.8
Precision Penning trap				
^{85}Rb	1.1	48.5	1068.7	1069.8
^{99}Cd	1.1	44.9	917.1	918.2
^{133}Cs	1.1	38.7	682.4	683.5

3.2 Dipolar Excitation

First of all, the amplitude of the rf excitation in the vicinity of the trap center as compared to the applied voltages is discussed. This discussion is similar for the dipolar and quadrupolar excitation as compared to the field geometries of ideal azimuthal multipoles and will be performed for the dipolar case only:

For an azimuthal dipolar excitation a rf voltage with the amplitude V_d and the frequency $\omega_d = 2\pi\nu_d$ is applied on a two-fold split ring electrode (Fig. 3.2). The excitation signal of the rf voltage is applied with a phase difference of π between the ring segments. The electrical field in the direction of $\vec{e}_d$ can approximated by the field created by a voltage between two infinitely large plates of a capacitor with a separation of $2\rho_0$:

$$\vec{E}_{ideal} = \frac{V_d}{2\rho_0} \cdot \sin(\omega_d t + \varphi_d)\vec{e}_d. \tag{3.12}$$

For the determination of the dipolar field components the circular symmetry of a Penning trap can be considered by the approach of an infinitely long hollow cylinder slitted axially in two parts. Performing a Fourier analysis of the radial potential leads to a correction factor of $c_1 = 4/\pi$. The electric field close to the trap center is then:

$$\vec{E}_{cyl} = c_1\vec{E}_{ideal} = \frac{4}{\pi}\frac{V_d}{2\rho_0} \cdot \sin(\omega_d t + \varphi_d)\vec{e}_d. \tag{3.13}$$

For a trap with hyperbolical shaped electrodes the dipolar component of the electrical field is reduced by the influence of the endcaps. The reduction factor can be determined by numerical simulations:

$$\vec{E}_{hyp} = a_{1,0} \cdot \vec{E}_{cyl} = a_{1,0} \cdot \frac{4}{\pi}\frac{V_d}{2\rho_0} \cdot \sin(\omega_d t + \varphi_d)\vec{e}_d. \tag{3.14}$$

Ions will be accelerated or decelerated depending on the orientation of the field vector $\vec{e}_d$ to the velocity vectors of the radial eigenmotions $\vec{e}_\pm$. With the vectors in phase the radius of the eigenmotion is increasing, with vectors counter phase it is decreasing.

In the following, the coefficients $a_{1,0}$ and c_1 are set to 1. The experimental most important cases are the resonance cases, where the radius of the eigenmotion of the ion increases linearly with the
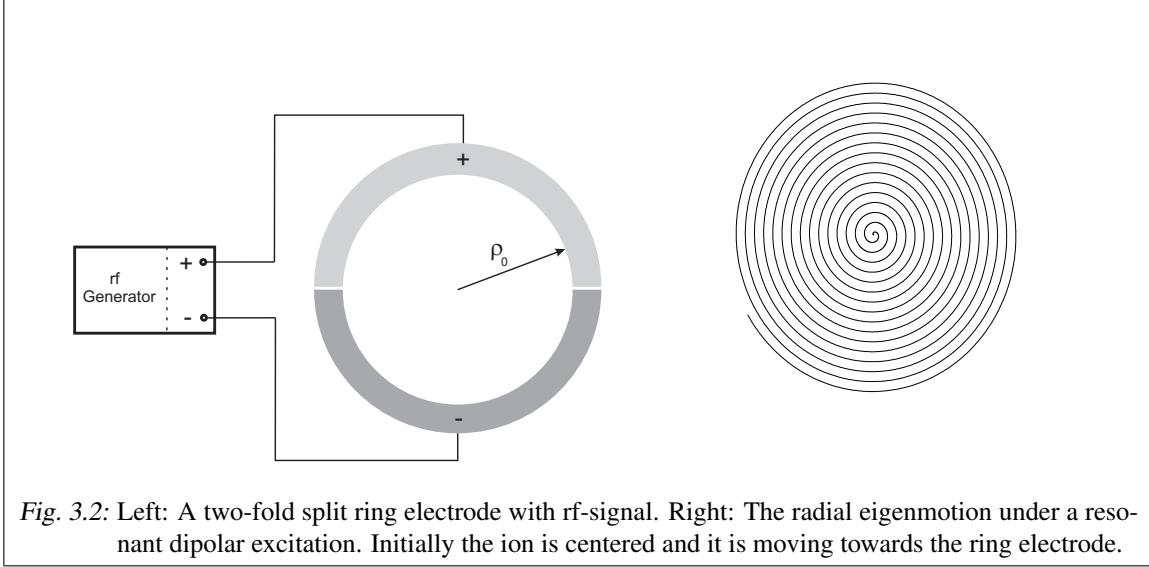
Fig. 3.2: Left: A two-fold split ring electrode with rf-signal. Right: The radial eigenmotion under a resonant dipolar excitation. Initially the ion is centered and it is moving towards the ring electrode.

excitation time. In general the energy of a particle with the mass m as a function of the excitation frequency and time is given by [LL79]:

$$E = \frac{1}{2m} \left| \int_{-\infty}^{+\infty} F(t)e^{-i\omega_R t}dt \right|^2 ,$$

$$= \frac{1}{2m} \left| \int_0^{T_d} qE_{hyp_d} \cos(\omega_d t)e^{-i\omega_R t}dt \right|^2 , \qquad (3.15)$$

where T_d is the excitation duration, ω_d is the excitation frequency and $\omega_R = \omega_\pm$ is the resonance frequency, the magnetron or reduced cyclotron frequency, respectively. The initial energy is assumed to be E_0. For excitation times larger than the excitation period ($T_d \gg \frac{1}{\nu_R}$) the energy is:

$$E = \frac{q^3}{2m} \frac{V_d^2}{4\rho_0^2} \cdot \frac{\sin^2\left((\omega_d - \omega_R)\frac{T_d}{2}\right)}{(\omega_d - \omega_R)^2}. \qquad (3.16)$$

This leads to a cyclotron radius of [Sch89].

$$\rho_+ \omega_d = \frac{V_d T_d}{4B\rho_0} \left| \frac{\sin\left((\omega_d - \omega_+)\frac{T_d}{2}\right)}{(\omega_d - \omega_+)\frac{T_d}{2}} \right| \qquad (3.17)$$

The result can be compared to a "sinc"-function $A = A_0 \left| \frac{\sin(x-x_0)}{x-x_0} \right|$ with the properties:

- The primary maximum is at x_0 with a height of A_0.

- Further maxima are at $x - x_0 \simeq n \cdot \pi$ with $n = \pm\frac{3}{2}, \pm\frac{5}{2}, \pm\frac{7}{2} \ldots$

- The minima are at $x - x_0 = n \cdot \pi$ with $n = \pm 1, \pm 2, \pm 3 \ldots$

In the following the energy absorption in the resonance case is described. As initial conditions it is assumed that the ions are in the center of the trap ($\rho_+ = \rho_- = 0$). With

$$\frac{\mathrm{d}E}{\mathrm{d}t} = \vec{F} \cdot \vec{v} \tag{3.18}$$

and an excitation of

$$\vec{F} = qE_d \cos(\omega_d t)\vec{e}_x \tag{3.19}$$

it leads to

$$\frac{\mathrm{d}E}{\mathrm{d}t} = \vec{F} \cdot \vec{v}$$
$$= qE_d \cos(\omega_d t) \left[\rho_+(t)\omega_+ \cos(\omega_+ t + \varphi_+) + \rho_-(t)\omega_- \cos(\omega_- t + \varphi_-)\right]. \tag{3.20}$$

The kinetic energy in the eigenmotions of a charged particle of the mass m at time t is given by

$$E_\pm(t) = \frac{m}{2}(\omega_\pm^2 - \omega_+\omega_-)\rho_\pm^2(t), \tag{3.21}$$

the derivative with respect to time is

$$\frac{\mathrm{d}E_\pm}{\mathrm{d}t} = \frac{m}{2}(\omega_\pm^2 - \omega_+\omega_-)\frac{\mathrm{d}(\rho_\pm^2(t))}{\mathrm{d}t} = m(\omega_\pm^2 - \omega_+\omega_-)\rho_\pm(t)\frac{\mathrm{d}\rho_\pm(t)}{\mathrm{d}t} \tag{3.22}$$

and inserting Eq. 3.20 for the resonance conditions ($\omega_d = \omega_\pm$ and $\varphi_\pm = 0$) of a pure eigenmotion ($\rho_\mp = 0$) yields

$$m(\omega_\pm^2 - \omega_+\omega_-)\rho_\pm(t)\frac{\mathrm{d}\rho_\pm(t)}{\mathrm{d}t} = qE_d \cos(\omega_\pm t)\rho_\pm(t)\omega_\pm \cos(\omega_\pm t). \tag{3.23}$$

Thus,

$$\int_0^{\rho_{\pm,max}} \mathrm{d}\rho_\pm = \frac{qE_d}{m(\omega_\pm - \omega_\mp)} \int_0^{T_d} \cos^2(\omega_\pm t)\mathrm{d}t \tag{3.24}$$

and

$$\rho_\pm(T_d) \simeq \frac{qE_d}{m(\omega_\pm - \omega_\mp)} \cdot \frac{T_d}{2}, \tag{3.25}$$

because for $T_d \gg \nu_\pm$:

$$\int_0^{T_d} \cos^2(\omega_\pm t)\mathrm{d}t = \frac{T_d}{2}. \tag{3.26}$$

3.3   Quadrupolar Excitation

Applying an azimuthal quadrupolar rf potential of the form

$$\Phi_q = -V_q\frac{1}{\rho_0^2}\cos(\omega_q t + \varphi_q)\left(x^2 - y^2\right) \tag{3.27}$$

results in a coupling of the radial eigenmotions and an interconversion of those. Using the $\vec{E}$-field derived from the potential Φ_q

$$\vec{E}_q = \frac{V_q}{\rho_0^2}\cos(\omega_q t + \varphi_q)(2x\vec{e}_x - 2y\vec{e}_y),\tag{3.28}$$

leads to the equations of motion in the radial plane

$$\ddot{x} - \omega_c\dot{x} - \left(\frac{\omega_z^2}{2} + 2\frac{qV_q}{m\rho^2}\cos(\omega_q t + \varphi_q)\right)x = 0,$$

$$\ddot{y} - \omega_c\dot{y} - \left(\frac{\omega_z^2}{2} - 2\frac{qV_q}{m\rho^2}\cos(\omega_q t + \varphi_q)\right)y = 0.\tag{3.29}$$

Their analytical solution as described in König *et al.* [KBK$^+$95] leads to the time depend evolution of the radii ρ_+ and ρ_-:

$$\rho_+(t) = \left[\rho_+(0)\cos(\omega_B t) - \frac{1}{2}\frac{\rho_+(0)[(\mathrm{i}\omega_q - \omega_c)] + \rho_-(0)k_0\mathrm{e}^{\mathrm{i}\Delta\varphi}}{\omega_B}\sin(\omega_B t)\right]\mathrm{e}^{\mathrm{i}\frac{1}{2}(\omega_q-\omega_c)t},$$

$$\rho_-(t) = \left[\rho_-(0)\cos(\omega_B t) + \frac{1}{2}\frac{\rho_+(0)[(\mathrm{i}\omega_q - \omega_c)] + \rho_+(0)k_0\mathrm{e}^{\mathrm{i}\Delta\varphi}}{\omega_B}\sin(\omega_B t)\right]\mathrm{e}^{\mathrm{i}\frac{1}{2}(\omega_q-\omega_c)t}.\tag{3.30}$$

with

$$\omega_B = \frac{1}{2}\sqrt{(\omega_q - \omega_c)^2 + k_0},\tag{3.31}$$

$$k_0 = 2\frac{qV_q}{m\rho_0^2}\frac{1}{\omega_+ - \omega_-},\tag{3.32}$$

and

$$\Delta\varphi = \varphi_q - (\varphi_+ + \varphi_-).\tag{3.33}$$

Fig. 3.3: Left: A four-fold split ring electrode connected to an rf generator for quadrupolar excitation. Right: The radial eigenmotions under a resonant quadrupolar excitation. The initially pure magnetron motion as indicated with a dashed circle is converted into cyclotron motion.
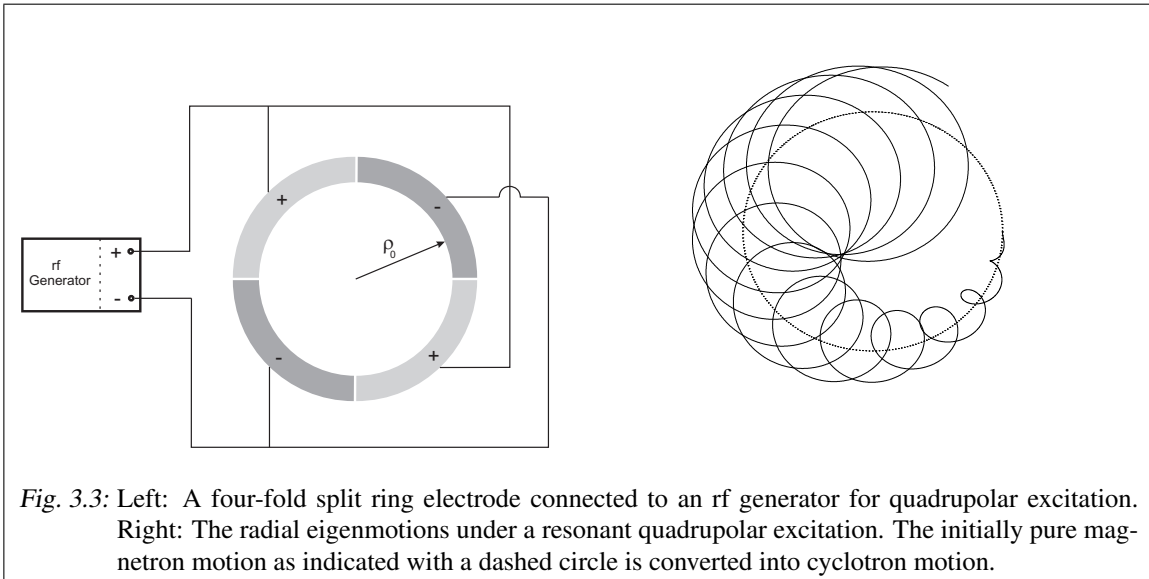
The Eq. 3.30 shows a coupling between the radial eigenmotions. For the resonance case with $\omega_q = \omega_c$ the radii evolve in the following way:

$$\rho_+(t) = \rho_+(0) \cos\left(\frac{k_0}{2}t\right) - \rho_-(0) e^{\imath \Delta \varphi} \sin\left(\frac{k_0}{2}t\right),$$

$$\rho_-(t) = \rho_-(0) \cos\left(\frac{k_0}{2}t\right) + \rho_+(0) e^{\imath \Delta \varphi} \sin\left(\frac{k_0}{2}t\right) \tag{3.34}$$

In a scenario with an initial magnetron radius $\rho_-(0) = \rho$ and an initial cyclotron radius $\rho_+(0) = 0$. According to Eq. 3.32 and 3.34 a full conversion from magnetron to cyclotron motion is occurring at excitation times of:

$$T_q = \frac{(2n+1)\pi}{V_q}(\omega_+ - \omega_-)\frac{m\rho_0^2}{2q}, \qquad (n = 0, 1, \dots). \tag{3.35}$$

If $\omega_q \neq \omega_c$ the eigenmotions are not completely converted.

Similarly as in the case of the dipolar excitation the influence of the trap geometry to the amplitude of quadrupolar excitation can be derived starting from an ideal azimuthal quadrupolar potential and introducing the correction coefficients for the cylindrical symmetry $c_2 = 4/\pi$ and the influence of the endcaps $a_{2,0} = 0.78$ [BBB+08]:

$$\vec{E}_q(x, y, t) = -2 \cdot \frac{4 \cdot 0.78}{\pi} \frac{V_q}{\rho_0} \cos(\omega_q t + \varphi_q) \cdot (x\vec{e}_x - y\vec{e}_y). \tag{3.36}$$

3.4 Time-of-Flight Ion Cyclotron Resonance method

In the following a method for the detection of the radial energy, and thus the cyclotron radius, will be described. This together with a quadrupolar excitation leads to the determination of the cyclotron frequency ω_c. A circulating particle has the radial energy E_r:

$$E_r = \frac{1}{2}m\omega^2\rho^2 \approx \frac{1}{2}m\omega_+^2 r_+^2, \tag{3.37}$$

which can be reduced to the component from the cyclotron motion in a Penning trap since the component of the magnetron motion is negligible $\omega_+ \gg \omega_-$ in the ISOLTRAP experiment (compare Tab. 3.1).

It is also possible to describe the energy as a function of the orbital magnetic moment $\vec{\mu}$. A circulating particle with a frequency ω creates a current of

$$I = \frac{qv}{2\pi\rho_c}\pi r^2, \tag{3.38}$$

where r is the radius of the circular area $F = \pi r^2$ with the normal vector $\vec{f}$. The magnetic moment μ is then defined as

$$|\vec{\mu}| = I \cdot F|\vec{f}| = q\frac{\omega}{2\pi} \cdot \pi r^2. \tag{3.39}$$

Then a charged particle in the magnetic field has the radial energy

$$
\begin{aligned}
E_r &= |\mu|B \\
&= I \cdot \pi\rho_+^2 B \\
&= \frac{q\omega_+}{2\pi}\pi\rho_+^2 B \\
&= \frac{1}{2}q\omega_+\rho_+^2 B.
\end{aligned} \tag{3.40}
$$

Also here only the cyclotron component is significant, and thus the radial energy is mainly carried in the cyclotron mode. Under the assumption $\omega_+ \approx \omega_c$ the Eq. 3.37 and 3.40 are identical.

A particle with a magnetic moment, which is ejected into a magnetic field gradient in axial direction, experiences an accelerating force in the same direction [Jac83]

$$\vec{F} = -\vec{\nabla}(\vec{\mu} \cdot \vec{B}) = -\frac{E_r}{B}\frac{\partial B}{\partial z}\vec{e_z}. \tag{3.41}$$

Thus the time of flight ToF(z) between the trap center at a location z_0 to a detector positioned at z_1 (compare Fig. 3.5) is a function of the initial axial energy E_0, the electrostatic potential $\Phi(z)$ along

Fig. 3.4: Magnetic moment of a moving charged particle in magnetic field.

Fig. 3.5: Principle of the ToF Ion Cyclotron method, a particle with a magnetic moment is ejected from a trap at the position z_0 into a magnetic field towards a detector at z_1. Particles with a higher magnetic moment will be faster at the detector than those with a lower one [GKT80].
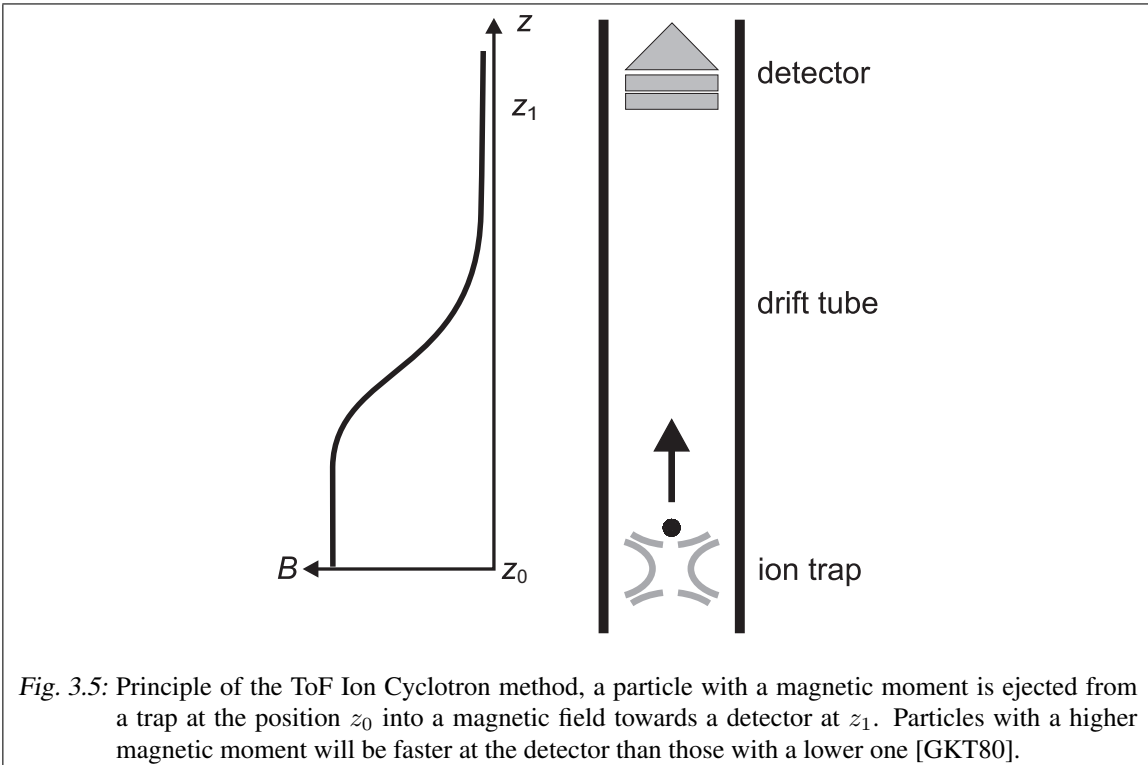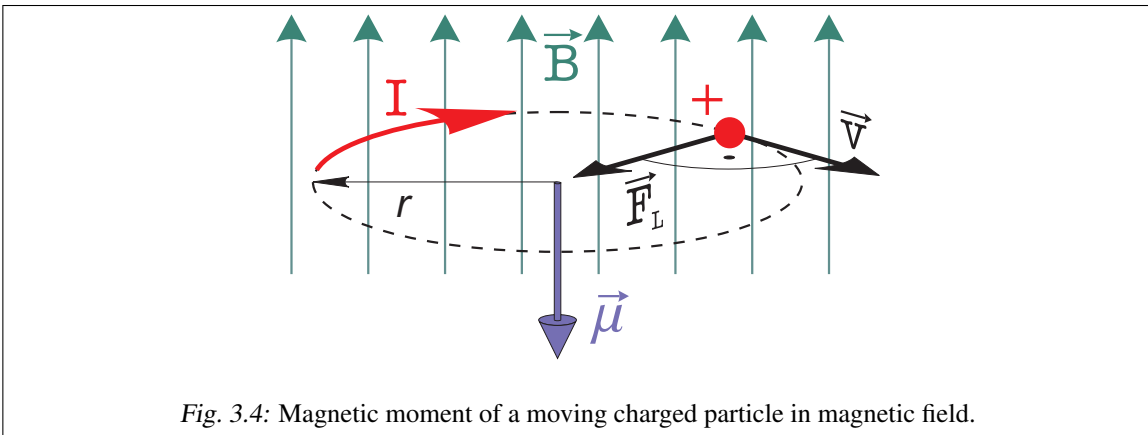
the way, and the changing magnetic field $B(z)$:

$$\text{ToF}(z) = \int_{z_0}^{z_1} \sqrt{\frac{m}{2\left(E_0 - q\Phi(z) - \mu B(z)\right)}} \mathrm{d}z. \tag{3.42}$$

The $\text{ToF}(z)$ is a measure for the orbital magnetic moments, and thus for the cyclotron radius. The excitation/detection combination is called Time-of-Flight Ion-Cyclotron-Resonance Method: The charged particles are brought on a magnetron radius $\rho_-(0)$ by use of a dipolar excitation on the magnetron frequency. Afterwards a quadrupolar excitation is applied such that in resonance a full conversion is performed according to Eq. 3.35 and the ToF is recorded as a function of the excitation frequency [GKT80].

3.5 Mass selective buffer gas cooling

In principle, a decrease of the ion-motion amplitudes could be achieved by exposing the ions to a buffer gas. In a Penning trap the interaction of the ions with buffer-gas atoms causes a centering of the axial and the cyclotron motion, while the radius of the magnetron motion is increased [SBB$^+$91, KBK$^+$95] as given on the left hand side of Fig. 3.6. Assuming that the kinetic energy of the ion is larger than the thermal energy of the gas $E_{kin} \geq k_B T_{gas}$ and the mass of the ions is larger than the mass of the buffer gas atoms $m_{ion} \gg m_{gas}$ the phases φ_+, φ_- are not important. The charged particles collide with neutrals, where the interaction can be described as a viscous-drag force

$$\vec{F}_{damp} = -\delta m \vec{v}, \tag{3.43}$$

with m the mass and $\vec{v}$ the velocity of the ion. The δ is described as

$$\delta = \frac{e}{mK}, \tag{3.44}$$

where K is the ion mobility

Fig. 3.6: Left: Ion trajectory in a Penning trap with a buffergas environment, the cyclotron radius is cooled, while the magnetron radius increases. Right: The same as left, but with an additional quadrupolar excitation with $\nu_q = \nu_c$ of the ion.
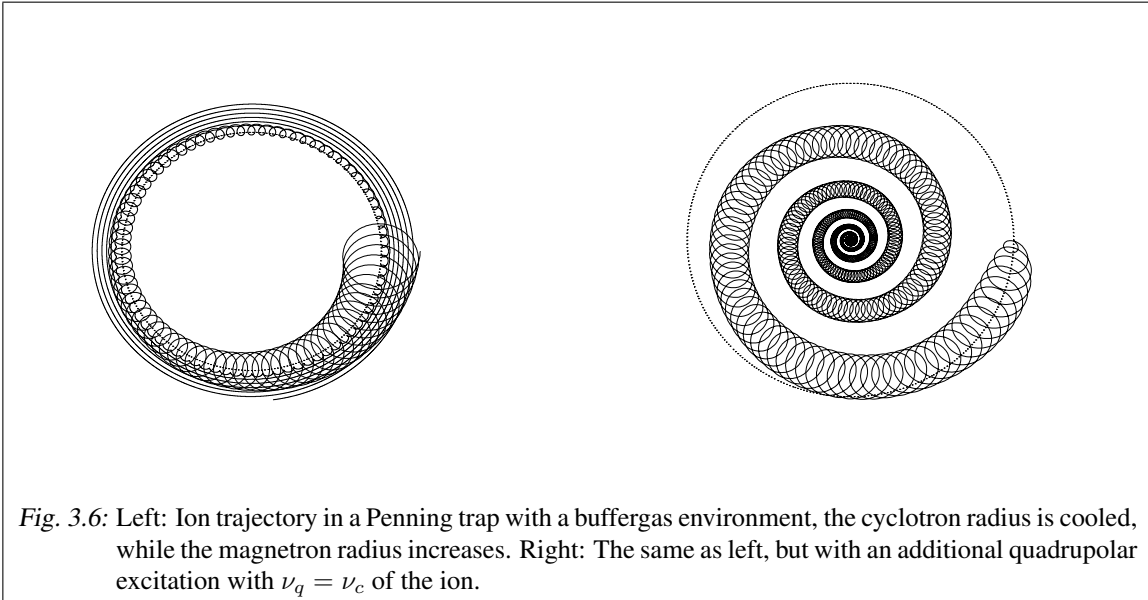
$$K = K_0 \frac{T/T_0}{p/p_0} \tag{3.45}$$

as a function of the temperature T and the pressure p normalized to $T_0 = 273\,\text{K}$ and $p_0 = 10^5\,\text{Pa}$. The mobility under normal conditions K_0 can be found for several kind of ions in several gases in [EMA$^+$78].

A loss of the ions by the increase of the magnetron radius and thus by collision with the ring electrode is prevented by coupling the magnetron and the cyclotron mode, which is displayed on the right hand side of Fig. 3.6. The velocity dependent interaction is stronger in the cyclotron mode than in the magnetron mode, and thus in the case of the coupling. This is realized by applying an azimuthal quadrupole excitation with a frequency of $\omega_c = (q/m)B$. Thus the cooling technique is mass selective, since the non-resonantly excited ions will be lost.

3.6   The real Penning trap

Everything described before is given for an ideal Penning trap where the ring and endcap electrodes are of infinite dimension. Due to finite electrode sizes and bores in the endcaps for the ion injection and ejection is the electrical field inside a Penning trap not ideally quadrupolar. Corrections of the potential are performed by implementing correction electrodes. Also the magnetic field as e.g. for ISOLTRAP is only homogeneous to $\Delta B/B < 10^{-7}$ in the vicinity of the trap center. The remaining imperfections result in a shift of the eigenfrequencies [BG86]. Thus the electrical potential in the vicinity of the trap center ($r/d \ll 1$) is given in cylindrical coordinates at the position [BG86] by

$$\Phi(\rho, z) = \frac{1}{2}\Phi_0 \left[\frac{C_2}{d^2}\left(z^2 + \frac{\rho^2}{2}\right) + \frac{C_4}{d^4}\left(z^4 - 3z^2\rho^2 + \frac{3}{8}\rho^4\right) \right.$$
$$\left. + \frac{C_6}{d^6}\left(z^6 - \frac{15}{2}z^4\rho^2 + \frac{45}{8}z^2\rho^4 - \frac{5}{16}\rho^6\right) + \dots \right]. \tag{3.46}$$

whereas the C_2 represents the term. For an ideal trap $C_2 = 1$ and $C_n = 0$ for all $n > 2$. The terms describing the octupol (C_4) and the dodecapol contributions (C_6) are highly undesired and result in a shift of the eigenfrequencies, and thus also on the sum of $\omega_+ + \omega_-$, where a resonant quadrupolar excitation results in a conversion between the two radial modes

$$\Delta(\omega_+ + \omega_-)^{elec} = \frac{V_0}{2d^2 B}\left[\frac{3}{2}\frac{C_4}{d^2}(\rho_-^2 - \rho_+^2)\right]$$
$$+ \left[\frac{15}{4}\frac{C_6}{d^4}(A_z^2(\rho_-^2 - \rho_+^2) - (\rho_-^4 - \rho_+^4))\right], \tag{3.47}$$

and thus their influence has to be minimized. Higher order terms are neglected for to vicinity of trap center.

Similarly the ideally homogeneous magnetic field has superimposed small components of higher order contributions, which can be described by

$$B_z = B_0\left[1 + \beta_2\left(z^2 - \frac{\rho^2}{2}\right)\right], \tag{3.48}$$

where β_2 denotes the relative strength of the lowest order perturbation of the magnetic field [BMSS90]. The frequency shift of the conversion frequency is given by

$$\Delta(\omega_+ + \omega_-)^{mag} = \beta_2\omega_c\left(A_z^2 - \frac{\rho_-^2}{2}\right). \tag{3.49}$$

By a systematic investigation of ω_+ and ω_c in the trap as described by Beck *et al.* [BBB$^+$09] the residual uncertainties can be minimized. Nevertheless a cross check of the setup performance is obligatory using well known references.

The described frequency shifts are induced by radial symmetric fields, an other shift of the eigenfrequencies arises for a misalignment of the symmetry axis of the trap electrodes to the axis of the magnetic field described by a finite tilting angle θ

$$B_x = B \sin \theta \cos \varphi, \tag{3.50}$$
$$B_y = B \sin \theta \sin \varphi, \tag{3.51}$$
$$B_z = B \cos \theta, \tag{3.52}$$

whereas φ denotes the angle between the abscissa and the plane containing the symmetry axis and the magnetic field axis. Furthermore a misplacement of ring segments of the split ring electrode may cause an additional component to the electrostatic potential. The lowest order of this pertubation can be described by an azimuthal elliptical term, and thus the electrical potential can be written cartesian coordinates as

$$\Phi = \frac{U_0}{2d^2} \left(z^2 - \frac{x^2 + y^2}{2} - \epsilon \frac{x^2 - y^2}{2} \right). \tag{3.53}$$

The strength of the distortion (ellipticity) is given by ϵ. The frequency shift for the sum of the two radial eigenfrequencies as a function of the of the ellipticity ϵ and the tilting angle θ is given to

$$\Delta(\omega_+ + \omega_-) \approx \omega_- \left(\frac{9}{4} \theta^2 - \frac{1}{2} \right), \tag{3.54}$$

which is to first order mass independent [Boe09].

4. EXPERIMENTAL SETUP

4.1 ISOLDE

Experiments with radioactive ions are a resource of information e.g. for nuclear physics, solid state physics and biophysics. For pushing frontiers of the current knowledge in these sciences technical development for high-efficiency and low-noise detectors is necessary. Furthermore a high intensity, highly pure, and very exotic Radioactive Ion Beam (RIB) is required.

ISOLDE is such a RIB facility [Kug00] at the European Particle Physics Laboratory CERN in Geneva, Switzerland. It is designed to produce exotic nuclei by nuclear reactions like fragmentation, spallation, and fission, triggered by a pulse of high-energy protons (1-1.4 GeV) with intensities of up to $3 \cdot 10^{13}$ particles impinging on a thick heated target. The resulting RIB intensity depends on several parameters as

$$I_{RIB} = (\sigma_{prod} \cdot N_{tar} \cdot I_{pb}) \cdot \epsilon_{rel}\epsilon_{ion}\epsilon_{p-acc}, \tag{4.1}$$

where σ_{prod} is the isotopic production cross section of the interaction of the primary proton beam of the intensity I_{pb} on a target of the thickness N_{tar}. Furthermore, the efficiencies for the release from the target and the ion source ϵ_{rel}, for the ionization ϵ_{ion}, and for the separator downstream ϵ_{p-acc} have to be considered for a realistic yield estimate [BCE$^+$08]. Note that, with this method not all elements can be delivered [LCD$^+$97], e.g., the refractory elements are not released from the target $\epsilon_{rel} \ll 1$ due to long time scales for the diffusion through a thick target, while in general the alkali elements have a high release and a very high ionization efficiency. In Fig. 4.1 the ionization methods that are available at ISOLDE for different elements are shown (left) as well as the Cd yields for two different target materials, plotted as a function of mass number (right).
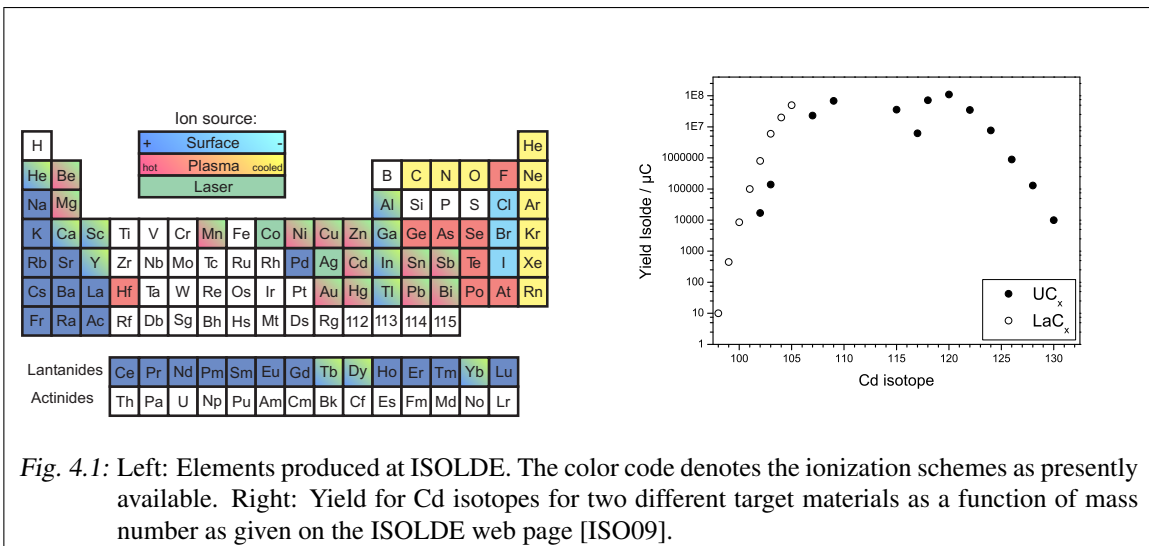
Fig. 4.1: Left: Elements produced at ISOLDE. The color code denotes the ionization schemes as presently available. Right: Yield for Cd isotopes for two different target materials as a function of mass number as given on the ISOLDE web page [ISO09].

Tab. 4.1: List of beamtimes that are discussed in this work showing the measured nuclides and the used targets and ion sources. The "n-conv" denotes the presence of a neutron converter.

Beamtime	Nuclides	Target	Ion source
05/2005	^{112,114,116,118,120,121}Ag	UC$_x$ & n-conv. [CLGK03]	RILIS [JCF$^+$97]
10/2005	^{114,120,122,123}Cd	UC$_x$ & n-conv. [CLGK03]	RILIS [KFA$^+$03]
07/2006	^{124,126}Cd	UC$_x$ & n-conv. [CLGK03]	RILIS [JCF$^+$97]
05/2007	$^{115,117,119-121,123}$Cd	UC$_x$ & n-conv. [CLGK03]	RILIS [KFA$^+$03]
06/2007	$^{99-109}$Cd	Sn liquid metall	FEBIAD hot plasma [SR92]
05/2008	^{126,128}Cd	UC$_x$ & n-conv. [CLGK03]	RILIS [KFA$^+$03]

The later discussed nuclides have been measured during six different beam times as presented in Tab. 4.1, which were dedicated to the mass measurement of neutron-deficient Cd, neutron-rich Cd, or neutron-rich Ag, and thus different target-ion source combinations were chosen. The neutron-deficient Cd is not expected to be contaminated by long-lived alkalis, and thus a Forced Electron Beam Ion Arc Discharge (FEBIAD) plasma source [SR92] was selected for a high ionization efficiency, while for the neutron-rich nuclides a neutron converter [CLGK03] and the Resonance Ionization Laser Ion Source (RILIS) had to be used for the suppression of neutron deficient Cs contaminations. In addition, for the run in May 2008 a temperature regulated quartz transfer line was used to reduces the amount of
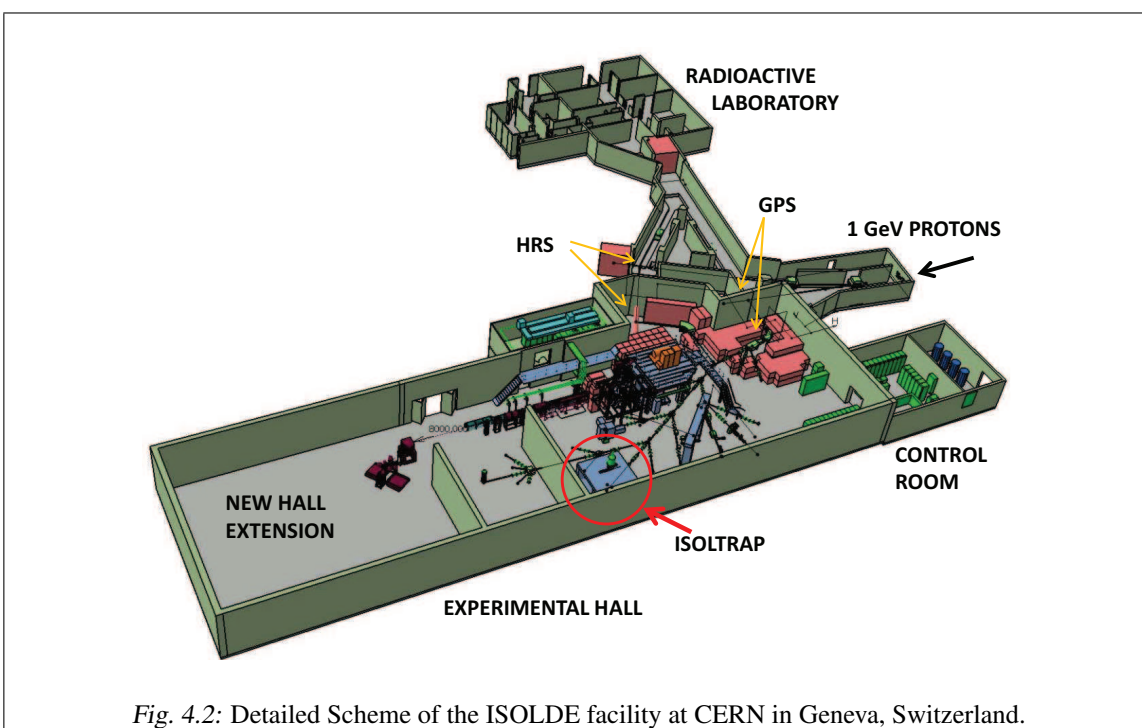
Fig. 4.2: Detailed Scheme of the ISOLDE facility at CERN in Geneva, Switzerland.

released Cs [BCE$^+$08]. Thus, it was even possible to approach the nuclide ^{128}Cd.

After the ion source, which is on a potential of 30 or 60 keV, the RIB is accelerated towards ground potential and transferred via the ISOLDE beam distribution system to either the magnet of the General Purpose Separator (GPS) or the two magnets of the High Resolution Separator (HRS) with a resolving power of $m/\Delta m = 1000$ and 5000, respectively. In the case of the HRS a movable pair of electrodes is available to select a more narrow part of the beam. Figure 4.2 gives an overview of the ISOLDE hall with beam lines from the target stations, via the magnets towards the experiments. The central beam line is divided into four sections, each equipped with wire-grid scanners and Faraday-cup detectors for determination of the beam position and intensity, respectively. At its end the ISOLTRAP experiment is placed.

4.2   ISOLTRAP

The ISOLTRAP setup consists of three main functional parts: a linear radio frequency (rf) Paul trap and two Penning traps. In the following, the experimental setup as shown in Fig. 4.3 is briefly described. More detailed information can be found in [MBB$^+$08b]. In the upper left part of Fig. 4.3 a typical sequence of an experiment is indicated in form of trigger pulses. Longer pulses represent longer times e.g. gates for rf excitation applied to the ring electrodes of the Penning traps.

The radio frequency quadrupole ion buncher and cooler (RFQ buncher) is a linear Paul trap consisting of four rods, each 26-fold axially segmented for superposing an axial DC potential to the radial AC potential of U_{rf}=80 V$_{pp}$, ν_{rf}=1 MHz. [HDK$^+$01, Her03]. The shape of the axial DC potential and a simplified scheme of the trap is shown in Fig. 4.4. The whole RFQ buncher including its electronics is placed in a high voltage cage, which provides the possibility of floating this part of the setup to up to 60 kV. This offset potential is adjusted to the ISOLDE target potential for decelerating the ions at the first three electrodes, guiding them to the potential minimum of about -17 V as compared to the cage potential at segments 24 and 25, and blocking them at the last segment. The ions are cooled in a buffer-gas environment with helium at a pressure of about 10^{-1} Pa to accumulate and cool the ion beam. The potential of the last segments can be switched between two sets of voltages, one set for trapping and one for ejecting the ions as a bunch.

In the following, the experimental steps as mentioned in Fig. 4.3 are denoted with boldface numbers in brackets. After the accumulation (**1**) and an additional cooling time the ions are ejected (**2**) pass a drift section including a deflector pair and an einzellens on the way to the first pulsed drift tube. When the ions are passing this drift tube, its potential is switched from about -2.5 keV compared to the buncher-cage potential to ground (**3**) [Her03]. Afterwards the ions are transferred by the help of electrostatic steerers and lenses from the horizontal to the vertical beam line. The ion transfer is monitored and optimized by measuring the number of ions with multichannel plate detectors at several positions in the ISOLTRAP beam line as marked with blue in Fig. 4.3.

In front of the preparation Penning trap the energy of the ions is reduced furthermore using a second pulsed drift tube (**4**) to allow trapping of the ions at about ground potential. These ions can be caught by switching the first of the 13 electrodes of the cylindrical preparation Penning trap [RHBB$^+$97] from 100 V to ground (**5**). This trap is filled with helium buffer gas of a pressure of $10^{-2} - 10^{-1}$ Pa. In the next 100 ms the ions are cooled especially in their axial and their cyclotron motion, while the blow up of the magnetron radius due to the interaction with the buffer gas is negligible for an injection close to the geometric axis. The following mass-selective buffer gas cooling [SBB$^+$91] is realized by a short resonant dipolar rf excitation of the magnetron motion (**6**), which leads to a magnetron radius larger than the radius $r_D = 1.5$ mm of the bore in the last trap elec-

Fig. 4.3: Detailed Scheme of the ISOLTRAP setup. The three main functional parts (RFQ buncher, prepa-
ration and precision Penning trap), the vacuum vessel and the magnets (black), the detectors
(blue), the pulsed drift tubes (green) and the other electrodes (red) are shown. In the upper left
part a scheme of the experimental sequence is given. The numbers relate the experimental step
to the part, where it is performed.

trode. Then an azimuthal rf excitation in quadrupolar geometry is applied (**7**). For the resonant case
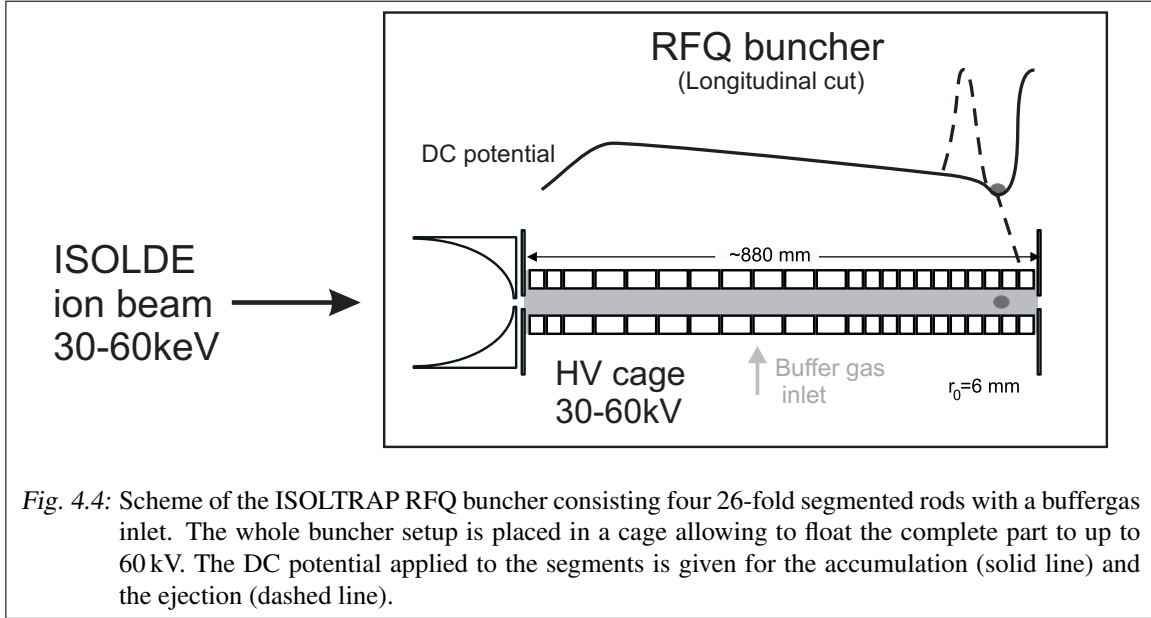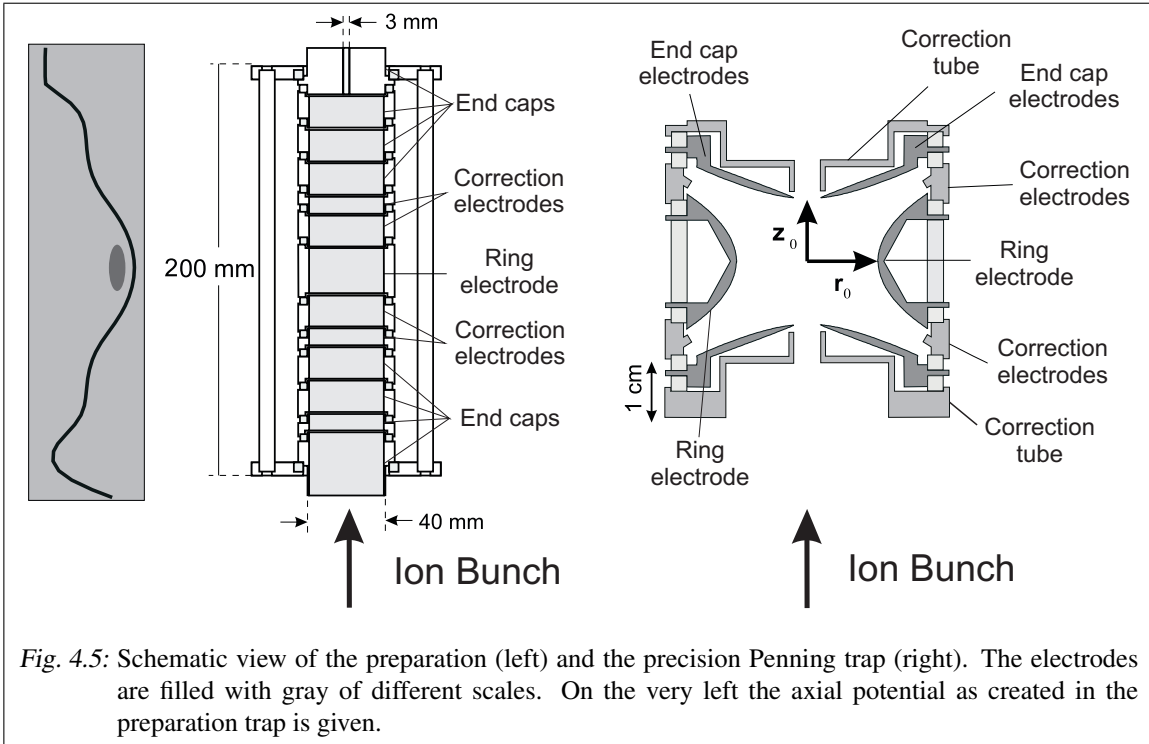($\nu_{rf} = \nu_c$, see Sec. 3) the magnetron motion is converted into cyclotron motion, which is cooled by

Fig. 4.4: Scheme of the ISOLTRAP RFQ buncher consisting four 26-fold segmented rods with a buffergas inlet. The whole buncher setup is placed in a cage allowing to float the complete part to up to 60 kV. The DC potential applied to the segments is given for the accumulation (solid line) and the ejection (dashed line).

collisions with the buffer gas. The resonance frequencies ν_c are in the range of a $0.5 - 1\,\mathrm{MHz}$ for the magnetic field of 4.7 T, thus the method can achieve a resolution $R = m/(\Delta m)$ of about $40\,000$, which is in general sufficient for a removal of isobaric contamination. The time between the excitation and the ejection is dedicated to the further cooling of the cyclotron motion, which is needed for centering the ions at the given buffer gas pressure. For the ejection (**8**) the electrodes of the trap are switched to form a potential ramp.

In Fig. 4.6 (left) a cooling resonance for the case of $^{99}\mathrm{Cd}^+$ is given, which shows the number of ions as a function of excitation amplitude for the quadrupolar excitation. For the resonance case $^{99}\mathrm{Cd}^+$ could be centered and transferred to the detector, whereas the few counts at the high-frequency side of the main peak are most-probably the isobaric contaminations $^{99}\mathrm{Ag}^+$ or $^{99}\mathrm{Zr}^+$. In this case a resolving power of $m/\Delta m \approx 20\,000$ is sufficient to separate the ion of interests from the contaminations.

The ejected ion cloud has a very low spatial and time distribution. Together with a well timed and well defined capture pulse at the entrance of the precision Penning trap this results in a low axial amplitude as compared to the trap dimensions (**9**). Low amplitudes are required to prevent the accumulation of effects on the ion trajectory due to field imperfections and inhomogeneities and thus the uncertainties stay low. Further reduction of these uncertainties is achieved by performing an electric and magnetic field optimization as described in [BBB$^+$09] and a stabilization of the magnetic field by decreasing temperature fluctuations in the warm bore of the super conducting magnet and the pressure fluctuations in the dewar of the magnet [MJAB$^+$08].

The preceding experiments are performed in a trap consisting of a magnetic field $B = 5.9\,\mathrm{T}$ and an electrostatic field created by applying a difference potential of $8.4\,\mathrm{V}$ between the ring electrode with $r_0 = 13\,\mathrm{mm}$ and the endcaps with $z_0 = 11.18\,\mathrm{mm}$. The next step is the phase-locked magnetron excitation (**10**), which is a dipolar rf excitation $\nu_{rf} \approx 1.1\,\mathrm{kHz}$ synchronized to the ejection of the ions from the preparation Penning trap. By use of this method the magnetron phase of the ions after non-central injection is not contributing to the uncertainty in magnetron radius. In the following a dipolar excitation of the cyclotron motion at ν_+ of a possible contamination (**11**) can be applied (marked with a dashed line in Fig. 4.3 (top)). A Gaussian envelope of this excitation is applied in order to keep the

Fig. 4.5: Schematic view of the preparation (left) and the precision Penning trap (right). The electrodes are filled with gray of different scales. On the very left the axial potential as created in the preparation trap is given.

perturbation of the ion of interest as low as possible [VRGA$^+$04].

Time steps (**1**) to (**11**) are performed to prepare a clean and cooled ion ensemble ideally consisting only of a few ions with a defined magnetron radius. The parameters of the following quadrupolar excitation (**12**) are chosen such, that in resonance a full conversion from magnetron to cyclotron motion is performed. By ejecting the ions afterwards from the trap and measuring their ToF (**13**) to the channeltron detector [YBF$^+$06] the cyclotron radius is determined and thus the the conversion is quantified.

The whole experimental cycle is controlled by CS (for "control system"), a LabVIEW based software package developed at GSI [BBB$^+$04, YBB$^+$05]. Its main part is a so called sequencer, which is sending the experimental values such as voltages, excitation frequencies, and length of time pulses to the devices at the initialization. At the beginning of a cycle the time pattern is generated by a 7811R, an FPGA card by National Instruments, as given schematically in Fig. 4.3 for triggering switches, excitations, and (together with the ejection of the precision Penning trap) the ToF-recording. After the cycle finishes, the recorded data are written to a file and the sequencer receives a "cycle-end". Afterwards the new value of the scan variable is sent to the corresponding device and a new cycle is started. This is repeated until a scan range is completed and a ToF-spectrum containing typically about 3000 ions is obtained as given in Fig. 4.6 (bottom). Measuring the ToF as a function of the quadrupolar excitation frequency the cyclotron frequency $\nu_c = q/mB$ can be determined up to a precision of $8 \cdot 10^{-9}$ by fitting the theoretical line shape to the data [KBK$^+$95, KBB$^+$03] as described in more detail in the next chapter.

Using this method to determine the mass of an ion with the same precision requires the calibration of the magnetic field a very well known mass. For this purpose a reference ion source is mounted perpendicular at the beginning to the ISOLTRAP beam for switching quickly between the radioactive ions and the reference ions. For the creation of the ions a commercial pellet [Hea09] containing a
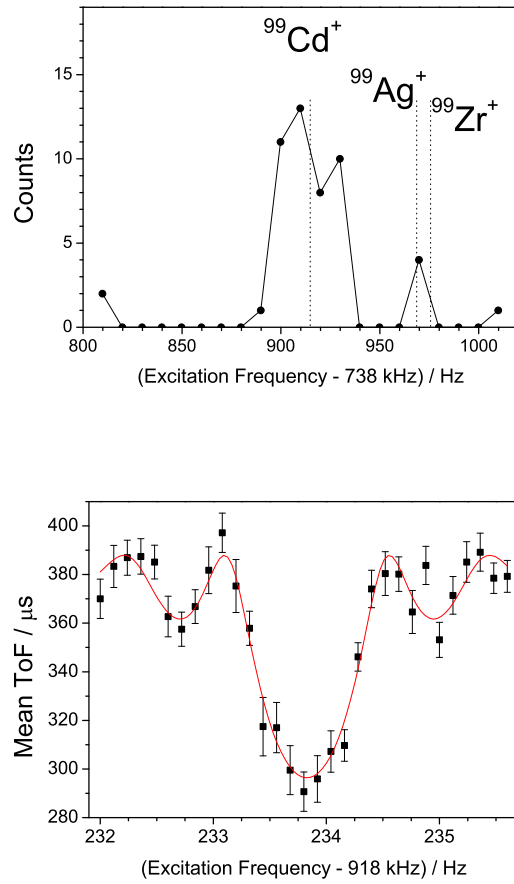
Fig. 4.6: Cooling resonance (top) for ^{99}Cd$^+$ with the expected resonance frequency ν_c as well as a ToF resonance for the same nuclide (bottom).

substrate of alkali elements is heated to surface ionize and evaporate the particles. The energy of the ions is adjusted for an optimal transition towards the and capture in the RFQ buncher.

5. ANALYSIS AND EVALUATION

From a ToF-resonance as shown in Fig. 4.6 to a mass value, as listed in the Atomic-Mass Evaluation (AME) (e.g. [AW95, AWT03]) many analysis and evaluation steps have to be performed. The resonance has to be analyzed and checked for potentially present contaminations. Furthermore, the magnetic field has to be calibrated i.e., the reference measurements have to be analyzed to extract a value for the cyclotron frequency of the reference ion at the time of measurement of the short-lived nuclide. In principle, the experimental results at ISOLTRAP are ratios

$$r = \frac{\nu_{c,ref}}{\nu_{c,int}} \tag{5.1}$$

between the cyclotron frequency of the reference ion and that of the ion of interest. Thus the result remains independent of the uncertainty and value of the reference mass m_{ref}. The atomic mass of the investigated radio nuclide m_{int} is determined to

$$m_{int} = \frac{\nu_{c,ref}}{\nu_{c,int}}(m_{ref} - m_e) + m_e, \tag{5.2}$$

where the mass of the ion is the atomic mass reduced by the mass of an electron m_e. The binding energy of the electron is typically in the range of a few eV and therefore it can be neglected in the discussion as the uncertainty of the final results are about two orders of magnitude larger. A more specific way to describe the mass is by use of the mass excess value ME

$$ME = m - A\mathrm{u}, \tag{5.3}$$

with m the mass of the nuclide, u the atomic mass unit and A being the "mass number" of a nuclide. In general the ME is given in keV by application of the conversion 1u= $931494.009(71)\,\mathrm{keV}/c^2$ [WAT03]. Note, typically c^2, the speed of light in vacuum, is not written ($c = 1$).

5.1 Analysis

For the final experimental values given at ISOLTRAP, the following uncertainties have to be considered:

- the uncertainty for the determination of the ToF,

- the uncertainty due to the magnetic field drift,

- the relative mass dependent uncertainty, and

- the residual systematic uncertainty of ISOLTRAP.

The analysis starts with the examination of the ToF-ICR curves. A typical measurement consists of 41 frequency points and about 20 repetitions. For each frequency step the single events are recorded and the mean ToF is calculated. Figure 5.1 shows on the top an example ToF spectra after different excitations for ^{133}Cs$^+$ and on the bottom the corresponding ToF-ICR curve. To underline the shift of the Mean ToF about 1000 ions per frequency step are recorded. For the case of an off-resonant excitation (1) a longer and more spread ToF distribution than for a resonant excitation (2) is obtained. For the fit of the expected line shape, as given in [KBK$^+$95], the uncertainty of the ToF distribution is adjusted for all frequency points such that a reduced $\chi^2 \approx 1$ is achieved, to which the uncertainty of the extracted center frequency is correlated to. In general, the statistical uncertainty of the ToF-ICR method is given with [Bol01, KBB$^+$03]

$$\left(\frac{\delta m}{m}\right)_{stat} \propto \frac{m}{T_{rf} q B \sqrt{N_{tot}}}, \tag{5.4}$$

where $1/T_{rf}$ describes the Fourier limit of the excitation as the inverse of the excitation time, B is the magnetic field strength, q the charge and m the mass of the ion in the trap. Furthermore the statistical uncertainty decreases with an increasing number of ions.
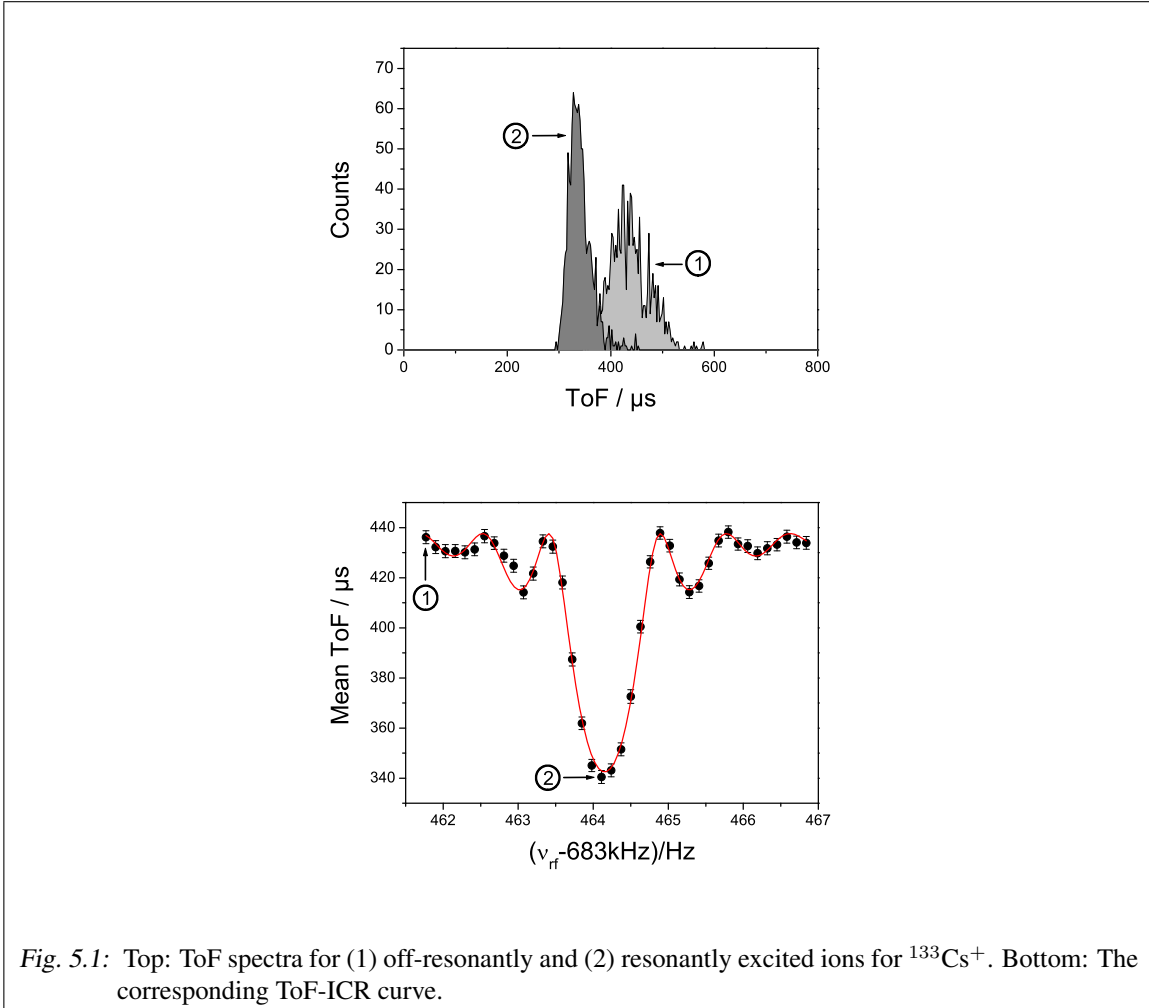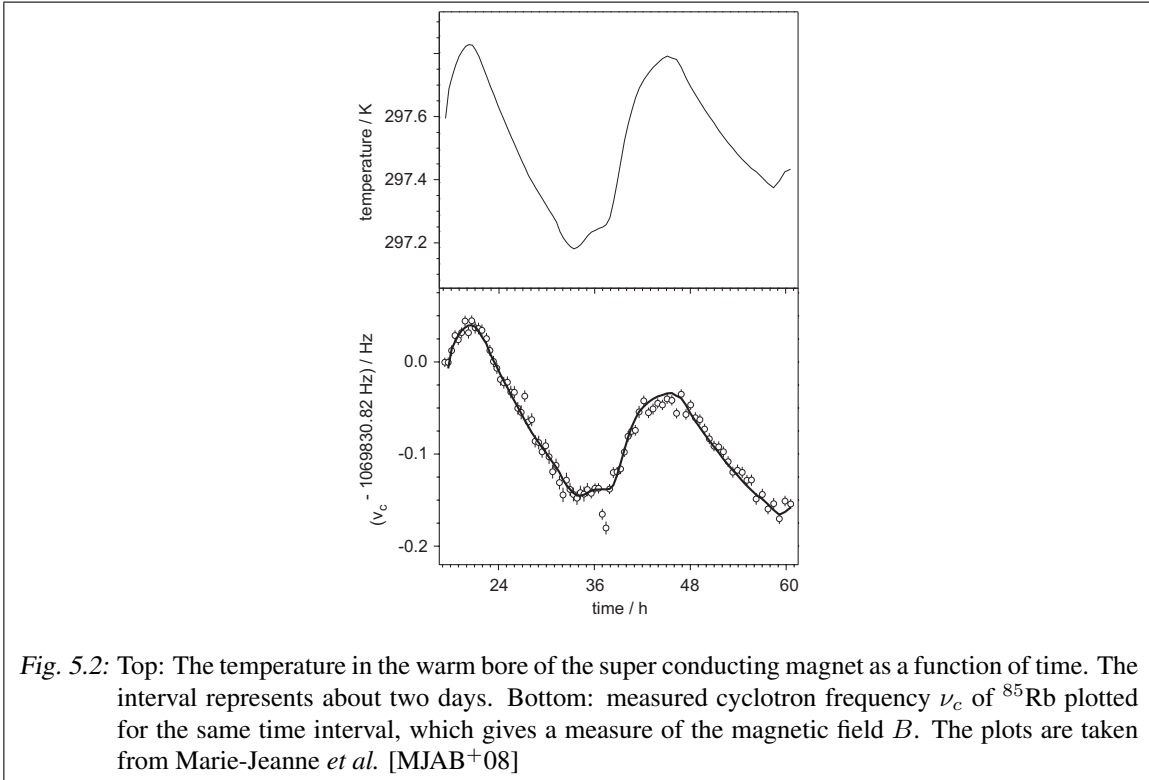

Fig. 5.1: Top: ToF spectra for (1) off-resonantly and (2) resonantly excited ions for ^{133}Cs$^+$. Bottom: The corresponding ToF-ICR curve.

On the other hand a present contamination is increasing the uncertainty of the measurement. A test tool for this is the so called count-rate class analysis. The centroid of the fit is investigated as a function of detected ions per measurement cycle. If another species in addition to the ion of interest is present in the trap, the centroid may shift as a function of ion number [BKK+92]. Thus all detected ions are divided into at least three count-rate classes with preferably the same statistics. For each class, the cyclotron frequency is determined separately. For a contamination present in the trap there is a systematic trend of the centroid towards lower frequencies for increasing ion number in the trap [KBB+03]. As a correction the cyclotron frequency as a function of count rate is extrapolated towards one ion only. In general, the use of this method results in a more conservative value for the uncertainty, which is preferred even if no contaminant is expected.

Another contribution to the uncertainty is the magnetic field drift, which is the only time dependent uncertainty. The magnetic field is calibrated before and after the actual cyclotron frequency measurement of the exotic ion. The magnetic field is "decaying" due to the flux-creep effect [AK64]. In addition, this trend is modulated with fluctuations of the magnetic field in the trap region caused by temperature variations and (at ISOLTRAP rather negligible) unstable pressure in the helium back line of the dewar for the cryogenic helium. On the timescales of the experiment the relative decay of the magnetic field can be approximated by a linear reduction with time:

$$\frac{\delta B}{\delta t} \frac{1}{B} = -2.30(3) \cdot 10^{-9}/\text{h}, \tag{5.5}$$

which has been extracted from a measurement for several days on the stable ^{85}Rb [KBB+03].

Fig. 5.2: Top: The temperature in the warm bore of the super conducting magnet as a function of time. The interval represents about two days. Bottom: measured cyclotron frequency ν_c of ^{85}Rb plotted for the same time interval, which gives a measure of the magnetic field B. The plots are taken from Marie-Jeanne *et al.* [MJAB+08]

Together with the temperature modulation the order of magnitude of these effects is given in Fig. 5.2. The plot on the top displays the measured temperature close to the vacuum vessel in the

warm bore of the super conducting magnet. The temperature dependent magnetic susceptibility of apparatus parts changes slightly the magnetic field and the cyclotron frequency ν_c is following the behavior as indicated in the lower plot of Fig. 5.2 by open circles. The line represents the scaled temperature evolution superposed by a linear decay (For more info see [MJAB$^+$08]). For this reason, the interpolation of the magnetic field has an uncertainty of [KBB$^+$03]

$$\frac{\sigma_B(\nu_{ref})}{\nu_{ref}} = 6.35(45) \cdot 10^{-11} \text{min}^{-1} \cdot \Delta t, \tag{5.6}$$

where Δt is the time interval between two reference measurements. To the uncertainty of the frequency ratio this quantity is added quadratically.

Another uncertainty arrives from imperfection of the quadrupolar electrostatic field and the misalignment of the magnetic field axis to the geometric axis of the trap electrodes [BBK$^+$96, BG86]. This results in a mass independent shift of $\nu_+ + \nu_-$ as given in Eq. (3.54). Thus a correction accounting for the mass difference between the ion of interest and the reference ion has to be performed for the frequency ratio r by systematic investigations using carbon clusters [KBB$^+$03]:

$$\frac{r - r_{th}}{r} = -1.6(4) \cdot 10^{-10} \text{u}^{-1} \cdot (m - m_{ref}), \tag{5.7}$$

where $r - r_{th}$ is the difference between the measured frequency ratio and the frequency ratio for an ideal Penning trap, i.e. the inverse of the mass ratio. After the correction the uncertainty of the measured frequency ratio has to be increased by the same quantity

$$\frac{\sigma_m(\nu_{ref})}{\nu_{ref}} = 1.6 \cdot 10^{-10} \text{u}^{-1} \cdot (m - m_{ref}) \tag{5.8}$$

quadratically.

Accounting for the ToF distribution, the magnetic field uncertainty, and the mass dependent shift of the frequency ratio a residual uncertainty was determined to

$$\left(\frac{\delta m}{m}\right)_{res} \leq 8 \cdot 10^{-9}, \tag{5.9}$$

which is considered to be the present systematic limit of the ISOLTRAP apparatus [KBB$^+$03].

5.2   Evaluation

In case the investigated nuclide has a long-lived exited isomeric state, it has to be decided whether the frequency ratio can be assigned to one of the states, or a correction for a mixture of both states has to be performed. An identification of the state is possible via the different half-lives as compared to the release time and in case of high excitation energies for the isomeric state via a comparison with the previous results. In addition, the state can be derived by looking at the total angular momentum J, if the production mechanism favors either high-J or low-J states. If no assignment is possible, the measured result has to be adjusted by half of the excitation energy and thus the uncertainty has to be increased by 0.29 times the excitation energy of the excited isomeric state [WAT03]. For this reason the experimental results can have different values and smaller uncertainties than the final mass value.

The mass doublets as obtained by e.g. Penning trap mass spectrometry are included in the atomic-mass evaluation (AME) [AWT03], which combines all different kinds of experimental nuclear physics

results connecting two or more masses, e.g. α and $\beta^{\pm}$ decays, neutron and proton transfer reactions, and exchange reactions.

The data obtained at ISOLTRAP are frequency ratios r (Eq. 5.1) and thus to be used as input data for the matrix calculation they have to be linearized as described in [BAA$^+$00]. The Eq. 5.2 can be rewritten using the mass excess values for the nuclide of interest and the reference nuclide, ME_{int} and ME_{ref}, respectively.

$$ME_{int} - r \cdot ME_{ref} = m_e(1-r) + A_{ref}\left(r - \frac{A_{int}}{A_{ref}}\right) \cdot \mathbf{u}. \tag{5.10}$$

Applying a three-digit truncated approximation

$$C = \left(\frac{A_{int}}{A_{ref}}\right)_{trunc} \tag{5.11}$$

as used in the AME for convenient plotting format, results in a relation of the form of a linear equation

$$ME_{int} - C \cdot ME_{ref} = \Delta \tag{5.12}$$

with

$$\Delta = ME_{ref}(r - C) + m_e(1-r) + A_{ref}\left(r - \frac{A_{int}}{A_{ref}}\right) \cdot \mathbf{u}. \tag{5.13}$$

The technical realization of the evaluation is described in [WAT03]. Here, a brief scheme of the calculation is given: A matrix of the over-determined system of Q data and M masses, with $(Q > M)$, is represented by the links between two to four masses m_μ have the value $q_i \pm dq_i$ where dq_i is the accuracy (1σ)

$$\sum_{\mu=1}^{M} k_i^\mu m_\mu = q_i \pm dq_i. \tag{5.14}$$

Using the example of the linearized frequency ratio the matrix elements correspond to $m_a = ME_a + A \cdot \mathbf{u}$, $m_b = C \cdot ME_b + A \cdot \mathbf{u}$, $k_i^a = +1$, $k_i^b = -1$ and $dq_i = \Delta$.

Writing (M, Q) in matrix notation gives $\mathbf{K}$ as the matrix of coefficients with $\mathbf{K}|m\rangle = |q\rangle$. Note, that almost all coefficients $\mathbf{K}$ are zero. For a linearized frequency ratio, as in case of Penning trap mass spectrometry, results in a line of $\mathbf{K}$ with only two non-zero elements. Furthermore, the diagonal weight matrix $\mathbf{W}$ is defined by the elements $w_i^i = 1/(dq_i dq_i)$. The solution using the least-square method leads to the construction

$$^{\mathbf{t}}\mathbf{KWK}|m\rangle = {}^{\mathbf{t}}\mathbf{KW}|q\rangle, \tag{5.15}$$

where $\mathbf{A}={}^t\mathbf{KWK}$ is the normal matrix, a square matrix of the order M, positive-definite, symmetric, and regular and hence invertible [ADLW86]. Thus the vector of adjusted masses $|\overline{m}\rangle$ is determined by

$$|\overline{m}\rangle = \mathbf{A}^{-1}\,{}^{\mathbf{t}}\mathbf{KW}|q\rangle \tag{5.16}$$

where the diagonal elements of $\mathbf{A}^{-1}$ are the squared uncertainties on the adjusted masses and the non-diagonal ones $(a^{-1})_\mu^\nu$ are the coefficients for the correlation between the masses m_ν and m_μ.

Furthermore, two important terms have to be introduced for the discussion of data, namely the "influence" (how much a datum affects a particular mass) and the "significance" (how much a datum affects the rest of the table) of a datum. The influence of a datum q_i on a mass m_μ is a measure to which part this experiment is determining that mass via the given link. The sum of all influences on each mass

is exactly 1 and the significance of a datum q_i is the sum of the influences to all connected masses, which cannot be bigger than 1. It is the policy of the AME that only data having a "significance" of more than one ninth are used in the matrix calculations [WAT03]. This minimizes the propagation of inaccurate data with no sacrifice in overall precision.

6. RESULTS OF MASS MEASUREMENTS AND ATOMIC MASS EVALUATION

The frequency ratios between reference ions and the ions of interest, as obtained from the experiments, are given in Tab. 6.1. For the neutron deficient Cd isotopes the reference was ^{85}Rb$^+$, while the neutron-rich Ag and Cd isotopes were measured with ^{133}Cs$^+$ as a reference in order to have a minimal mass-difference dependent uncertainty.

6.1 Results on Neutron-Deficient Cd Nuclides

In the following the data on neutron-deficient Cd isotopes are discussed first, as their discussion is slightly different than the one for the neutron-rich nuclides. For the neutron-deficient nuclides a comparison with recent results from two other Penning trap experiments is possible. Campaigns dedicated to neutron deficient nuclides around ^{100}Sn where performed by SHIPTRAP at GSI [BAB$^+$05] and by JYFLTRAP at IGISOL [JEH$^+$06]. Both measurements deviate slightly from each other, and thus a third measurement at a different place could bring clarification.
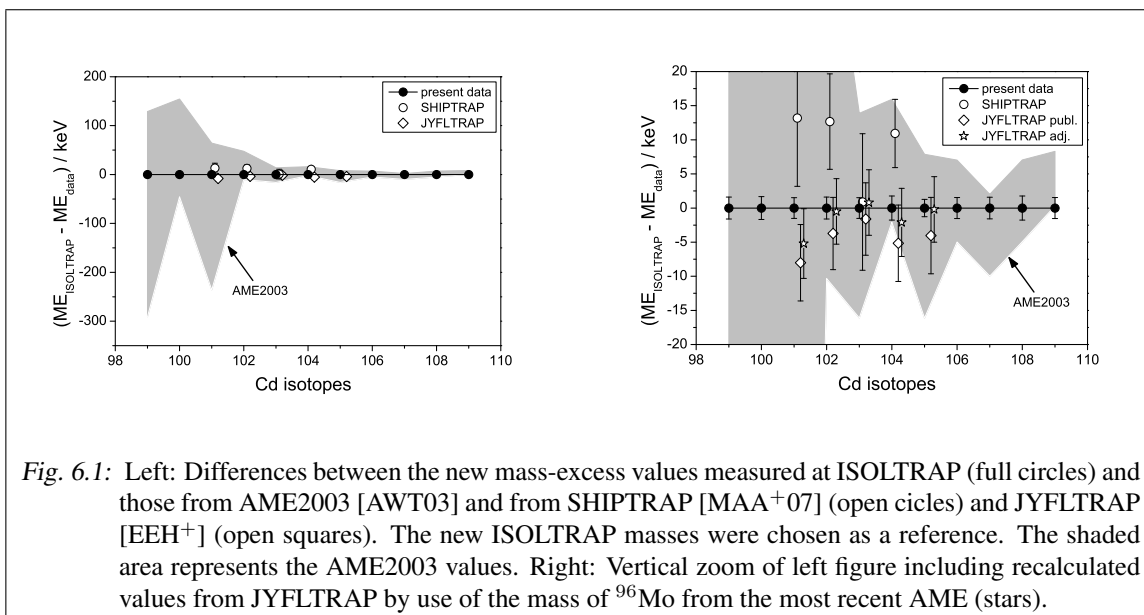
Fig. 6.1: Left: Differences between the new mass-excess values measured at ISOLTRAP (full circles) and those from AME2003 [AWT03] and from SHIPTRAP [MAA$^+$07] (open cicles) and JYFLTRAP [EEH$^+$] (open squares). The new ISOLTRAP masses were chosen as a reference. The shaded area represents the AME2003 values. Right: Vertical zoom of left figure including recalculated values from JYFLTRAP by use of the mass of ^{96}Mo from the most recent AME (stars).

As shown in Fig. 6.1, the measurements performed on the neutron-deficient Cd at ISOLTRAP (full symbols) agree with the literature values of the latest Atomic-Mass Evaluation (AME2003) [AWT03] within the uncertainties. Note that the mass of ^{99}Cd was determined experimentally for the first time. This plot also contains the recent mass excess values obtained by SHIPTRAP ($^{101-104}$Cd [MAA$^+$07]) and by JYFLTRAP ($^{101-105}$Cd [EEH$^+$]), as published and as adjusted (Table 6.2). In the case of the SHIPTRAP measurements a tendency to higher mass excess values is observed.

Tab. 6.1: The half-lives [AWT03] and ratios $r = \nu_c(\{\text{Rb,Cs}\}^+)/\nu_c(^A\{\text{Ag,Cd}\}^+)$ between the cyclotron frequencies of the reference nuclides ^{85}Rb and ^{133}Cs and the silver and cadmium nuclides.

Nuclide	Half life	$r = \nu_c(^{85}\text{Rb}^+)/\nu_c(^A\{\text{Cd}\}^+)$
^{99}Cd	16(3) s	1.165 032 756 0(202)
^{100}Cd	49.1(0.5) s	1.176 755 855 2(208)
^{101}Cd	1.36(5) min	1.188 512 101 2(189)
^{102}Cd	5.5(0.5) min	1.200 240 767 7(218)
^{103}Cd	7.3(0.1) min	1.212 005 235 3(250)
^{104}Cd	57.7(1.0) min	1.223 740 297 6(228)
^{105}Cd	55.5(0.4) min	1.235 512 679 7(182)
^{106}Cd	stable	1.247 254 328 2(215)
^{107}Cd	6.50(2) h	1.259 033 102 3(225)
^{108}Cd	stable	1.270 781 503 2(270)
^{109}Cd	461.4(1.2) d	1.282 567 977 2(219)

Nuclide	Half life	$r = \nu_c(^{133}\text{Cs}^+)/\nu_c(^A\{\text{Ag,Cd}\}^+)$
^{114}Cd	stable	0.857 024 906 4(316)
^{120}Cd	50.80(21) s	0.902 218 928 1(304)
^{122}Cd	5.24(3) s	0.917 294 267 6(351)
^{123}Cd	2.10(2) s	0.924 845 957 9(1984)
^{124}Cd	1.25(2) s	0.932 374 283 5(766)
^{126}Cd	517(17) ms	0.947 458 503 6(340)
^{126}Cd	517(17) ms	0.947 458 423 6(1162)
^{128}Cd	280(40) ms	0.962 547 294 8(818)
^{112}Ag	3.130(9) h	0.842 004 298 4(193)
^{114}Ag	4.6(1) s	0.857 066 003 9(369)
^{115}Ag	53.46(10) h	0.864 590 002 2(692)
^{116}Ag	2.68(19) min	0.872 133 648 1(261)
^{117}Ag	73.6(1.4) s	0.879 660 816 4(298)
^{118}Ag	3.76(15) s	0.887 207 174 8(200)
^{119}Ag	6.0(5) s	0.894 737 713 2(430)
^{120}Ag	1.23(4) s	0.902 286 018 9(363)
^{120}Ag	1.23(4) s	0.902 286 164 4(922)
^{121}Ag	790(20) ms	0.909 820 365 4(378)
^{121}Ag	790(20) ms	0.909 820 403 5(896)
^{123}Ag	296(6) ms	0.924 907 151 8(8668)

Tab. 6.2: The mass excess (ME) of the neutron deficient Cd isotopes with $A = 99 - 109$ for the measurements performed at ISOLTRAP (this work), SHIPTRAP [MAA$^+$07], and JYFLTRAP [EEH$^+$]. The adjusted JYFLTRAP ME values calculated from the frequency ratios published in [EEH$^+$] using a reference from the current AME are given in the last column.

Nuclide	ME(ISOLTRAP) / keV	ME(SHIPTRAP) /keV	ME(JYFLTRAP) / keV published [EEH$^+$]	ME(JYFLTRAP) / keV adjusted
^{99}Cd	-69931.1(1.6)			
^{100}Cd	-74194.6(1.6)			
^{101}Cd	-75836.4(1.5)	-75849(10)	-75827.8(5.6)	-75831.2(5.1)
^{102}Cd	-79659.6(1.7)	-79672(7)	-79655.6(5.3)	-79659.1(4.8)
^{103}Cd	-80651.2(2.0)	-80651(10)	-80648.5(5.3)	-80652.0(4.8)
^{104}Cd	-83968.5(1.8)	-83979(5)	-83962.9(5.6)	-83966.4(5.0)
^{105}Cd	-84334.0(1.4)		-84330.1(5.5)	-84333.8(4.8)
^{106}Cd	-87130.4(1.7)			
^{107}Cd	-86990.4(1.8)			
^{108}Cd	-89252.7(2.1)			
^{109}Cd	-88503.7(1.7)			

To discuss the influences and the consistency of all data available, two calculations of the AME were performed. A first evaluation included the values of SHIPTRAP and JYFLTRAP and a second one also values from ISOLTRAP. New averaged values are obtained, which are given in the last two columns of Table 6.3 and demonstrate the influence of the ISOLTRAP data.

In the following the results obtained in this work are compared to data which were available for the Atomic-Mass Evaluation in 2003 [AWT03]. In Fig. 6.2 differences between mass-excess values obtained from ISOLTRAP and from the other two Penning trap experiments and the AME2003 for the neuron-deficient Cd are plotted as well as from mass-excess values calculated from the input data of the AME2003.

The SHIPTRAP data by Martín *et al.* [MAA$^+$07] were already included in the mass evaluation. The JYFLTRAP frequency ratios from [EEH$^+$] were included in the present evaluations. Using the ISOLTRAP mass-excess values a new atomic-mass evaluation was performed to check the influence of the new data on the AME network. The individual cases are discussed in the following sections. Note, that there is an important general observation: Since the last published evaluation (in 2003 [AWT03]), the masses of many nuclides have changed. This includes ^{96}Mo, the reference mass used by JYFLTRAP to derive the masses in [EEH$^+$], which moved by 3.2 keV. Elomaa *et al.* [EEH$^+$] reported deviations of 1.8σ - 2.1σ from the SHIPTRAP mass values (^{101,102,104}Cd). When these masses are recalculated using the new ^{96}Mo mass value, the adjusted JYFLTRAP values are in perfect agreement with those of ISOLTRAP and the deviation from the SHIPTRAP values is reduced to slightly over 1σ (see Fig. 6.1(b) and Tab. 6.2).

The reasons for the ^{96}Mo mass change are multiple, mostly related to the removal or replacement of conflicting data that were linked to ^{96}Mo (causing a -3.3-keV shift). The question of links is a key point here. It is important to remember that it is not a mass that is measured in a trap, but a cyclotron frequency ratio i.e., a link between two nuclides. As the reference a nuclide is chosen that already
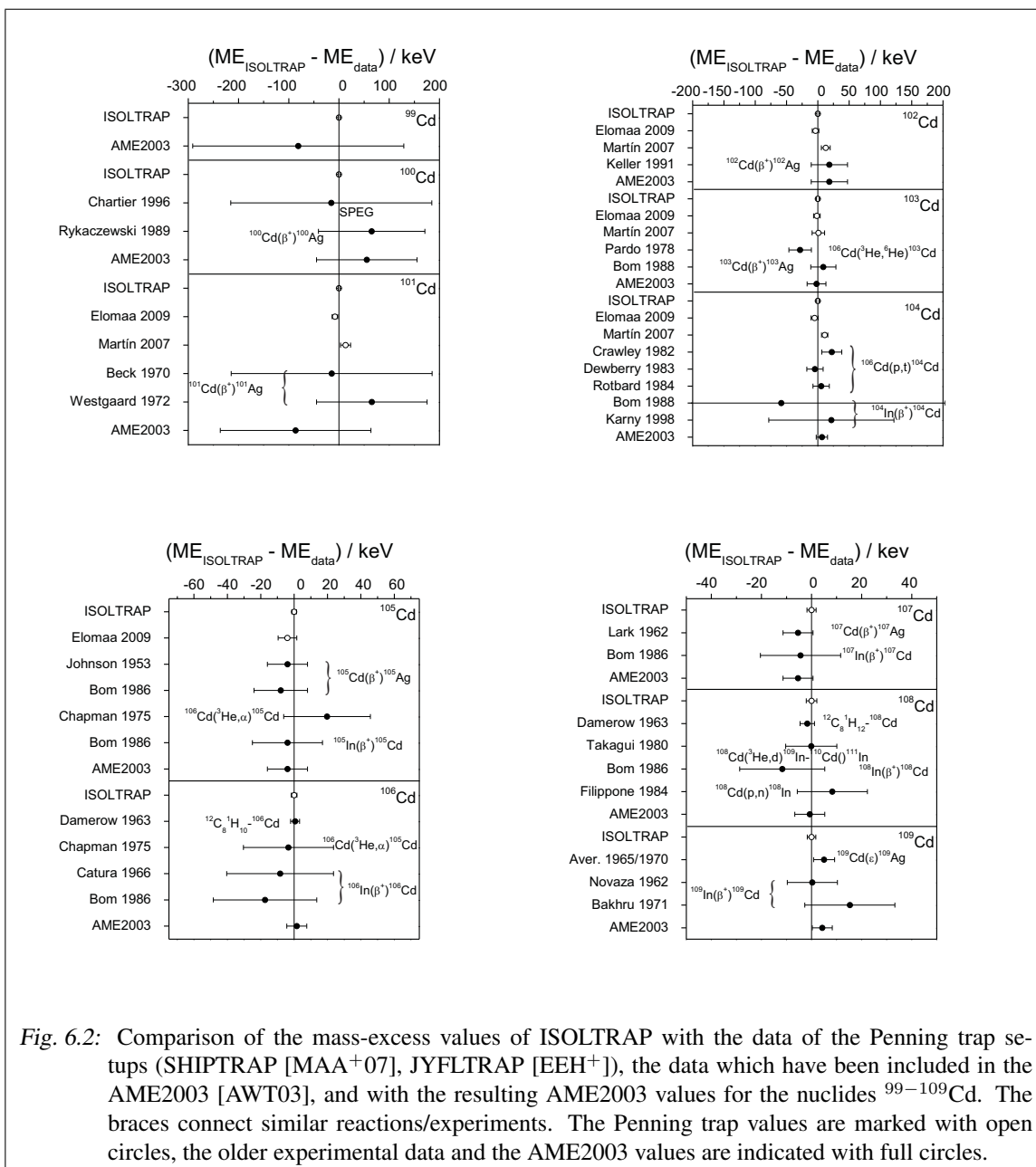
Fig. 6.2: Comparison of the mass-excess values of ISOLTRAP with the data of the Penning trap se-
tups (SHIPTRAP [MAA$^+$07], JYFLTRAP [EEH$^+$]), the data which have been included in the
AME2003 [AWT03], and with the resulting AME2003 values for the nuclides $^{99-109}$Cd. The
braces connect similar reactions/experiments. The Penning trap values are marked with open
circles, the older experimental data and the AME2003 values are indicated with full circles.

has a small uncertainty in its mass. In the case of ^{96}Mo, the uncertainty was 1.9 keV. As JYFLTRAP
reported several frequency ratios involving this nuclide, the ensemble of these links also contributed
to a reduction in the ^{96}Mo uncertainty (to 1.5 keV) as well as the remaining 0.1 keV shift. Hence
this is a case which illustrates the importance of the mass evaluation. For this reason the following
discussion refers to JYFLTRAP data recalculated with the new ^{96}Mo mass instead of the published
values [EEH$^+$]. This avoids conflicts, which are already solved in the present adjustment.

Like JYFLTRAP, the SHIPTRAP measurements contribute only slightly to the final mass results
as compared to ISOLTRAP. In the AME, there is a distinction between "influence" (how much a
datum affects a particular mass) and "significance" (how much a datum affects the rest of the table).

Tab. 6.3: The mass excess (ME) of the neutron deficient Cd isotopes with $A = 99 - 109$ for the measurements performed at ISOLTRAP (this work), those listed in the AME2003 [AWT03], those obtained in an atomic-mass evaluation before the ISOLTRAP data entered (including SHIP-TRAP [MAA$^+$07] and JYFLTRAP data [EEH$^+$]) and the newly adjusted values (last column). The symbol # marks the AME value of ^{99}Cd as extrapolated from systematics.

Nuclide	ME(ISOLTRAP) / keV	ME(AME2003) /keV	ME(AME before) /keV	ME(AME after) / keV
^{99}Cd	-69931.1(1.6)	-69850(210)#	-69850(210)#	-69931.1(1.6)
^{100}Cd	-74194.6(1.6)	-74250(100)	-74252(65)	-74194.6(1.7)
^{101}Cd	-75836.4(1.5)	-75750(150)	-75835.8(4.8)	-75836.0(1.4)
^{102}Cd	-79659.6(1.7)	-79678(29)	-79664.4(4.1)	-79659.5(1.7)
^{103}Cd	-80651.2(2.0)	-80649(15)	-80656.3(4.2)	-80652.0(1.8)
^{104}Cd	-83968.5(1.8)	-83975(9)	-83968.7(4.7)	-83968.3(1.6)
^{105}Cd	-84334.0(1.4)	-84330(12)	-84334.4(4.9)	-84333.8(1.3)
^{106}Cd	-87130.4(1.7)	-87132(6)	-87128.2(5.0)	-87130.4(1.7)
^{107}Cd	-86990.4(1.8)	-86985(6)	-86986.3(5.7)	-86990.1(1.7)
^{108}Cd	-89252.7(2.1)	-89252(6)	-89251.9(5.5)	-89252.6(2.1)
^{109}Cd	-88503.7(1.7)	-88508(4)	-88508.2(3.4)	-88504.7(1.6)

It is the policy of the AME that only data having a "significance" of more than one ninth are used in the flow-of-information matrix [WAT03]. This minimizes the propagation of inaccurate data with no sacrifice in overall precision.

The SHIPTRAP data [MAA$^+$07], obtained by measuring the link ^{85}Rb - ^{A}Cd, contribute less than the cut-off criterion for the case of the cadmium mass values as given in Tab. 6.4. Moreover, they have no influence on the value of ^{85}Rb as it was measured by [BPR$^+$99] to an accuracy of about 11 eV. Thus, the "significance" of the SHIPTRAP data is concentrated on the mass being investigated. As a consequence, the SHIPTRAP data shown in Tab. 6.2 are excluded from the evaluation.

This is different for the data from JYFLTRAP. As can be seen from Tab. 6.4, the JYFLTRAP data have low influence on the cadmium mass values. However, JYFLTRAP has investigated the link ^{96}Mo - ^{A}Cd. As the mass value of ^{96}Mo was previously only known to 1.9 keV, there is also a flow of information from the JYFLTRAP data towards ^{96}Mo. The "influence" of the JYFLTRAP data reduces the uncertainty of the ^{96}Mo mass value to 1.5 keV as shown in Fig. 6.3 and therefore the "significance" of the JYFLTRAP data is increased. Therefore these data are included in the evaluation.

Another example for insignificant data in the new AME is the ^{101}Cd(β^+)^{101}Ag-decay Q-value, which was determining the mass of ^{101}Cd entirely in the AME2003. At present both masses are determined by Penning trap mass spectrometry results (^{101}Ag is determined by ISOLTRAP [Her09]), which are at least 20-times more precise. Via the link of the β-decay is almost no flow of information and thus, it is taken out of the evaluation.

The comparison for the neutron-deficient cadmium nuclides of the input data to the new AME value is shown in Fig. 6.4. Note, that due to feedback from the new data the plotted mass-excess values can shift as compared to Fig. 6.2.
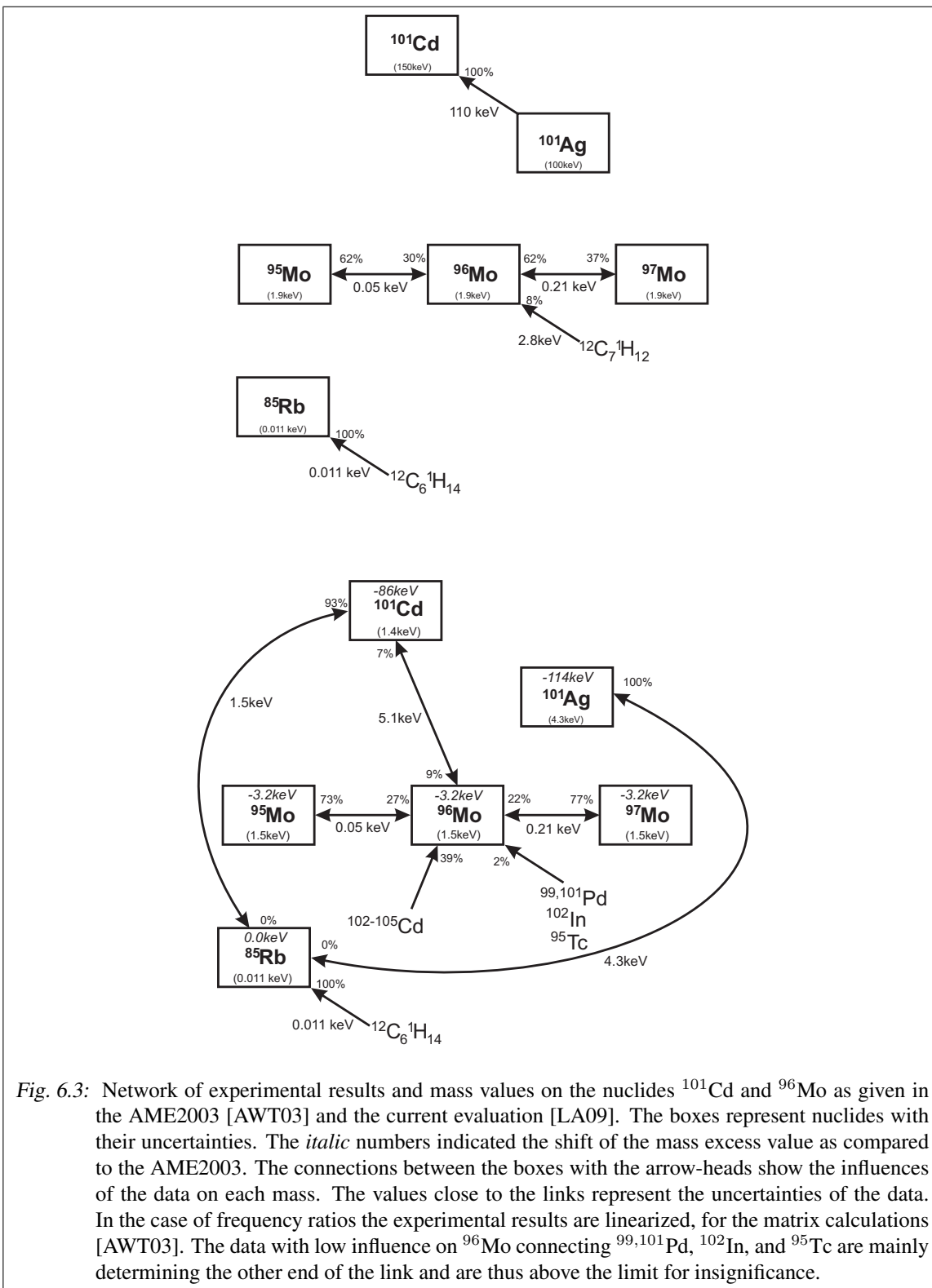
Fig. 6.3: Network of experimental results and mass values on the nuclides ^{101}Cd and ^{96}Mo as given in the AME2003 [AWT03] and the current evaluation [LA09]. The boxes represent nuclides with their uncertainties. The *italic* numbers indicated the shift of the mass excess value as compared to the AME2003. The connections between the boxes with the arrow-heads show the influences of the data on each mass. The values close to the links represent the uncertainties of the data. In the case of frequency ratios the experimental results are linearized, for the matrix calculations [AWT03]. The data with low influence on ^{96}Mo connecting ^{99,101}Pd, ^{102}In, and ^{95}Tc are mainly determining the other end of the link and are thus above the limit for insignificance.

Tab. 6.4: Influences of the experimental data from ISOLTRAP (this work) and from JYFLTRAP [EEH$^+$] on the current AME on the mass excess values of ^{A}Cd and ^{96}Mo. The given influences of the SHIPTRAP data [MAA$^+$07] are hypothetical, these data have not been included due to their low significance.

| Nuclide | Influences of experimental data | | | |
| | on the Cd nuclides | | | on ^{96}Mo |
	ISOLTRAP	SHIPTRAP^a	JYFLTRAP	JYFLTRAP
^{101}Cd	92.9%	2%	7.1%	9.0%
^{102}Cd	89.4%	6%	10.6%	9.9%
^{103}Cd	84.7%	3%	12.3%	9.9%
^{104}Cd	90.3%	10%	9.7%	9.3%
^{105}Cd	92.9%		6.4%	10.2%

^{a} hypothetically

^{99}Cd

The mass of ^{99}Cd was determined for the first time by ISOLTRAP. Before, only an AME2003 extrapolation of the mass excess was available which agrees with the new value determined with ISOLTRAP.

^{100}Cd

So far, the mass excess of ^{100}Cd was determined using the SPEG mass spectrometer value of -74180(200) keV [CAM$^+$96] and via the Q-value of the β^+-decay of ^{100}Cd to ^{100}Ag of 3890 keV [RPG$^+$89]. The experimental result obtained at ISOLTRAP agrees very nicely with the earlier experiments, but the uncertainty is by more than a factor of 50 smaller. The new compilation of the AME uses the ISOLTRAP data with 100% of influence for the determination of the ME of ^{100}Cd, and the connection by ^{100}Cd$(\beta^+)^{100}$In changes the mass excess of ^{100}In from a mass-excess value of -64170 keV to -64330(180) keV.

^{101}Cd

The mass excess of ^{101}Cd has been determined at SHIPTRAP and JYFLTRAP. Both values have a discrepancy of 1.5σ relative to each other. The mass excess determined at ISOLTRAP is between the two earlier results, and deviates by 14 keV (1.3σ) from the SHIPTRAP results and agrees within the uncertainty with the result from JYFLTRAP. All three values agree with the AME2003 mass-excess determined by [Bec70, WZN72]. The new AME value is influenced by 92.9% by the ISOLTRAP result and by 7.1% by the JYFLTRAP result.

^{102}Cd

For this nuclide the mass excess has been also determined at SHIPTRAP and at JYFLTRAP. The two values have a discrepancy of 12 keV corresponding to 1.4σ. The ISOLTRAP value agrees well with the measurements at JYFLTRAP but deviates by 1.3σ from the values determined with SHIPTRAP. Also in this case all three Penning trap measurements agree with the mass excess listed in the AME2003 which includes experimental data by [KBK$^+$91]. In the new compilation of the mass values for the AME, the ISOLTRAP result contributes with 89.2% and the JYFLTRAP value with
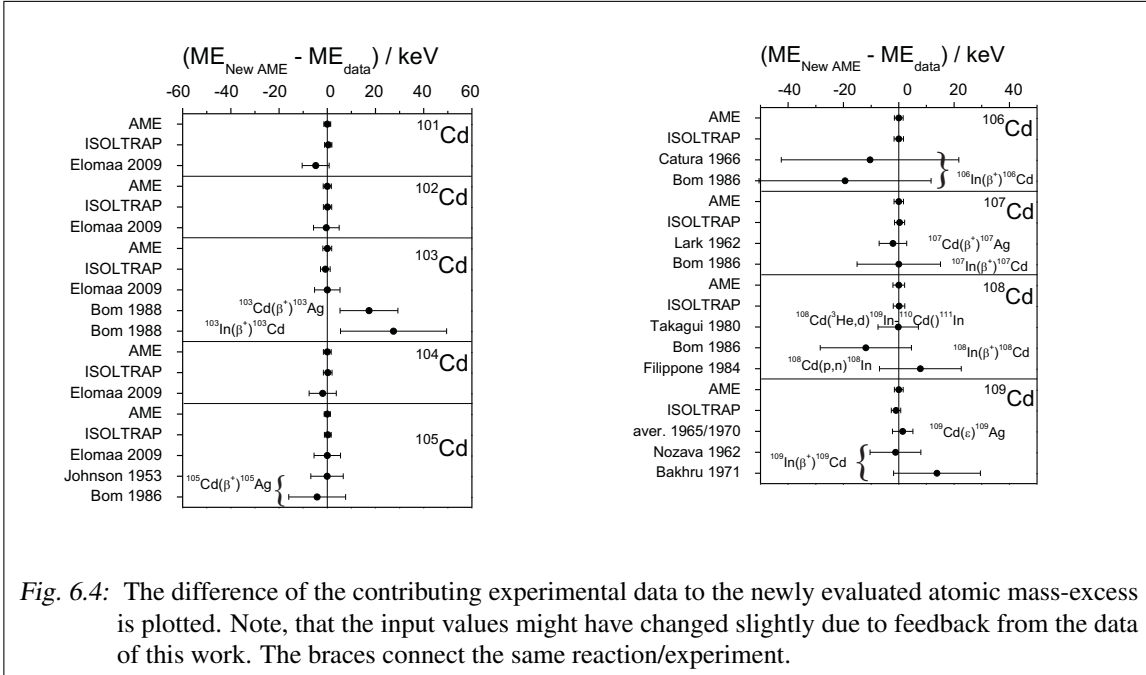
10.8%.

Fig. 6.4: The difference of the contributing experimental data to the newly evaluated atomic mass-excess is plotted. Note, that the input values might have changed slightly due to feedback from the data of this work. The braces connect the same reaction/experiment.

^{103}Cd

In this case all three Penning trap measurements agree nicely with each other. Furthermore the three measurements are within the uncertainty of the AME2003 value, which includes experimental data by [BHC$^+$88, PKBR78]. The newly determined AME value is influenced by 84.7% and 12.3% by the ISOLTRAP and the JYFLTRAP value, respectively. There are small contributions coming from the β-decays ^{103}Cd(β)^{103}Ag (2.4%) and ^{103}In(β)^{103}Cd (0.6%).

^{104}Cd

For $A = 104$ the results of ISOLTRAP and JYFLTRAP agree within the experimental uncertainties, while the SHIPTRAP result deviates from the ISOLTRAP and the JYFL-TRAP value by about 11 keV (2σ) and 12 keV (1.7σ), respectively. All values agree perfectly with the AME2003, which includes experimental data by [CBB$^+$82, DKN83, RVV$^+$84, BHC$^+$88, KBC$^+$98], mass excess while reducing the uncertainty. The newly-obtained AME value is to 90.3% determined by the ISOLTRAP value and by 9.7% by the JYFLTRAP result.

^{105}Cd

The two direct mass measurements with the mass excess values of JYFLTRAP and ISOLTRAP agree perfectly within their uncertainties. The previous mass excess value tabled in AME2003 (including experimental data by [BCH$^+$86, CD75, Joh53]) is also in agreement within the uncertainties. The new AME value is determined to 92.9% by ISOLTRAP and to 6.4% by JYFLTRAP. The β^+-decay of ^{105}Cd [BCH$^+$86, Joh53] contributes with 0.7% the mass excess of ^{105}Cd. In addition, the seven-fold reduction of the uncertainty of ^{105}Cd mass results also in an improvement of the ME of ^{105}Ag by a factor of more than two to -87070.8(4.5) keV.

^{106}Cd

The mass of ^{106}Cd was determined by the difference of C_8H_{10}-^{106}Cd and has been measured to 171789.3(2.7) keV [DRJ63] contributing to the average value in the AME2003 with 89.0%. Also the single-neutron pick-up reaction ^{106}Cd(^{3}He,α)^{105}Cd ($Q_0 = 9728(25)$ keV) [CD75] enters with 4.4% and the β^+-decay of ^{106}In with $Q = 6516(30)$ keV [CR66] and $Q = 6507(29)$ keV [BCH$^+$86] (3.5%) to the mass excess of the AME2003. The measurement at ISOLTRAP agrees with these previous results, but has a four times smaller uncertainty. The new AME result has a 99.7% influence from the ISOLTRAP data. The β^+-decay of ^{106}In [BCH$^+$86, CR66] contributes with only 0.3%. Those have been included due to their significance as links in the mass network.

^{107}Cd

The mass excess of ^{107}Cd was determined by the Q-value measurements of two β^+-decays: $Q(^{107}\text{Cd}(\beta^+)^{107}\text{Ag})$=1417(4) keV [LGJW62] and $Q(^{107}\text{In}(\beta^+)^{107}\text{Cd})$=3426(11) keV [BCH$^+$86], which entered with 96.3% and 3.7%, respectively, to calculate the AME2003 mass excess. This value agrees with the one from the present work. After reevaluating all data the new AME value is determined to 91.5% by the ISOLTRAP data. The rest is coming from the β^+-decay Q-values of ^{107}Cd(β^+)^{107}Ag [LGJW62] and ^{107}In(β^+)^{107}Cd [BCH$^+$86] with 8.2% and 0.3%, respectively.

^{108}Cd

The mass-excess value of ^{108}Cd in the AME2003 is calculated including an experimental value from the Minnesota, 16-inch, double-focussing mass spectrometer, namely the difference of $m(C_8H_{12}-^{108}\text{Cd}) = 189715.6(2.9)$ keV [DRJ63] with 67.9% influence and the Q-value of the differential reaction of ^{108}Cd(^{3}He,d)^{109}In-^{110}Cd()^{111}In, $Q_0 = -806.5(2.6)$ [TD80] (27.1%). A small contribution comes from the average of a β^+-decay Q-value of ^{108}In [BCH$^+$86] Q=5125(14) keV and the ^{108}Cd(p,t)^{108}In reaction [FDPA84] with a weight of 5.0%. The ISOLTRAP value compares to the AME2003 within the uncertainties. The result of a new calculation of the AME is determined to 94.0% by the ISOLTRAP value with a three times smaller uncertainty. The value of the differential reaction [TD80] contributes with 5.7% and the average of the β-decay and the (p,n) reaction with 0.3%.

^{109}Cd

The main contribution for the mass-excess value of the AME2003 came from an electron-capture measurement of ^{109}Cd to ^{109}Ag with a Q-value of 214(3) keV as an average of two experiments [LSW65, GGG$^+$70] (84.7%). The other 15.3% were given by two β^+-decay Q-value measurements Q=2015(8) keV and 2030(15) keV [Noz62, BLBR71]. The ISOLTRAP measurement agrees with the earlier values and decreases the experimental uncertainty. After a new evaluation the AME value is now influenced with 82.9% by the ISOLTRAP data, with 13.7% by the electron capture ^{109}Cd(e$^-$)^{109}Ag [LSW65, GGG$^+$70] and with 3.5% by β^+-decay of the ^{109}In [Noz62, BLBR71].

6.2 Results on Neutron-Rich Ag and Cd Nuclides

On the neutron-rich side the problem of isomerism is present. In Fig. 6.5(a) the results of the ISOL-TRAP campaigns for Ag nuclides are compared to the mass-excess values, as given in [AWT03] for the ground state and the excited isomeric state. The results for ^{114,116}Ag are assigned to the ground states, due to the longer half-lives as compared with the excited state. The value measured for ^{118}Ag is assigned to the exited isomeric state, due to the agreement with the mass excess value as given in

[AWT03]. In addition the value of the excitation energy of $\approx 128\,\text{keV}$ is about an order higher than the measured uncertainty. Furthermore with the count rate analysis procedure [KBB⁺03] no hint for a close by contamination was found. In the cases of ^{115,117,119}Ag the results needed to be adjusted, because it could not been distinguished between the isomeric and the ground state, nor could it be excluded that only one of the states is present.
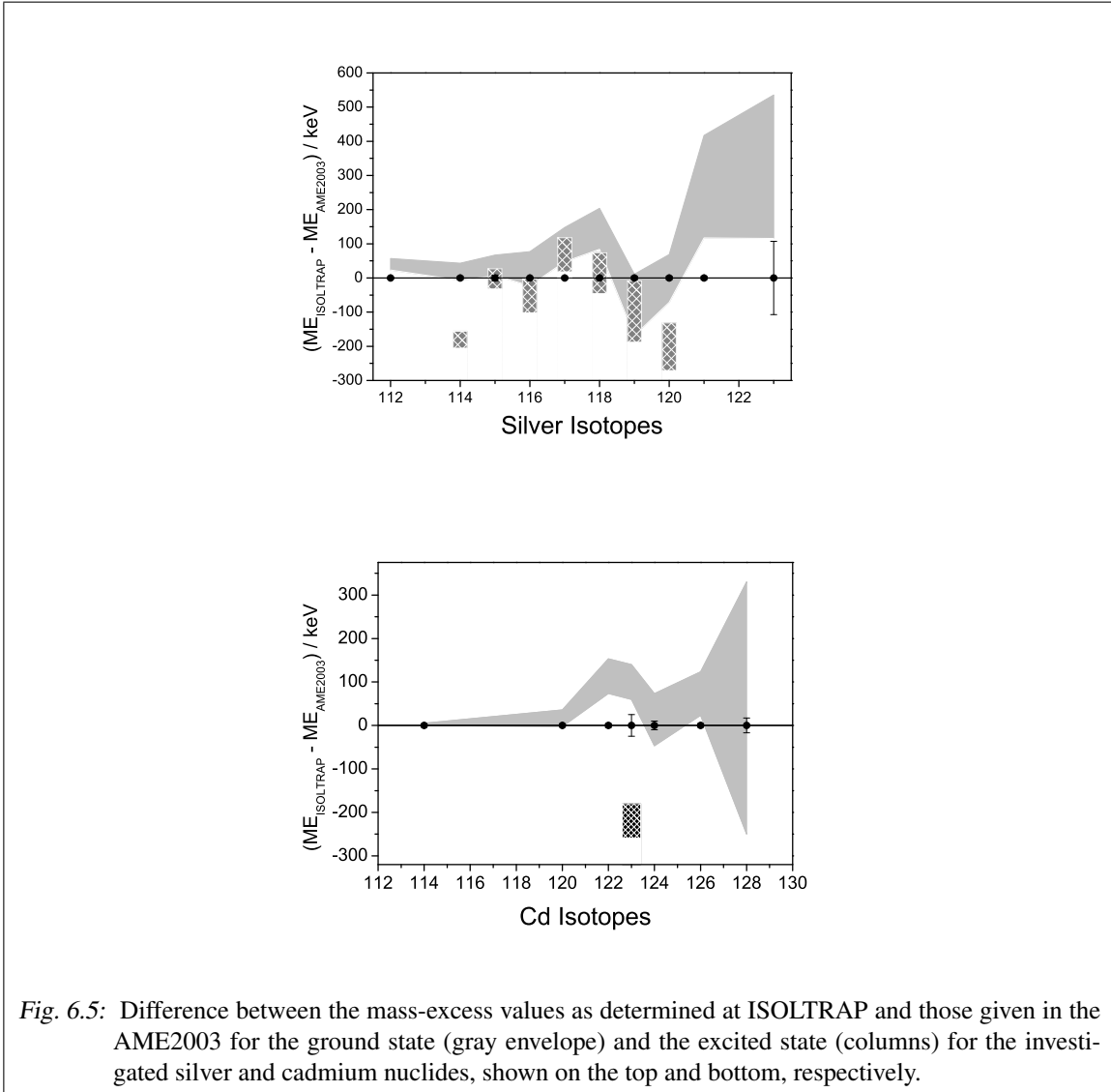

Fig. 6.5: Difference between the mass-excess values as determined at ISOLTRAP and those given in the AME2003 (gray envelope) and the excited state (columns) for the investigated silver and cadmium nuclides, shown on the top and bottom, respectively.

In next paragraphs the influence of the ISOLTRAP frequency ratios as measured for the neutron-rich cadmium and silver nuclides on the mass network is discussed. In Fig. 6.6 and Tab. 6.5 the corresponding mass-excess values are compared with the values entering into the evaluation and the values of the AME2003 [AWT03].
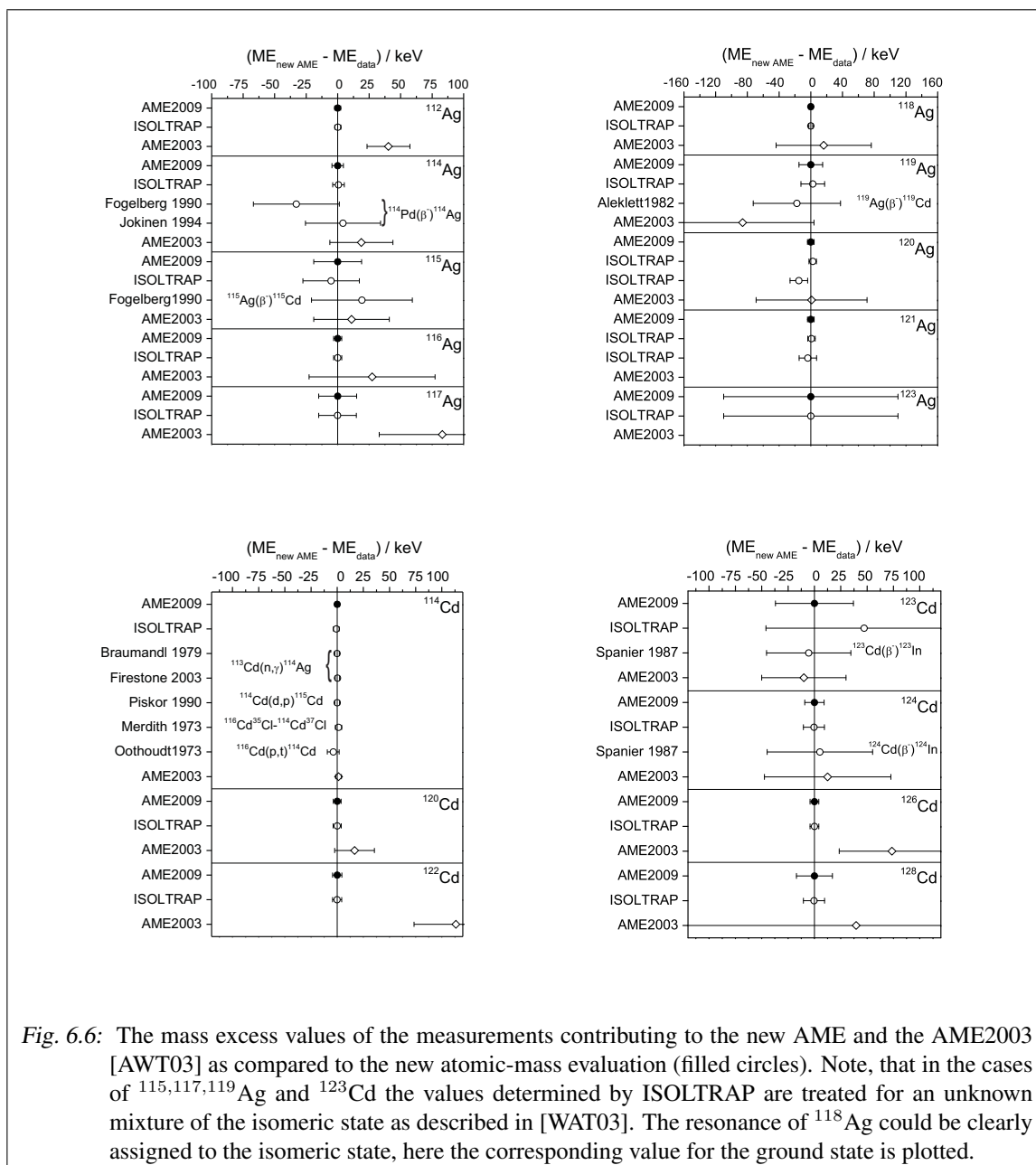
Fig. 6.6: The mass excess values of the measurements contributing to the new AME and the AME2003 [AWT03] as compared to the new atomic-mass evaluation (filled circles). Note, that in the cases of ^{115,117,119}Ag and ^{123}Cd the values determined by ISOLTRAP are treated for an unknown mixture of the isomeric state as described in [WAT03]. The resonance of ^{118}Ag could be clearly assigned to the isomeric state, here the corresponding value for the ground state is plotted.

Tab. 6.5: The mass excesses as determined by ISOLTRAP (not adjusted for isomeric mixtures) and as listed in the AME2003 [AWT03]. Furthermore, the excitation energy and half-life of the isomeric state [ABBW03], the adjusted ME value and finally a new atomic-mass evaluation including the masses of the neutron-rich Cd and Ag isotopes are given as discussed in the text.

Nuclide	Run #	ME(ISOLTRAP) measured /keV	ME(AME2003) /keV	excitation energy of the isomeric state /keV	half-life of the isomeric state	ISOLTRAP adjusted /keV	new adjusted values /keV
^{112}Ag	1	-86583.8(2.4)	-86624(17)				-86583.7(2.4)
^{114}Ag	1	-84930.8(4.6)	-84949(25)	199(5)	1.50(5) ms		-84930.2(4.5)
^{115}Ag	4	-84952.9(8.6)	-84990(30)	41.16(0.10)	18.0(0.7) s	-84974(22)	-84979(19)
^{116}Ag	1	-82542.7(3.2)	-82570(50)	81.90(0.20)	8.6(0.3) s		-82542.7(3.2)
^{117}Ag	4	-82172.3(3.7)	-82270(50)	28.6(0.2)	5.34(5) s	-82187(15)	-82187(15)
^{118}Ag	1	-79426.3(2.5)	-79570(60)	127.49(0.05)	2.0(0.2) s	-79553.8(2.5)	-79553.8(2.5)
^{119}Ag	4	-78638.7(5.3)	-78560(90)	#20(20)	2.1(0.1) s	-78648(14)	-78646(15)
^{120}Ag	1	-75651.5(4.7)	-75650(70)	203.0(1.0)	371(24) ms		
^{120}Ag	4	-75634(11)	-75650(70)	203.0(1.0)	371(24) ms		-75649.1(4.2)
^{121}Ag	1	-74392.6(4.7)	-74660(150)				
^{121}Ag	4	-74388(11)	-74660(150)				-74391.8(4.3)
^{123}Ag	4	-69630(110)	#-69960(210)				-69630(110)
^{114}Cd	2	-90018.7(3.9)	-90020.9(2.7)				-90019.6(2.1)
^{120}Cd	2	-83957.4(3.8)	-83974(19)				-83957.4(3.7)
^{122}Cd	2	-80616.5(4.4)	-80730(40)				-80616.6(4.4)
^{123}Cd	2	-77210(25)	-77310(40)	316.52(0.23)	1.82(3) s	-77367(93)	-77320(37)
^{124}Cd	3	-76697(10)	-76710(60)				-76697.5(9.2)
^{126}Cd	2	-72256.5(4.2)	-72330(50)				-72256.5(4.2)
^{126}Cd	5	-72266(14)	-72330(50)				
^{128}Cd	5	-67250(17)	-67290(290)				-67250(17)

^{114}Cd

The measurement performed at ISOLTRAP agrees perfectly with the value given in the AME2003. The $ME(^{114}$Cd$)$ was determined to 70.6% by the Q-values of two measurements of the n,γ reaction ^{113}Cd(n,γ)^{114}Cd (1414(30) keV [BSVE79] and 1452(25) keV [FLM$^+$06]). A contribution of 10.6% comes from the reaction Q-value of ^{114}Cd(d,p)^{115}Cd Q=3916.30(0.59) keV [PS90] and 8.2% by the mass difference between ^{12}C$_8$ ^{1}H$_{18}$ and ^{114}Cd given with 237487.6(2.9) μu [DRJ63]. The mass duplet of ^{116}Cd^{35}Cl-^{114}Cd^{37}Cl=4348.7(1.2) μu [MSB$^+$73] ^{114}Cd and the (p,t) reaction of ^{116}Cd (Q=-6363(5) keV [OH73]) influenced the mass excess with 8.1% and 2.5%, respectively. The $ME(^{114}$Cd$)$ of the new evaluation is determined to 57.9% by the (n,γ) reaction, to 28.5% by the ISOLTRAP result, to 6.9% by the (d,p) reaction, to 5.1% by the CdCl mass duplet, and to 1.6% by the (p,t) reaction.

^{120}Cd

The ME given in the AME2003 and the result from ISOLTRAP agree within the uncertainties. Previously the AME ME-value was determined by the ^{124}Sn(^{3}He,^{7}Be)^{120}Cd reaction with a Q-value of -5098(30) keV [SSFC76]. In the new evaluation the mass is entirely determined by the present work.

^{122}Cd

The ISOLTRAP result conflicts by 2.8σ with the value given in the AME2003, which was determined by two-proton exchange reaction ^{124}Sn(^{18}O,^{20}Ne)^{122}Cd with a Q-value of -1246(43) keV [GZL$^+$97]. The new AME value is completely determined by the result of the present work due to its low uncertainty.

^{123}Cd

This nuclide has a long-lived (1.82(3)s) excited state (316.52(0.23) keV). The ISOLTRAP result could not be assigned to either the ground state or the isomere, so the value was corrected to -77367(93) keV. Due to the high uncertainty this value only contributes 16.2%, while the main influence to the ME comes from the β^--decay of ^{123}Cd (Q-value 6115(33) keV [SAEF87]). This decay was determining the mass of ^{123}Cd to 100% in the AME2003.

^{124}Cd

The ME of ^{124}Cd of the AME2003 was determined by its β^--decay Q-value of 4166(39) keV [SAEF87]. This value and the result obtained at ISOLTRAP agree perfectly with each other. In the new evaluation the ME value is determined to 97.8% by ISOLTRAP and to 2.2% by the β^--decay Q-value.

^{126}Cd

The mass-excess value in the AME2003 came from a β^--decay of ^{126}Cd with Q=5486(36) keV [SAEF87]. This result and the weighted average of the two ISOLTRAP values deviate by about 1.5σ. In the present version of the AME the $ME(^{126}$Cd$)$ is determined entirely by the ISOLTRAP results.

^{128}Cd

The measurement at ISOLTRAP agrees perfectly with ME-value of the AME2003 originating from the reaction ^{128}Cd(β^-)^{128}In (Q=7070(290) keV [SAEF87]). The new value is entirely determined by the result of the present work.

^{112}**Ag**

The AME2003 value and the ISOLTRAP value deviate by about 40 keV (2.3σ). In the AME2003 the mass excess value was determined to 69.7% by the Q-value of 299(20) keV of the β-decay ^{112}Ag(β^-)^{112}Cd [IRYY62] and to 30.3% by the Q-value of 3967(20) keV of the decay ^{112}Pd(β^-)^{112}Ag [NWSK54]. In the new evaluation the mass is completely determined by the ISOL-TRAP value.

^{114}**Ag**

The isomeric state with an excitation energy of 199(5) keV has a half-life of 1.5 ms, which is too short to be considered in the experiment. The value from ISOLTRAP and that from the AME2003 agree within their uncertainties. The mass in the AME 2003 was determined to 50.3% by the β^--decay of ^{114}Pd [FZE$^+$90, FLM$^+$06] with Q-values of 1414(30) keV and 1451(25) keV, respectively, and to 49.7% by the β^--decay of ^{114}Ag [FZE$^+$90] with a Q-value of 5018(35) keV. After the new evaluation the ^{114}Ag mass is almost entirely determined by the ISOLTRAP value (98.3%). A feedback of 1.7% from ^{114}Pd(β^-)^{114}Ag remains. This connection contributes significantly to the mass value of ^{114}Pd, which is -83483(16) keV as compared to the AME2003 value of -83497(24) keV.

^{115}**Ag**

The ISOLTRAP value was adjusted to -84974(22) keV to account for a possible mixing with the long-lived isomeric state (18.0(0.7)s) with an excitation energy of 41.16(0.10) keV. The adjusted value agrees with the value from the AME2003, which was completely determined by three measurements of the reaction ^{115}Ag(β^-)^{115}Cd [BPFC64, MT78, FZE$^+$90] with the Q-values of 3180(100) keV, 3105(100) keV and 3091(40) keV, respectively. The adjusted ISOLTRAP value contributes with 76.3% to the new evaluation and the rest of 23.8% comes from the β-decay Q-values.

^{116}**Ag**

Due to the comparable short half-life (8.6(0.3)s) and the absence of a decay peak in the ToF spectrum, the ISOLTRAP result was assigned to the ground state. The new value agrees with the value of the AME2003, which was entirely determined by two Q-values of the β^--decay of ^{116}Ag [AHLR82, FZE$^+$90] (6028(130) keV and 6170(50) keV). In the new AME, the mass-excess of ^{116}Ag is determined to 100% by ISOLTRAP.

^{117}**Ag**

Due to the presence of a long-lived isomeric state (5.34(5)s) of the ^{117}Ag^m with an excitation energy of 28.6(0.2) keV the ISOLTRAP value had to be adjusted to ME=-82187(15) keV, which agrees within the uncertainties with the value of the AME2003. This has been determined completely by ^{117}Ag(β^-)^{117}Cd [AHLR82] with a Q-value of 4160(50) keV. The new AME value is entirely determined by the adjusted ISOLTRAP value.

^{118}**Ag**

The mass-excess value determined at ISOLTRAP was assigned to the isomeric state with an excitation energy of 127.49(0.05) keV. The resulting -79553.8(2.5) agrees nicely with the value of the AME2003, which has been determined by the link to the ^{118}Cd using the β^--decay results (Q-value of 7122(100) keV [AHLR82] and 7155(76) keV [ABG$^+$95]). After the reevaluation the mass of ^{118}Ag is entirely determined by ISOLTRAP.

^{119}**Ag**

The isomeric state ^{119}Ag^m with a half-life of 2.1(0.1)s is predicted to be at an excitation energy of 20(20) keV. For this reason the $ME(^{119}$Ag) was adjusted to -78648(14) keV. This value agrees with the AME2003 value from the β^--decay of ^{119}Ag [AHLR82] with a Q-value of 5350(40) keV. In the new evaluation the ME determined at ISOLTRAP is contributing with 97.3% and the other 2.7% come from ^{119}Ag$(\beta^-)^{119}$Cd.

^{120}**Ag**

Due to the short half-life of the isomeric state (371(24)ms) and the good agreement with the previous ground state mass the ISOLTRAP value was assigned to the latter. The two ME-values determined at ISOLTRAP agree within their uncertainties with the AME2003-value, which originates from two measurements of the ^{120}Ag$(\beta^-)^{120}$Cd decay with results Q=8200(100) keV [AHLR82] and Q=8450(100) keV [ABG$^+$95]. In the new evaluation the AME value is determined to 100% by the average of the 2 ISOLTRAP measurements.

^{121}**Ag**

The ISOLTRAP value and that from AME2003 deviate by about 1.8σ. The previous AME value was determined by the β^--decay of ^{121}Ag with a Q-value of 6400(120) keV[AHLR82]. In the new evaluation the $ME(^{121}$Ag) is determined by the weighted average between the two ISOLTRAP results.

^{123}**Ag**

The mass of ^{123}Ag has been measured for the first time. The result and the extrapolated value differ by about 1.4σ, which is consistent with the deviation of the ^{121}Ag. The new value in the AME is entirely determined by the ISOLTRAP result.
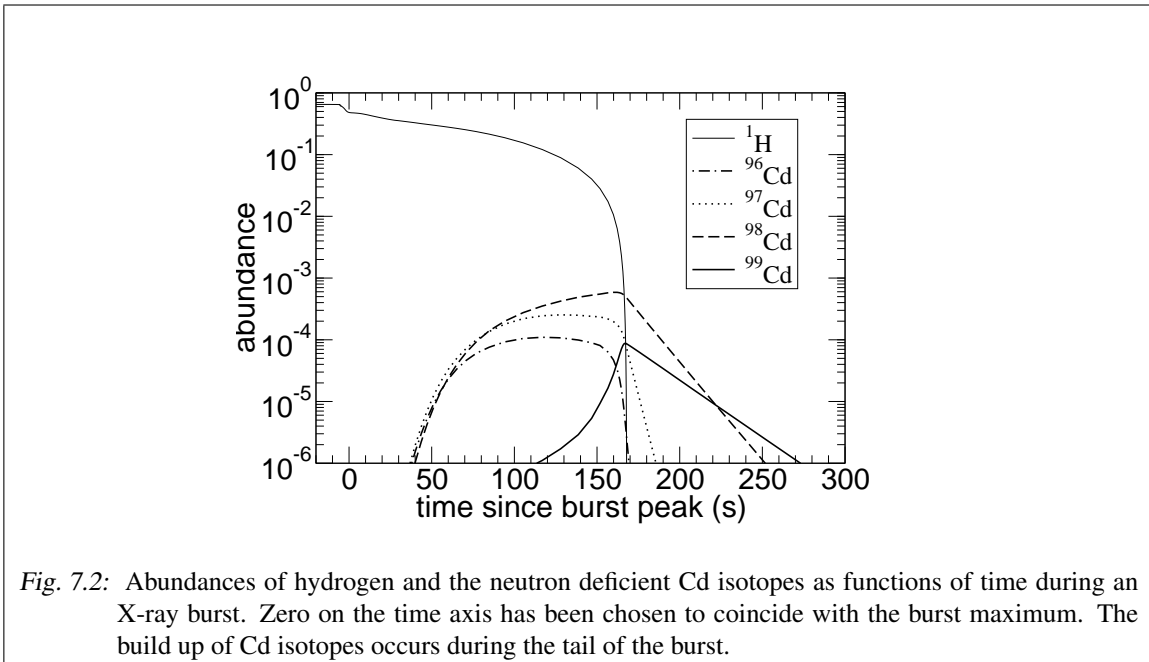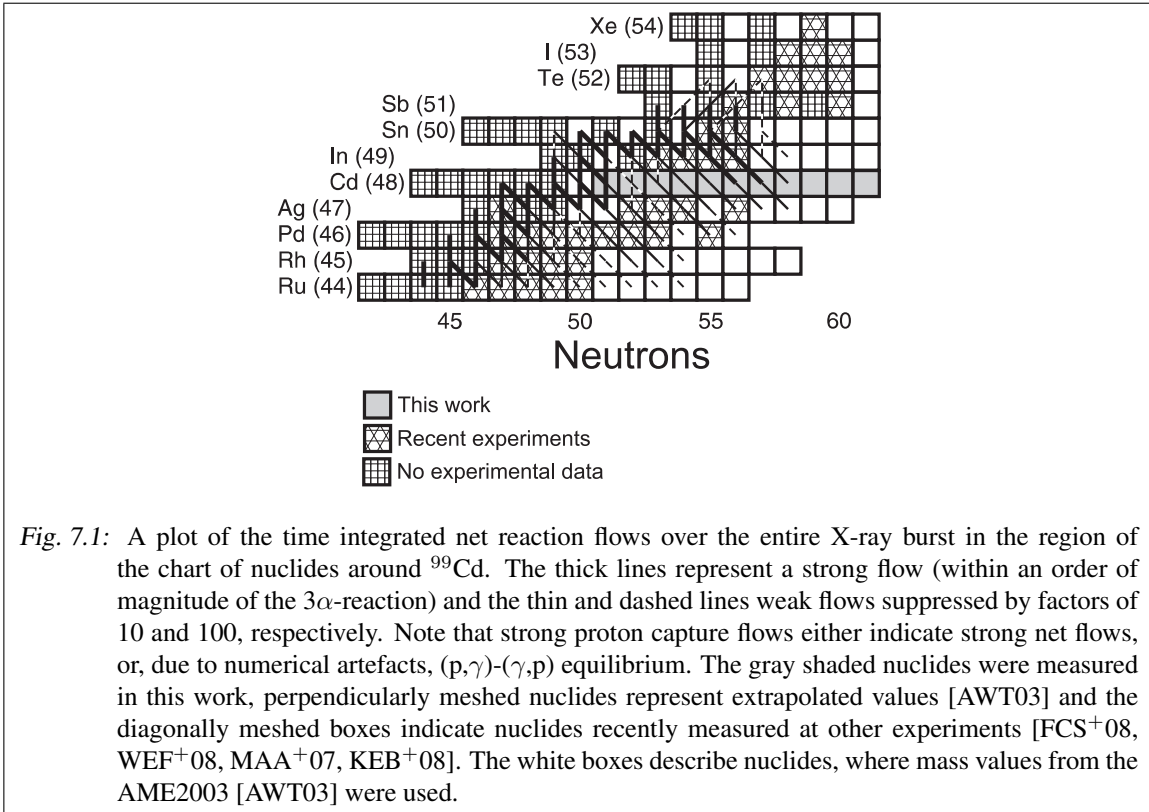
7. DISCUSSION

After the description of the results in the previous chapter, the impact of the new mass values on two different fields will be discussed. On the one hand it is the rp-process path in the vicinity of neutron-deficient nuclide ^{99}Cd and the consequence for the burst ashes resulting from reduced uncertainties for proton-separation energies S_p. On the other hand, results of the local probe for structural changes as described by the evolution of the δV_{pn}-values are discussed. Furthermore, the smoothing of trends in the S_{2n}, δV_{pn} and for the Garvey-Kelson relations are compared.

7.1 Impact of the neutron-deficient data on the knowledge of the rp-process path

^{99}Cd has been suggested as a possible branching point in the path of the astrophysical rp process in some X-ray bursts. Figure 7.1 shows the reaction flows during a type I X-ray burst calculated in a model based on a single-zone approximation and for parameters (accretion rate and initial composition) that are favorable for an extended rp process into the Sn region [SAB$^+$01, MGL$^+$07]. Here the reaction network [Cyb] was updated with results from recent Penning trap mass measurements (by e.g. LEBIT [SBB$^+$07], CPT [FCS$^+$08], JYFLTRAP [WEF$^+$08, KEB$^+$08] and SHIPTRAP [WEF$^+$08, MAA$^+$07]) and the new masses from this work.

Figure 7.1 shows a zoom in the vicinity of ^{99}Cd of the reaction paths as given in Fig. 2.4 for the entire burst. During the very end of the burst, as hydrogen abundance and temperature are dropping, the reaction path shifts towards ^{99}Cd (see Fig. 7.2). The amount of ^{99}Cd that can be built up by feeding from ^{98}Cd(β^+)^{98}Ag(p,γ)^{99}Cd depends critically on the remaining decrease of ^{99}Cd by proton captures before hydrogen is completely exhausted and the final abundances freeze out. This depends strongly on the proton separation energy of ^{100}In, $S_p(^{100}$In). If this quantity is low, proton captures are inhibited by photo-disintegration of ^{100}In, and ^{99}Cd remains abundant as the reaction flow proceeds via its slow β^+ decay. If $S_p(^{100}$In) is large, ^{99}Cd can be converted very effectively by a dominating reaction flow via ^{99}Cd(p,γ)^{100}In.

The AME2003 value for $S_p(^{100}$In) is 1.61(33) MeV as obtained adding mass errors quadratically. The large error originated from the extrapolated masses of ^{99}Cd ($\pm$ 0.21 MeV) and ^{100}In ($\pm$ 0.25 MeV). After our accurate measurement of the ^{99}Cd mass the uncertainty is almost exclusively due to the ^{100}In data. Including the newly evaluated value for the mass of ^{100}In we obtain now $S_p(^{100}$In) of 1.69(18) MeV. Figure 7.3 shows final abundances and overproduction factors relative to solar abundances for model calculations for various values of $S_p(^{100}$In). Clearly, $S_p(^{100}$In) is a critical quantity for determining the $A = 99$ abundance in the final reaction products (burst ashes). The 2σ range of the AME2003 mass uncertainties introduces more than an order of magnitude uncertainty in the $A = 99$ abundance. At the lower 2σ limit of $S_p(^{100}$In) $A = 99$ becomes one of the most abundant mass chains, even exceeding the $A = 98$ production by 50%, while at the upper limit it is one of the least abundant ones. The new measurements dramatically reduce the possible range of $A = 99$, excluding now an enhanced $A = 99$ production at the 2σ level. The largest reduction in the uncertainty comes from our precise measurement of the ^{99}Cd mass. However, the improvement in

Fig. 7.1: A plot of the time integrated net reaction flows over the entire X-ray burst in the region of the chart of nuclides around ^{99}Cd. The thick lines represent a strong flow (within an order of magnitude of the 3α-reaction) and the thin and dashed lines weak flows suppressed by factors of 10 and 100, respectively. Note that strong proton capture flows either indicate strong net flows, or, due to numerical artefacts, (p,γ)-(γ,p) equilibrium. The gray shaded nuclides were measured in this work, perpendicularly meshed nuclides represent extrapolated values [AWT03] and the diagonally meshed boxes indicate nuclides recently measured at other experiments [FCS$^+$08, WEF$^+$08, MAA$^+$07, KEB$^+$08]. The white boxes describe nuclides, where mass values from the AME2003 [AWT03] were used.

Fig. 7.2: Abundances of hydrogen and the neutron deficient Cd isotopes as functions of time during an X-ray burst. Zero on the time axis has been chosen to coincide with the burst maximum. The build up of Cd isotopes occurs during the tail of the burst.

precision of the mass of ^{100}In due to the β^+-decay of ^{100}In linked to ^{100}Cd (measured in this work) contributes significantly, leading to an additional reduction of the uncertainty by about a factor of 2.5.
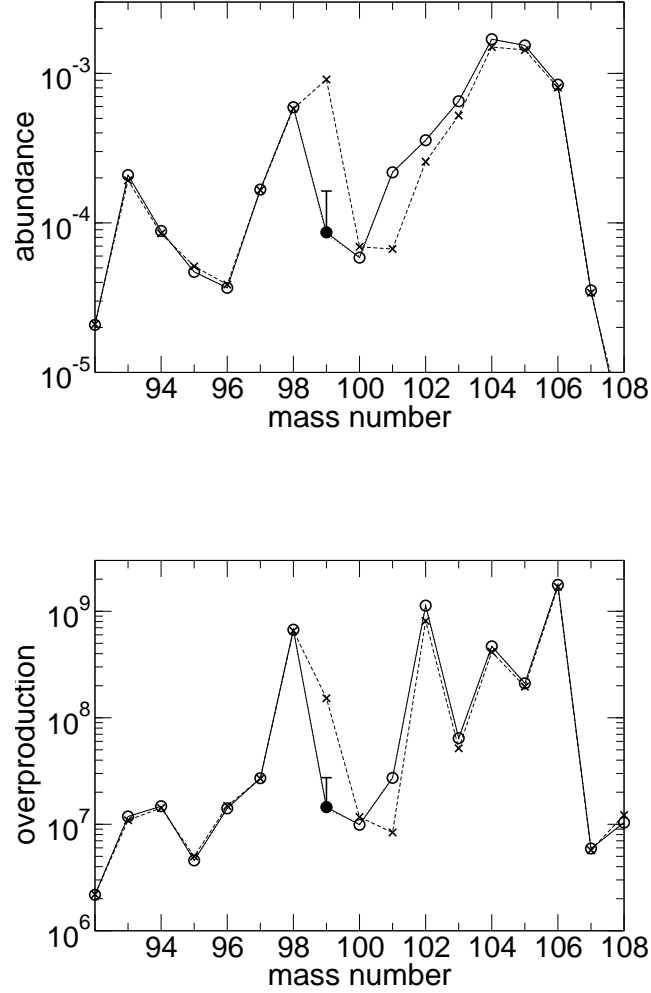
Fig. 7.3: (a) Final composition of the burst ashes for different values of $S_p(^{100}\text{In})$: with our new value for ^{99}Cd (circles connected by solid line), the lower 2σ limit allowed in AME2003 (crosses connected by dashed line) and the upper 2σ limit allowed in AME2003 (dotted line which basically coincides with solid line). The data point with our new ^{99}Cd mass and our new 2σ uncertainty is indicated as a filled circle with error bars. (b) Overproduction factors relative to the solar abundance, determined by assuming the entire mass chain has decayed into the first stable isotope. This is a p-nucleus for $A = 92$, 94, 96, 98, 102, and 106, while the other mass chains feed isotopes predominantly made by the s process.

The composition of the burst ashes is important for crust heating models and for judging whether the rp process is a possible production scenario for light p-nuclei. In terms of crustal heating, Gupta *et al.* [GBS⁺07] have shown that there are significant differences in total heat generation and distribution of heat sources as a function of depth for $A = 98$, 99, or 100 ashes. While a change in a single mass chain probably has only a small effect on the thermal structure of the neutron star, our work shows

that there are very large uncertainties in the prediction of the final composition of the burst ashes that need to be addressed. The present measurement is a first step in that direction. Uncertainties in other mass chains such as Ag, In, and Sn also need to be addressed.

In order to judge the suitability of a proposed nucleosynthesis scenario to explain the origin of the elements in the solar system, one key aspect is the pattern of overproduction factors, i.e. the ratio of the produced abundances to the solar abundances (see Fig. 7.3). The ratio of the overproduction factor of a given isotope to the highest overproduction factor of the pattern (or to an average of the highest overproduction factors when taking into account variations due to uncertainties) indicates the fraction of solar system material that could originate at most from this nucleosynthesis site. For a p-process scenario one would require large, comparable overproduction factors for p-nuclei, and significantly reduced overproduction factors for non-p nuclei. As Fig. 7.3 shows, the rp process in this particular X-ray burst would be a promising scenario to produce the p-nuclei ^{98}Ru, ^{102}Pd and ^{106}Cd. However, co-production of non-p nuclei such as isotopes fed by the $A = 99$, 104, and 105 mass chains potentially limits this scenario. The question is whether a possible co-production can be attributed to uncertainties in the nuclear physics input data such as β-decay half-lives and level densities, or whether the co-production is a fundamental issue with the proposed scenario. For the $A = 99$ case, this question has now been addressed with the present measurement. As Fig. 7.3 shows, at the 2σ level the AME2003 mass uncertainties allowed for co-production of as much as 20% of ^{99}Ru (a s-process nucleus) relative to the p-nucleus ^{98}Ru. With our new mass measurements, $A = 99$ co-production is now limited to a rather insignificant few %.

7.2 Mass Surface and Nuclear structure

The additional information needed for nucleosynthesis studies is provided by the nuclear models. With new masses included in the atomic-mass evaluation and some shifted mass-excess values it is possible to test the available models according to their prediction power for not yet measured masses. In Fig. 7.4 the difference of predictions by the models, which were described before, to the values taken from the new AME are plotted as a function of mass number for cadmium and silver nuclides. Here the values from the Weizsäcker-Bethe mass formula are only shown for completeness. The σ_{rms} deviation of the predicted values from the experimental data is given in Tab. 7.1 with the change as compared to the values of Tab. 2.1. The σ_{rms} for both elements give a measure of the quality independent of the pairing.

In general, all mass models have a problem towards neutron-rich nuclei, whereas the neutron-deficient side is reproduced quite well. Also most models reproduce the masses of either the silver or the cadmium nuclides better, which suggests an improvement of the pairing term. Moreover, with HFB17 the microscopic models reach the quality of the prediction of the microscopic-macroscopic mass formulas in the region of interest.

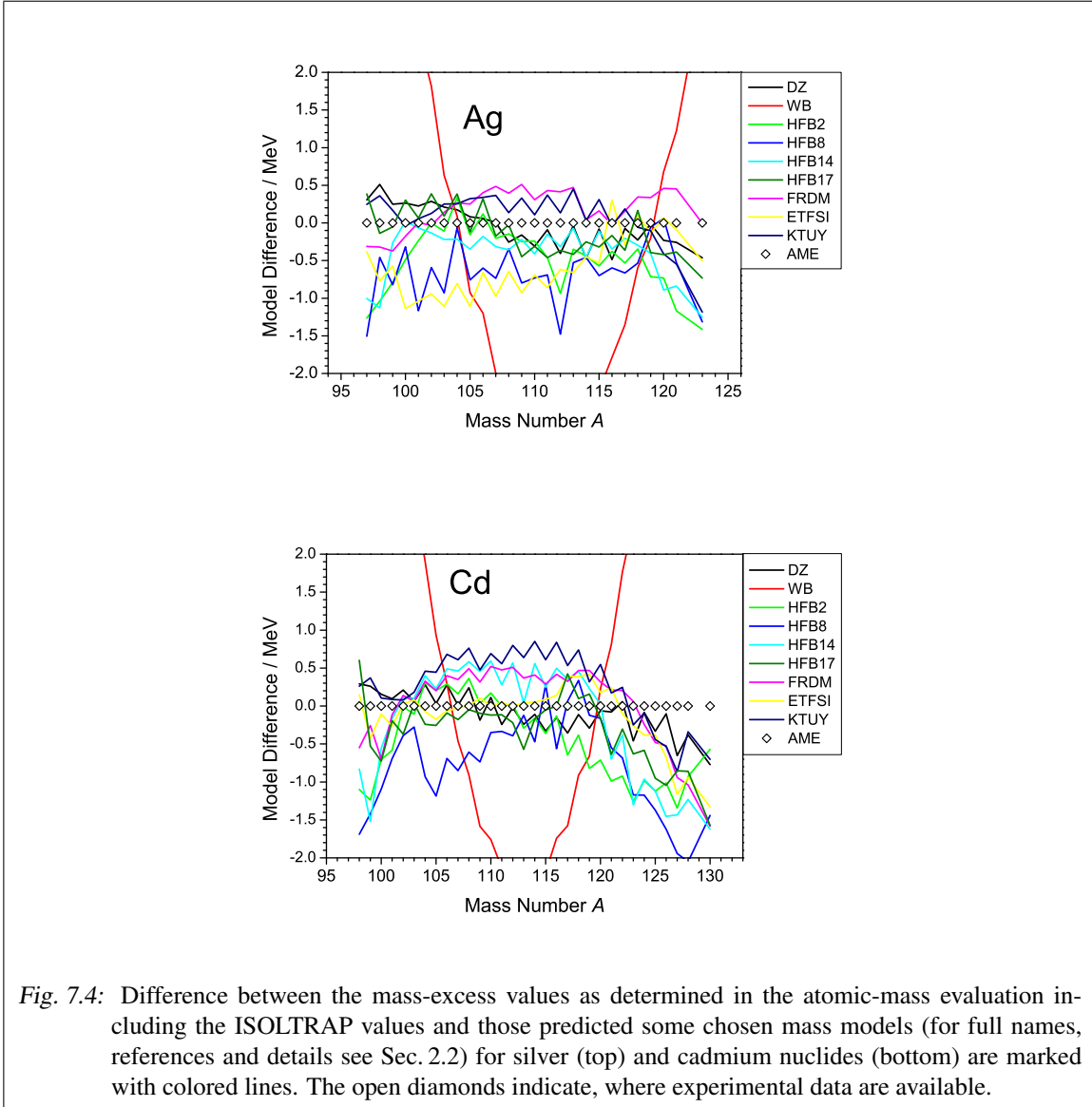### 7.2.1 Two-Neutron Separation Energy

Furthermore the obtained data give useful information on nuclear structure in the mass region. The two neutron separation energy

$$S_{2n}(N, Z) = ME(N - 2, Z) - ME(N, Z) + 2 \cdot ME(n) \tag{7.1}$$

is a major indicator for structural changes, where $ME(n)$ is the mass excess value of a neutron. In Fig. 7.5 the S_{2n}-values for the $Z = 47 - 50$ are compared for odd (top) and even (bottom) N separately. The new mass values for Cd isotopes straighten the trend of the S_{2n} for even N. Thus the shift of ^{122}Cd by about 110 keV to a less bound value results in a slight reduction of S_{2n} for $N = 74$

Tab. 7.1: Comparison of the mass models to the available mass data of Ag and Cd nuclides using the σ_{rms} deviation as given in Eq. 2.17. The change as compared to the Tab. 2.1 is given in brackets.

Mass Model	Ag	Cd	Ag & Cd
Number of Isotopes Used	26	32	58
	σ_{rms} / MeV		
DZ	0.27(+0.02)	0.28($\pm$0.00)	0.28
WB	2.97(-0.01)	4.39(+0.15)	3.82
HFB2	0.64(+0.08)	0.70(+0.03)	0.67
HFB8	0.77(+0.04)	0.97(+0.03)	0.88
HFB14	0.52(+0.06)	0.77(+0.05)	0.67
HFB17	0.54(+0.01)	0.33(+0.03)	0.46
FRDM	0.32(-0.03)	0.52($\pm$0.00)	0.44
ETFSI	0.71(+0.01)	0.43(+0.02)	0.57
KTUY	0.35(+0.09)	0.54($\pm$0.00)	0.46

Fig. 7.4: Difference between the mass-excess values as determined in the atomic-mass evaluation including the ISOLTRAP values and those predicted some chosen mass models (for full names, references and details see Sec. 2.2) for silver (top) and cadmium nuclides (bottom) are marked with colored lines. The open diamonds indicate, where experimental data are available.

and in a slight shift towards a higher value of S_{2n} for $N = 76$. Furthermore, the new mass value of ^{126}Cd reduces its S_{2n} by about 60 keV.

The corrections in the the silver chain are even more pronounced. The new mass values for ^{119,121}Ag straighten the kink at $N = 74$ and the new mass value of ^{123}Ag results in a smooth continuation. In all cases the reduced uncertainties of the mass-excess values improve the knowledge of the S_{2n} values.

In the case of the odd-N S_{2n}(Ag)-values the staggering is damped by the new measurements towards a straight line, which is hardly visible in the top of Fig. 7.5 due to the smallness of the effect, while for the odd-N S_{2n}(Cd)-values the shift is already visible around the only measured mass, although the experimental value of ISOLTRAP was adjusted for a potentially present excited isomeric state.
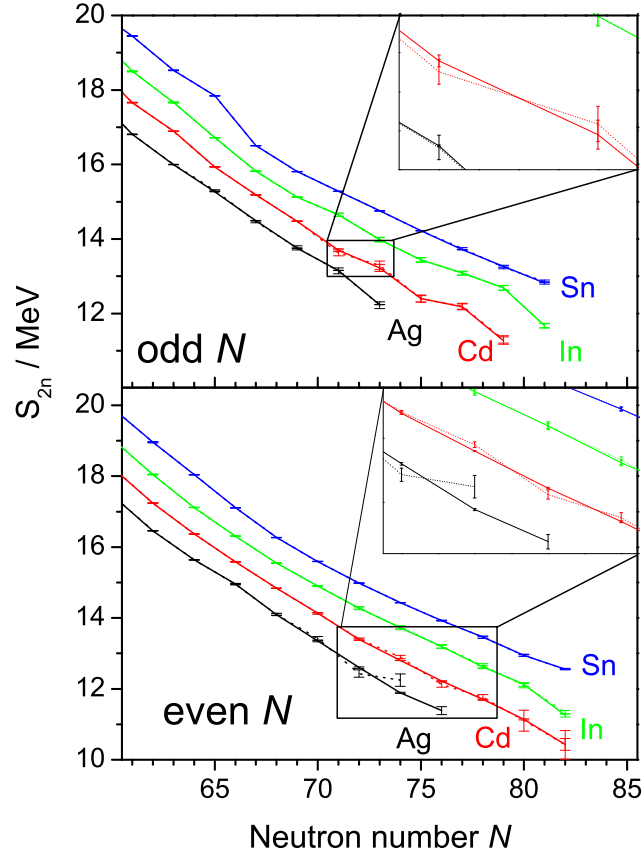
Fig. 7.5: The two neutron separation energy S_{2n} for the as a function of neutron number N for odd (top) and even (bottom) N separately to emphasize the different behaviors. The zooms show the regions of the strongest correction.

7.2.2 δV_{pn}-values

The more sensitive probe of structural changes is the δV_{pn}-value, the double difference of binding energies giving the average interaction of the last proton(s) with the last neutron(s) [ZWYG88, ZCB89] as described in Sec. 2.4. The new $^{112,114-121,123}$Ag and $^{114,120,122-124,128}$Cd mass measurements provide improved information on the average interaction between the last (two) proton(s) and the last (two) neutron(s) δV_{pn} [ZWYG88, ZCB89] below the neutron and proton shell closures $N = 82$ and $Z = 50$. Values of δV_{pn} for Sn, Cd, In and Ag were extracted from the new mass data. These new δV_{pn} results are illustrated in Fig. 7.6 with the solid lines using the new Cd and Ag mass measurements in this study together with mass values from the AME2003, where no new data are available. The dashed lines correspond to the pure AME2003 [AWT03] results.

The results for the even-even nuclei are shown in top-left of Fig. 7.6. The δV_{pn}(Sn) values as calculated from mass data given in the AME2003 reveal a zig-zag behavior as the number of the valance neutrons decreases towards the closed shell at $N=82$. The new δV_{pn}(Sn)-values (solid circles)
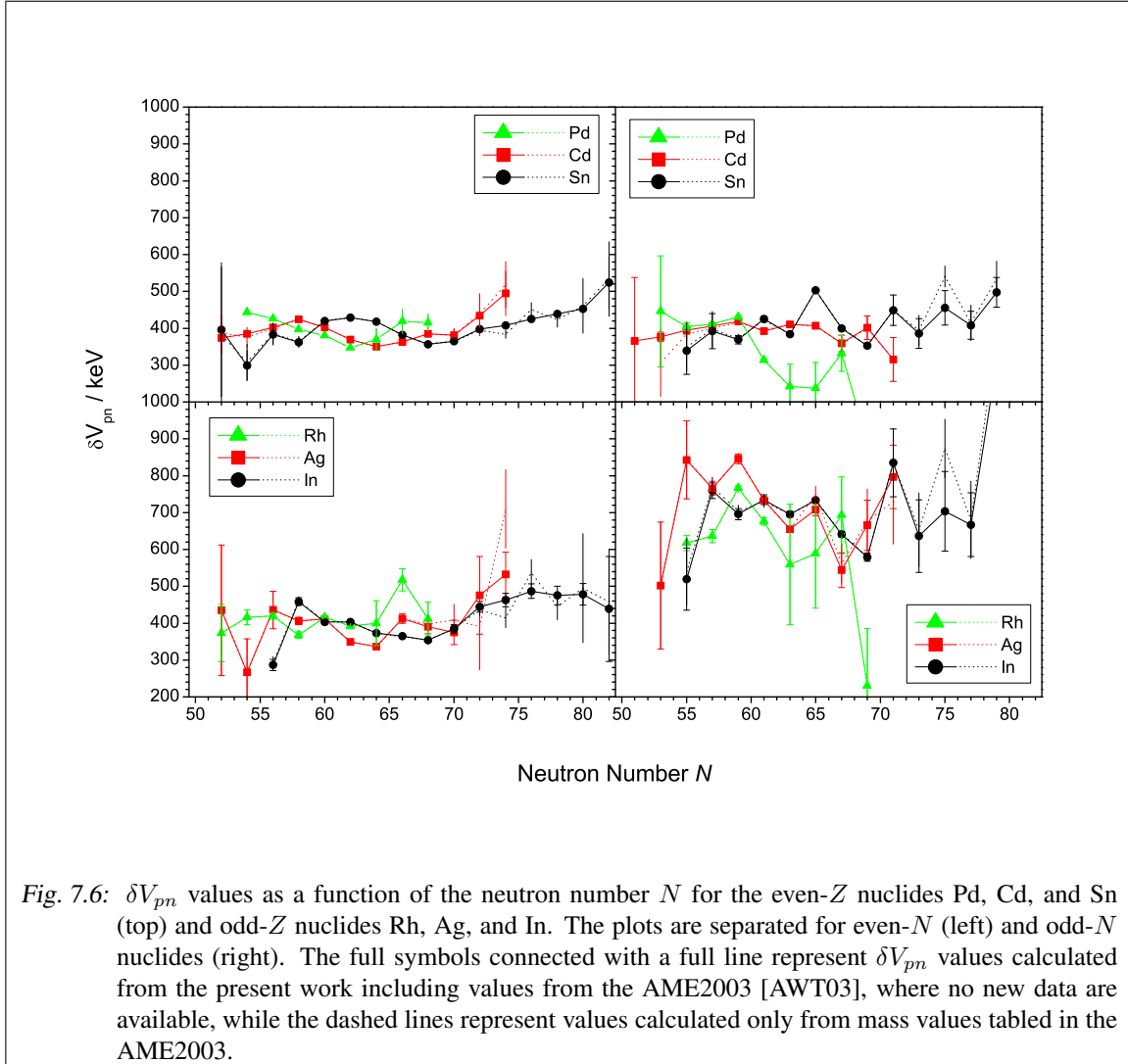
Fig. 7.6: δV_{pn} values as a function of the neutron number N for the even-Z nuclides Pd, Cd, and Sn (top) and odd-Z nuclides Rh, Ag, and In. The plots are separated for even-N (left) and odd-N nuclides (right). The full symbols connected with a full line represent δV_{pn} values calculated from the present work including values from the AME2003 [AWT03], where no new data are available, while the dashed lines represent values calculated only from mass values tabled in the AME2003.

result clearly in a damping of the zig-zag and thus show a much smoother increasing trend, which is expected for the proton-neutron interaction. Indeed, see Fig. 7.7, the results obtained for N=82 nuclei in the $^{132}_{50}$Sn region are comparable to the values for N=126 nuclei in the $^{208}_{82}$Pb region. Moreover, just as in the Pb region where δV_{pn}(Hg) values are higher than those Pb isotones, here the δV_{pn}(Cd) results are higher than those of Sn. Finally, Fig. 7.7 shows a crossing pattern in the Pb region as one crosses the magic number $N = 126$ [CLP$^+$09], which is also expected for the Sn region. For a final conclusion the mass of ^{130}Cd is needed.

Protons in Sn occupy orbits just below the $Z = 50$ closed shell whereas neutrons occupy orbits just below the $N = 82$ closed shell. The normal parity orbits in a major shell begin with high j angular momenta and low n principal quantum numbers whereas, near the end of the shell one finds orbits with low j and high n. As a result of this, if both protons and neutrons fill just below or just above a shell at the same time, the overlap between the proton and neutron wave functions may be expected to be large. The large δV_{pn}(Sn) result for the even-even nuclei, especially at $N = 82$, can be explained with this approach. Similarly, the zig-zag behavior in δV_{pn}(In) is mostly removed with the
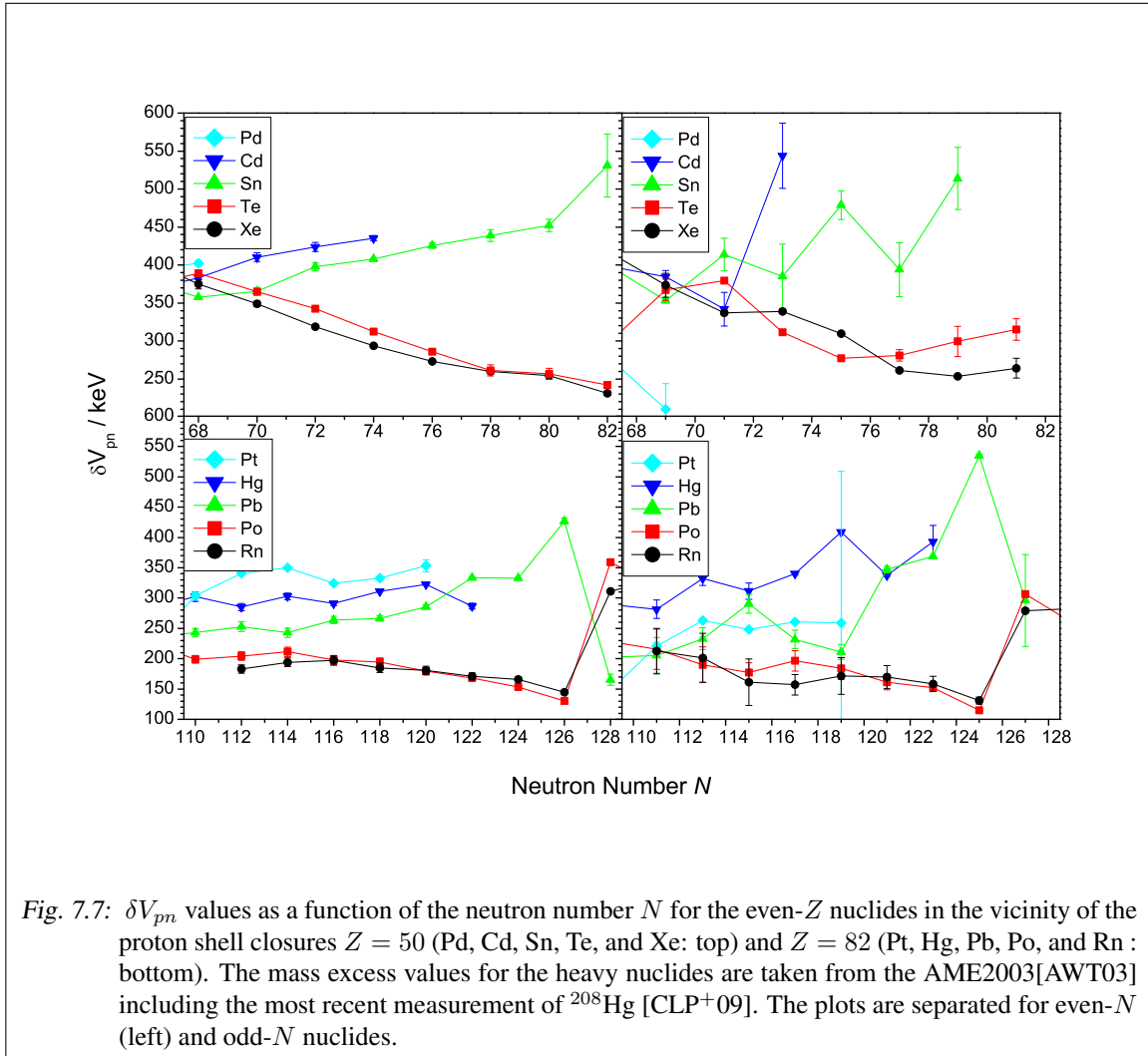
Fig. 7.7: δV_{pn} values as a function of the neutron number N for the even-Z nuclides in the vicinity of the proton shell closures $Z = 50$ (Pd, Cd, Sn, Te, and Xe: top) and $Z = 82$ (Pt, Hg, Pb, Po, and Rn : bottom). The mass excess values for the heavy nuclides are taken from the AME2003[AWT03] including the most recent measurement of ^{208}Hg [CLP$^+$09]. The plots are separated for even-N (left) and odd-N nuclides.

new Cd masses in Fig. 7.6.

A very large change in δV_{pn} is seen in ^{121}Ag$_{74}$ (Fig. 7.6), roughly about 200 keV. This $\delta V_{pn}(^{121}$Ag) value requires the masses of ^{121}Ag, ^{119}Ag, ^{120}Pd, and ^{118}Pd. The ^{121,119}Ag masses were measured in this work and the largest mass change happened for ^{121}Ag, which differs by about 270 keV from AME2003. Therefore, there is a drop in $\delta V_{pn}(^{121}$Ag) from 710(100) keV to 525(50) keV. In addition, including some recent mass measurements for Pd nuclei [HEE$^+$07] gives $\delta V_{pn}(^{121}$Ag)= 415(10) keV which is even somewhat lower. (However, in order to compare AME2003 with the new measurements here δV_{pn} is kept as 500 keV in the plot).

On the other hand for the odd neutron numbers (right top and bottom) in Fig. 7.6, it is hard to see the same smooth trend for δV_{pn}(Sn) as for even N. There remains a zig-zag trend for δV_{pn}(Sn) (right-top) and δV_{pn}(In) (right-bottom) for odd neutrons. In the present work, Cd masses were measured only for even neutron numbers except for ^{123}Cd$_{71}$. The largest change between AME2003 and our results among odd Z nuclei appears in $\delta V_{pn}(^{124}$In$_{75}$) which requires masses of ^{124}In, ^{123}In, ^{123}Cd and ^{122}Cd. Since only one odd neutron Cd mass (^{123}Cd) was measured in this study, $\delta V_{pn}(^{124}$In) is the only one nucleus which uses newly measured Cd masses including one with an odd neutron number. The new mass of ^{123}Cd differs about 110 keV from AME2003 and the $\delta V_{pn}(^{124}$In) value (right-bottom) decreases by about 140 keV from 875(80) keV to 735(50).

The remaining (smaller) zig-zag trend of δV_{pn} for odd-N Cd nuclei may be an artifact of the fact that most of the odd-N Cd masses have not been re-measured. Therefore, it will be interesting to see wether the oscillations for the other δV_{pn} values will be further damped by new mass values of additional odd-A Cd isotopes.

7.2.3 Garvey-Kelson relations

Also by using the Garvey-Kelson mass relations [GK66, GGJ$^+$69] (introduced in Sec. 2.3) as valid for the investigated mass region more irregularities for the odd-N nuclides can be observed than for even-N nuclides. The values presented in Fig. 7.8 are calculated by the difference between the mass values of Cd isotopes as given in the AME and the mean of all possible Garvey-Kelson relations using the existing masses in the vicinity. The values obtained using the AME2003 (open circles) are compared with the values from a current evaluation (full circles), which includes also the Pd values from Hager et al [HEE$^+$07]. In general the new values are shifting towards the zero line, which corresponds to a better agreement between the values obtained from the Garvey-Kelson relations with the experimental data. Nevertheless for the neutron-rich odd-N cadmium isotopes ^{119,127}Cd are slightly outside of the one-σ_{rms} as given by the dotted line [BFH$^+$08], which is an agreement to the observation in the two-proton separation energy S_{2n} and the δV_{pn}. Beside the analogy, the uncertainties of the Garvey-Kelson relations are not clearly defined: On the one hand it is stated, that the prediction of masses for even-odd nuclides is more uncertain then for even-even ones, on the other hand it is stated that the agreement of the Garvey-Kelson relations is better towards closed shells then on the average [BFH$^+$08].

7.2.4 Correlation between δV_{pn} and orbital overlap of valence nucleons

Going back to the discussion of the δV_{pn} and extract those values as a function of neutron number from the recent AME [LA09] reveals a characteristic behavior. This AME includes in addition to the present results also the recent results of other groups on the neutron-deficient [WEF$^+$08, KEB$^+$08, MAA$^+$07, FCS$^+$08] and on the neutron-rich side of the valley of stability [HEE$^+$07]. Figure 7.9
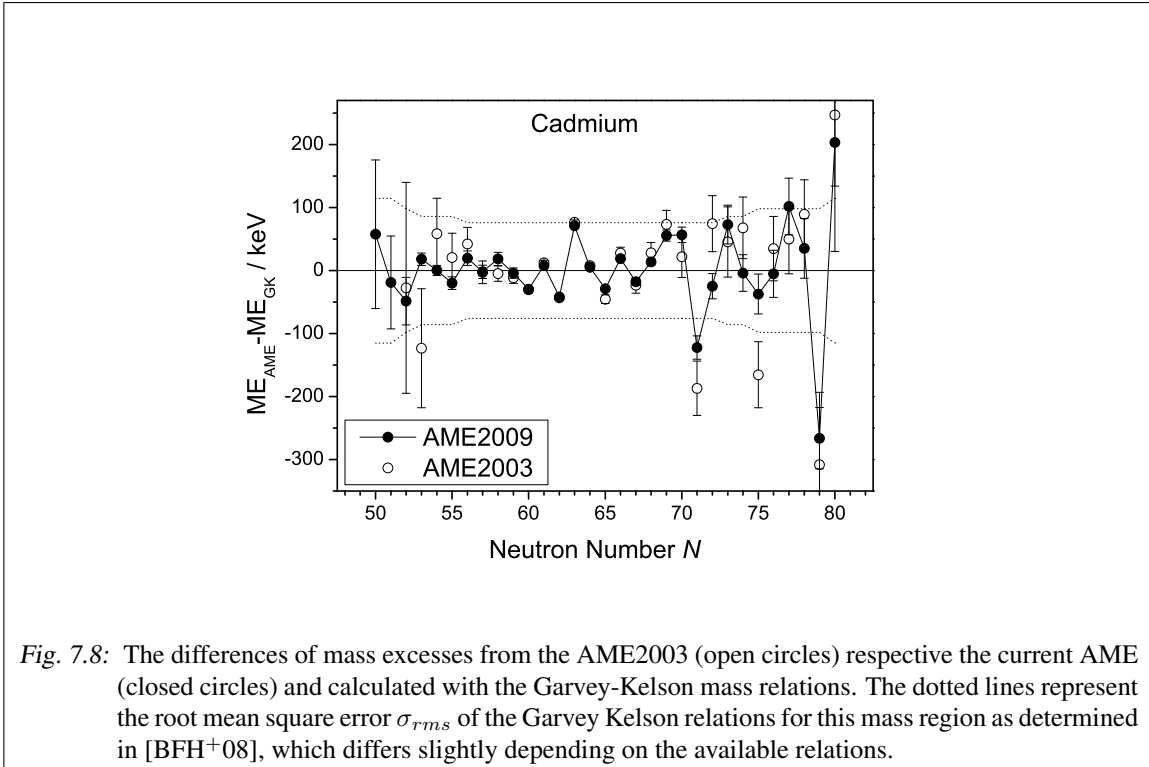

Fig. 7.8: The differences of mass excesses from the AME2003 (open circles) respective the current AME (closed circles) and calculated with the Garvey-Kelson mass relations. The dotted lines represent the root mean square error σ_{rms} of the Garvey Kelson relations for this mass region as determined in [BFH$^+$08], which differs slightly depending on the available relations.

shows the δV_{pn} values for even-even Pd, Cd, and Sn nuclides between the neutron shell-closures N=50 and 82. As can be observed there is a smooth trend in the δV_{pn} values over the entire shell. They increase from N=50 towards a local maximum, decrease a bit at about midshell and afterwards increase again towards $N = 82$. Furthermore, the inflexion point is shifting from Pd to Sn to more neutron-rich nuclei. To explain this behavior of the δV_{pn}-values of the even-even nuclei, the orbits of the last protons and the last neutrons are derived from the ground state total angular momentum J and parity Π of the odd-even $(Z - 1, N)$ and the even-odd $(Z, N - 1)$ nuclei, respectively. The orbits in a nucleus are filled with pairs of nucleons, where each pair couples to a favorable total angular momentum of zero. Thus, near closed shells the total angular momentum J and the parity Π of the ground state of an odd-even and an even-odd nucleus describe the orbit of the investigated valence nucleons. For the example of ^{128}Cd the neutron orbit is derived from the ground state of ^{127}Cd, as $J^{\Pi} = 3/2^+$ [END09]. The total angular momentum of 3/2 can only be created by the orbital angular momentum $l = 1$ coupling to the spin $s = +1/2$ or by $l = 2$ coupling to $s = -1/2$. The parity $\Pi = +1$ determines l to be even and thus the orbit has to be a $d_{3/2}$ state. The principle quantum number $n = 2$ can be derived from Fig. 2.7. In analogy for the valance-proton orbit of ^{128}Cd the ground state of the nuclide ^{127}Ag is investigated.

The strength of the δV_{pn} can be calculated by the overlap of the orbits of the last protons and last neutrons in the ground states. In the following, the overlap is estimated by the wave functions' principal (n_g) and orbital angular momentum quantum numbers (l_g):

$$O_{gg} = \frac{V_{gp}^2 V_{gn}^2}{1 + |n_{gp} - n_{gn}| + |l_{gp} - l_{gn}|}. \tag{7.2}$$

V is the filling factor of the orbits described by the pairing model (Sec. 2.2), which is for the ground state $V_g^2 = 0.5$. The index $_g$ denotes, that this are the quantum numbers of the discussed ground states orbits of the $(Z - 1, N)$ (indexed with $_p$) and $(Z, N - 1)$ nuclides (indexed with $_n$).
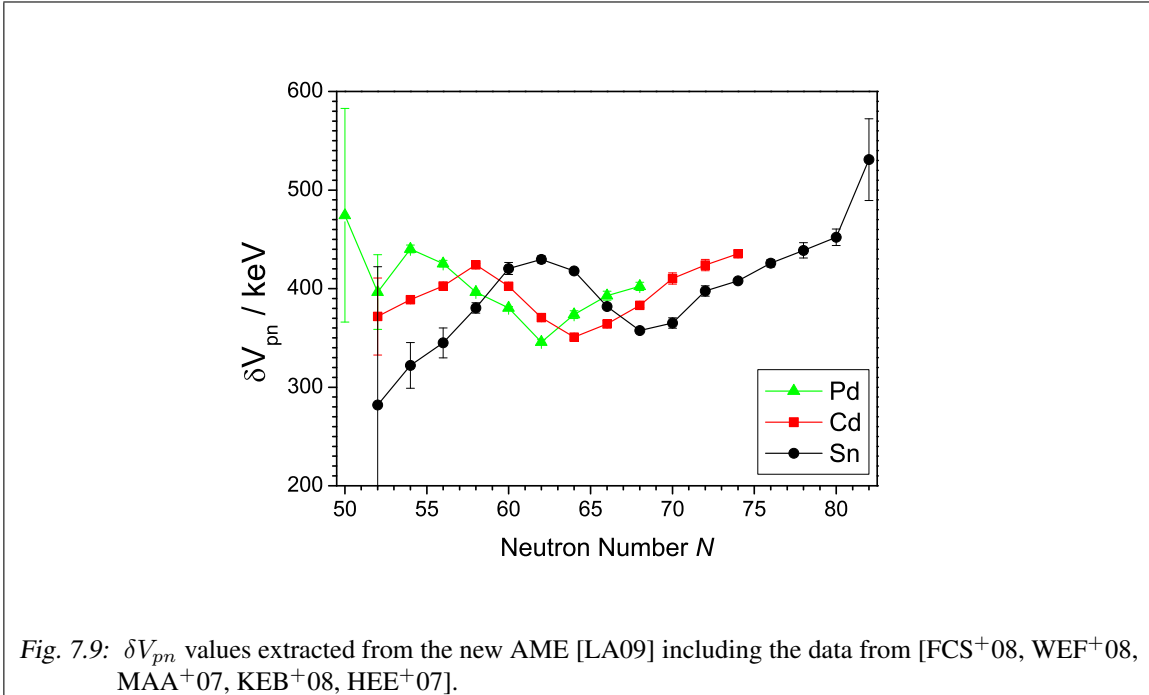

Fig. 7.9: δV_{pn} values extracted from the new AME [LA09] including the data from [FCS$^+$08, WEF$^+$08, MAA$^+$07, KEB$^+$08, HEE$^+$07].

In addition, the overlaps of the first excited states of the odd-even and even-odd nuclides with the ground state of the other nucleons orbits O_{eg} and O_{ge}, respectively, and the overlap of the excited states with each other have to be taken into account, specially for midshell nuclides. The weighted contributions of the next higher proton and neutron orbit are determined to

$$O_{eg} = \sum_e \frac{V_{ep}^2 V_{gn}^2}{1 + |n_{ep} - n_{gn}| + |l_{ep} - l_{gn}|},$$

$$O_{ge} = \sum_e \frac{V_{gp}^2 V_{en}^2}{1 + |n_{gp} - n_{en}| + |l_{gp} - l_{en}|},$$

$$O_{ee} = \sum_{ep} \sum_{en} \frac{V_{ep}^2 V_{en}^2}{1 + |n_{ep} - n_{en}| + |l_{ep} - l_{en}|}, \tag{7.3}$$

where the "$_e$" denotes the excited state. The filling factors V for the excited states are given as

$$V_e^2 = \frac{1}{2} \left[1 - \frac{\sqrt{(E_e + \Delta)^2 - \Delta^2}}{E_e + \Delta} \right]. \tag{7.4}$$

using the Eqs. (2.22) and (2.25) under the assumption that the Fermi level (λ) and the energy level closest to the Fermi level (ϵ_0) are zero. Here, E_e describes the energy of the excited state and Δ is the strength of the pairing interaction, fixed at $\Delta = 1\,\mathrm{MeV}$. The total overlap is then determined to

$$O = O_{gg} + O_{eg} + O_{ge} + O_{ee}, \tag{7.5}$$

where the O_{eg}, O_{ge}, and O_{ee} are determined by up to three states of each nucleon with excitation energies below $300\,\mathrm{keV}$.

In Fig. 7.10 the overlap of the last neutrons with the last protons is determined for the even-even Pd, Cd, Sn, Te, and Xe nuclides (solid black line) and has been adjusted to be comparable with the experimental δV_{pn} (red circles) $\delta V_{pn}^{over} = a_o \cdot O + b_o$, where a_o is a scaling factor of $200\,\mathrm{keV}$ and b_o is an offset of $320\,\mathrm{keV}$. Note that only single values of the three parameters Δ, a_o, and b_o are used for all nuclides in Fig. 7.10. The resulting trends are comparable with those obtained from the δV_{pn}. In the cases of the isotopic chains of Pd, Cd and Sn the presence of the inflexion points can be reproduced and also their positions. Beyond the shell closure for $Z = 50$ an agreement in the trends can be observed, although the values determined for the Xe isotopes is slightly too high.

The single particle approach used in this model is only valid for nuclides where collective effects are not important. An indication for collectivity is given by $R_{4/2}$, the energy ratio between the first 4^+ and the first 2^+ state. If this ratio is below 2, the nucleus can be described by the single particle approach, as in the case of the Sn nuclides. For higher $R_{4/2}$ the states are collective and can be described by mixing of shell model configurations [Cas00] as in the cases of Pd and Xe shown in Fig. 7.10 with a black dashed line. For very exotic nuclides the available experimental data concerning level energies and total angular momenta are not always available. In these cases they are estimated from systematic trends as published in [END09].

In Fig. 7.10 δV_{pn} values calculated by Stoitsov et al. using the nuclear density functional theory (DFT) [KS65, BHR03, SDNB06] are given with green dashed lines. These DFT values for the δV_{pn} are comparable to the experimental values. However, in contrast to the overlap values, the DFT values do not reproduce the basic trends especially for the Sn, Cd and Te. Thus, for a simple estimation of the interaction by connecting principal and agular quantum numbers weighted with a filling factor
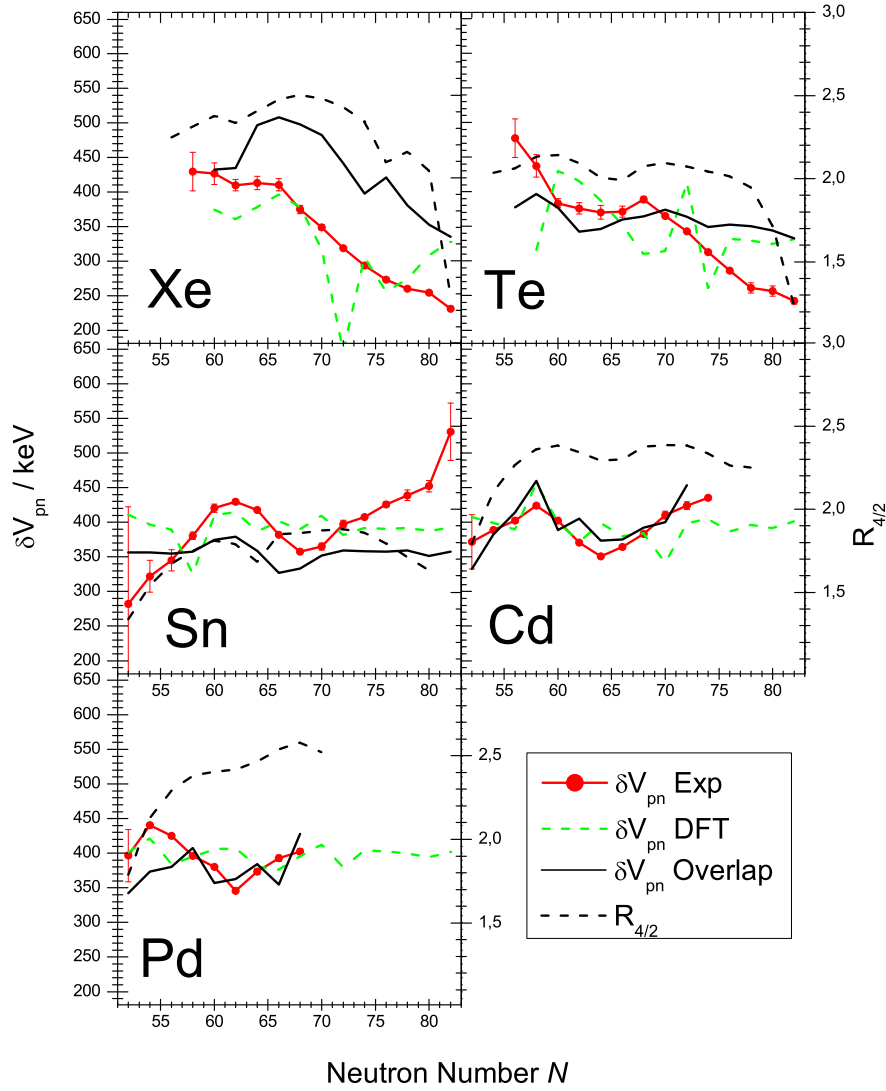
Fig. 7.10: Experimental δV_{pn} values (red circles, left ordinate) and those determined from nuclear density functional theory calculations [SCC$^+$07] (green dashed line, left ordinate) for Pd, Cd, Sn, Te, and Xe even-even nuclides as compared to the overlap of the last neutron and last proton orbits (black solid line, right ordinate). The black dashed line (left ordinate) indicates the $R_{4/2}$ of the even-even nuclides.

from the pairing model, the agreement of the overlap model with the experimental δV_{pn} values is remarkable.

It shall be added, that the overlap model is not expected to work so well further away from the close shells, because of the onset of collectivity. For a test of its validity it would be interesting to study in the vicinity of ^{208}Pb and beyond ^{132}Sn on the neutron-rich side.

8. SUMMARY AND CONCLUSION

In the present work, mass determinations of the eleven neutron-deficient nuclides $^{99-109}$Cd, of ten neutron-rich silver nuclides $^{112,114-121,123}$Ag, and seven neutron-rich cadmium nuclides $^{114,120,122-124,126,128}$Cd are reported. Due to the clean production of the neutron-deficient nuclides it was possible to reduce the experimental uncertainties down to 2 keV, whereas the measurements of neutron-rich nuclides were hampered by the presence of contaminations from more stable In and Cs nuclides. In the case of ^{99}Cd and ^{123}Ag the masses were determined for the first time and for the other nuclides the mass uncertainties could be reduced by up to a factor of 50 as in the case of ^{100}Cd.

In the case of a potential isomeric mixture as for ^{115,117,119}Ag and ^{123}Cd, where no assignment to either the ground state or the excited state was possible, the experimental results were adjusted accordingly. Afterwards all results were included in the framework of the atomic-mass evaluation and thus linked and compared with other experimental data. In the case of the neutron-deficient Cd nuclides a conflict between the mass values obtained in the present work and those published by the JYFLTRAP group [EEH$^+$] could be solved by performing an atomic-mass evaluation. Thus, it was revealed that reason for the conflict was a different value of the JYFLTRAP reference mass ^{96}Mo. Furthermore, a reduction of the mass uncertainty and a slight increase of the mass of ^{100}In were obtained.

These mass measurements are an important step towards an understanding of the physics of the rp process that will enable a more reliable determination of the composition of the produced material at $A = 99$. It has been shown that the mass of ^{99}Cd strongly affects the $A = 99$ production in an X-ray burst model, and that uncertainties have been significantly reduced from more than an order of magnitude to about a factor of 3. The dominant source of uncertainty is now the mass of ^{100}In.

In principle, other uncertainties will also contribute. These include those of masses of lighter Cd isotopes, where similar rp-process branchpoints occur and which might affect feeding into the ^{99}Cd branchpoint. In addition, nuclear reaction rate uncertainties will also play a role. However, as reaction rates affect branchings in a linear fashion, while mass differences enter exponentially, mass uncertainties will tend to dominate [Sch06]. Also, which reaction rates are important depends largely on nuclear masses. For example, for low $S_p(^{100}$In$)$ a (p,γ)-(γ,p) equilibrium will be established between ^{99}Cd and ^{100}In and the ^{100}In(p,γ) reaction rate would affect the $A = 99$ production, while for larger $S_p(^{100}$In$)$ the ^{99}Cd(p,γ) reaction rate might be more relevant. Therefore, the mass uncertainties should be addressed first. Once they are under control, further improvements might be possible by constraining proton capture rates.

The presented results are relevant for any rp-process scenario with a reaction flow through the ^{99}Cd region. Here, an X-ray burst model has been used to investigate in detail the impact of the present measurements on such an rp process. The νp process in core collapse supernovae might be another possible scenario for an rp process in the ^{99}Cd region. It it is planed to also explore whether in that case mass uncertainties have a similar impact on the final composition.

On the neutron-rich side of the valley of stability for the Cd and Ag chains of nuclides, the r process has not yet been reached. Further technical development on suppression of contaminants are required. This includes improvements on the ISOLDE side, e.g., by improving the selectivity of the

transfer line or on the ISOLTRAP setup by implementing an electrostatic ion beam trap for a fast and efficient isobaric selection.

Nevertheless the obtained results contribute to the knowledge of nuclear structure. The trends in the two-neutron separation-energy S_{2n} and the interaction between the last neutrons and last protons δV_{pn} were corrected to more smooth evolutions, as already seen in other regions of the nuclear chart. The strongest corrections have been observed for even-N nuclides, were more new experimental data are available. Thus, new measurements on odd-N nuclides are suggested. This also is underlined by the trends observed in the Garvey-Kelson relations for the neutron-rich Cd nuclides.

Furthermore, it has been shown, that the prominent structure of the δV_{pn} for an entire chain of nuclides including inflexion points can be reproduced by using simple relations between quantum numbers of the occupied orbits. This approach connects ten values for each nuclide with only one adjusted parameter. This has been investigated for 63 δV_{pn} values of even-even nuclides in the vicinity of $Z = 50$ and $50 \le N \le 82$. The simple model works remarkably well for the elements Cd, Sn, and Te. Small deviation have been observed for the Xe and Pd nuclides which were explained with the limitations of the model to the vicinity of the close shells, where the nuclides have only few valence protons and neutrons. Thus, it would be interesting to study the overlap model in the vicinity of the doubly magic nuclide ^{208}Pb and also for more neutron-rich nuclides in the region of ^{132}Sn.

BIBLIOGRAPHY

[ABBW03]   G. Audi, O. Bersillon, J. Blachot, A. H. Wapstra, *The evaluation of nuclear and decay properties*, Nucl. Phys. A, 729(1):3 – 128, the 2003 NUBASE and Atomic Mass Evaluations, **2003**

[ABG+95]   A. Aprahamian, D. S. Brenner, R. Gill, A. Piotrowski, R. F. Casten, Privat Communication to G. Audi, **1995**

[ADLW86]   G. Audi, W. G. Davies, G. E. Lee-Whiting, *A method of determining the relative importance of particular data on selected parameters in the least-squares analysis of experimental data*, Nucl. Instrum. Meth. A, 249(2–3):443–450, **1986**

[AG89]   E. Anders, N. Grevesse, *Abundances of the elements: Meteoritic and solar*, Geochim. Cosmochim. Acta, 53(1):197 – 214, **1989**

[AG03]   M. Arnould, S. Goriely, *The p-process of stellar nucleosynthesis: Astrophysics and nuclear physics status*, Phys. Rep., 384(1-2):1 – 84, **2003**

[AGT07]   M. Arnould, S. Goriely, K. Takahashi, *The r-process of stellar nucleosynthesis: Astrophysics and nuclear physics achievements and mysteries*, Phys. Rep., 450(4-6):97 – 213, **2007**

[AHLR82]   K. Aleklett, P. Hoff, E. Lund, G. Rudstam, *Total β-decay energies and mass systematics of neutron-rich silver and cadmium isotopes*, Phys. Rev. C, 26(3):1157–1166, **1982**

[AK64]   P. W. Anderson, Y. B. Kim, *Hard superconductivity: theory of the motion of Abrikosov flux lines*, Rev. Mod. Phys., 36(1):39–43, **1964**

[APDT95]   Y. Aboussir, J. M. Pearson, A. K. Dutta, F. Tondeur, *Nuclear mass formula via an approximation to the Hartree–Fock method*, At. Data Nucl. Data Tables, 61(1):127 – 176, **1995**

[AW95]   G. Audi, A. H. Wapstra, *The 1995 update to the atomic mass evaluation*, Nucl. Phys. A, 595(4):409 – 480, **1995**

[AWT03]   G. Audi, A. H. Wapstra, C. Thibault, *The AME2003 atomic mass evaluation (II). Tables, graphs and references*, Nucl. Phys. A, 729(1):337–676, **2003**

[BAA+00]   D. Beck, F. Ames, G. Audi, G. Bollen, F. Herfurth, H.-J. Kluge, A. Kohl, M. König, D. Lunney, I. Martel, R. B. Moore, H. Raimbault-Hartmann, E. Schark, S. Schwarz, M. de Saint Simon, J. Szerypo, the ISOLDE Collaboration, *Accurate masses of unstable rare-earth isotopes by ISOLTRAP*, Eur. Phys. J. A, 8(3):307–329, **2000**

[BAB$^+$05]   M. Block, D. Ackermann, D. Beck, K. Blaum, M. Breitenfeldt, A. Chauduri, A. Doe-mer, S. Eliseev, D. Habs, S. Heinz, F. Herfurth, F. P. Heßberger, S. Hofmann, H. Geissel, H.-J. Kluge, V. Kolhinen, G. Marx, J. B. Neumayr, M. Mukherjee, M. Petrick, W. Plass, W. Quint, S. Rahaman, C. Rauth, D. R. C. Scheidenberger, L. Schweikhard, M. Suhonen, P. G. Thirolf, Z. Wang, C. Weber, *The ion-trap facility SHIPTRAP*, Eur. Phys. J. A, 25:s1.49–s1.50, **2005**

[BAB$^+$08]   S. Baruah, G. Audi, K. Blaum, M. Dworschak, S. George, C. Guénaut, U. Hager, F. Herfurth, A. Herlert, A. Kellerbauer, H.-J. Kluge, D. Lunney, H. Schatz, L. Schweikhard, C. Yazidjian, *Mass measurements beyond the major r-process waiting point ^{80}Zn*, Phys. Rev. Lett., 101(26):262501, **2008**

[BB36]   H. A. Bethe, R. F. Bacher, *Stationary states of nuclei*, Rev. Mod. Phys., 8(2):82, **1936**

[BBB$^+$04]   D. Beck, K. Blaum, H. Brand, F. Herfurth, S. Schwarz, *A new control system for ISOLTRAP*, Nucl. Instrum. Meth. A, 527:567–579, **2004**

[BBB$^+$08]   M. Breitenfeldt, S. Baruah, K. Blaum, A. Herlert, M. Kretzschmar, F. Martinez, G. Marx, L. Schweikhard, N. Walsh, *The elliptical Penning trap: Experimental investigations and simulations*, Int. J. Mass Spectrom., 275(1-3):34 – 44, **2008**

[BBB$^+$09]   D. Beck, K. Blaum, G. Bollen, P. Delahaye, S. George, C. Guénaut, F. Herfurth, A. Herlert, D. Lunney, L. Schweikhard, C. Yazidjian, *Electric and magnetic field optimization procedure for Penning trap mass spectrometers*, Nucl. Instrum. Meth. A, 598(2):635 – 641, **2009**

[BBFH57]   E. M. Burbidge, G. R. Burbidge, W. A. Fowler, F. Hoyle, *Synthesis of the elements in stars*, Rev. Mod. Phys., 29(4):547–650, **1957**

[BBK$^+$96]   G. Bollen, S. Becker, H. J. Kluge, M. König, R. B. Moore, T. Otto, H. Raimbault-Hartmann, G. Savard, L. Schweikhard, H. Stolzenberg, *ISOLTRAP: a tandem Penning trap system for accurate on-line mass determination of short-lived isotopes*, Nucl. Instrum. Meth. A, 368(3):675 – 697, **1996**

[BCC06]   D. S. Brenner, R. B. Cakirli, R. F. Casten, *Valence proton-neutron interactions throughout the mass surface*, Phys. Rev. C, 73(3):034315, **2006**

[BCE$^+$08]   E. Bouquerel, R. Catherall, M. Eller, J. Lettry, S. Marzari, T. Stora, *Beam purification by selective trapping in the transfer line of an ISOL target unit*, Nucl. Instrume. Meth. B, 266(19-20):4298 – 4302, **2008**

[BCH$^+$86]   V. R. Bom, P. C. Coops, R. W. Hollander, E. Coenen, K. Deneffe, P. Van Duppen, M. Huyse, *The determination of the beta decay energies of $^{105-108}In$*, Z. Phys. A, 325:149–155, **1986**

[Bec70]   E. Beck, Proc. 2nd Int. Conf. Nuclei far from Stability NUFAST, 2, **1970**

[BFH$^+$08]   J. Barea, A. Frank, J. G. Hirsch, P. V. Isacker, S. Pittel, V. Velázquez, *Garvey-Kelson relations and the new nuclear mass tables*, Phys. Rev. C, 77(4):041304, **2008**

[BG86]   L. S. Brown, G. Gabrielse, *Geonium theory: Physics of a single electron or ion in a Penning trap*, Rev. Mod. Phys., 58(1):233–311, **1986**

[BHC+88]   V. R. Bom, R. W. Hollander, E. Coenen, K. Deneffe, P. Van Duppen, M. Huyse, *The beta-decay energies of ^{103}In and ^{104}In*, Z. Phys. A, 331:21–27, **1988**

[BHR03]   M. Bender, P.-H. Heenen, P.-G. Reinhard, *Self-consistent mean-field models for nuclear structure*, Rev. Mod. Phys., 75(1):121–180, **2003**

[Bil97]   L. Bildsten, *Thermonuclear burning on rapidly accreting neutron stars*, arXiv:astro-ph/9709094v1, **1997**

[BKK+92]   G. Bollen, H.-J. Kluge, M. König, T. Otto, G. Savard, H. Stolzenberg, R. B. Moore, G. Rouleau, G. Audi, I. Collaboration, *Resolution of nuclear ground and isomeric states by a Penning trap mass spectrometer*, Phys. Rev. C, 46(6):R2140–R2143, **1992**

[Bla06]   K. Blaum, *High-accuracy mass spectrometry with stored ions*, Phys. Rep., 425(1):1 – 78, **2006**

[BLBR71]   H. Bakhru, I. M. Ladenbauer-Bellis, I. Rezanka, *Level structure of ^{109}Cd from the decay of ^{109}In*, Phys. Rev. C, 3(2):937–944, **1971**

[BMSS90]   G. Bollen, R. B. Moore, G. Savard, H. Stolzenberg, *The accuracy of heavy-ion mass measurements using time of flight-ion cyclotron resonance in a Penning trap*, J. of Appl. Phys., 68(9):4355–4374, **1990**

[Boe09]   C. Boehm, *Setup of a carbon-cluster laser ion source and the application of the invariance theorem at ISOLTRAP*, Diploma thesis, **2009**

[Bol01]   G. Bollen, *Mass measurements of short-lived nuclides with ion traps*, Nuclear Physics A, 693(1-2):3 – 18, **2001**

[BPFC64]   E. L. Bahn, B. D. Pate, R. D. Fink, C. D. Coryell, *Decay of 20-minute ^{115}Ag*, Phys. Rev., 136(3B):B603–B617, **1964**

[BPR+99]   M. P. Bradley, J. V. Porto, S. Rainville, J. K. Thompson, D. E. Pritchard, *Penning Trap Measurements of the masses of ^{133}Cs, $^{87,85}Rb$, and ^{23}Na with uncertainties ≤ 0.2 ppb*, Phys. Rev. Lett., 83(22):4510–4513, **1999**

[BQ81]   M. Brack, P. Quentin, *The Strutinsky method and its foundation from the Hartree-Fock-Bogoliubov approximation at finite temperature*, Nucl. Phys. A, 361(1):35 – 82, **1981**

[Bro05]   B. A. Brown, *Lecture notes in nuclear structure physics*, http://www.nscl.msu.edu/ brown/Jina-workshop/BAB-lecture-notes.pdf, **2005**

[BSVE79]   F. Braumandl, K. Schreckenbach, T. Von Egidy, *Precision measurements of neutron binding energies of ^{28}Al, ^{92}Zr, ^{114}Cd, ^{165}Dy, ^{168}Er, ^{200}Hg, and ^{239}U*, Nucl. Instr. Meth., 166(2):243 – 250, **1979**

[CAM+96]   M. Chartier, G. Auger, W. Mittig, A. Lépine-Szily, L. K. Fifield, J. M. Casandjian, M. Chabert, J. Fermé, A. Gillibert, M. Lewitowicz, M. Mac Cormick, M. H. Moscatello, O. H. Odland, N. A. Orr, G. Politi, C. Spitaels, A. C. C. Villari, *Mass measurement of ^{100}Sn*, Phys. Rev. Lett., 77(12):2400–2403, **1996**

[Cas00]   R. F. Casten, *Nuclear structure from a simple perspective*, 2nd Ed., Oxford University Press, **2000**

[CBB$^+$82]   G. M. Crawley, W. Benenson, G. Bertsch, S. Gales, D. Weber, B. Zwieglinski, *Pairing model predictions for (p, t) experiments on the cadmium isotopes*, Phys. Lett. B, 109(1-2):8 – 10, **1982**

[CBB$^+$03]   J. Clark, R. C. Barber, C. Boudreau, F. Buchinger, J. E. Crawford, S. Gulick, J. C. Hardy, A. Heinz, J. K. P. Lee, R. B. Moore, G. Savard, D. Seweryniak, K. S. Sharma, G. Sprouse, J. Vaz, J. C. Wang, Z. Zhou, *Improvements in the injection system of the Canadian Penning trap mass spectrometer*, Nucl. Instr. Meth. B, 204:487 – 491, **2003**

[CBCM05]   R. B. Cakirli, D. S. Brenner, R. F. Casten, E. A. Millman, *Proton-neutron interactions and the new atomic masses*, Phys. Rev. Lett., 94(9):092501, **2005**

[CD75]   R. Chapman, G. D. Dracoulis, *The reaction $^{106}Cd(^3He,\alpha)^{105}Cd$*, J. Phys. G, 1(6):657–664, **1975**

[CLGK03]   R. Catherall, J. Lettry, S. Gilardoni, U. Köster, *Radioactive ion beams produced by neutron-induced fission at ISOLDE*, Nucl. Instr. Meth. B, 204:235 – 239, **2003**

[CLP$^+$09]   L. Chen, Y. A. Litvinov, W. R. Plaß, K. Beckert, P. Beller, F. Bosch, D. Boutin, L. Caceres, R. B. Cakirli, J. J. Carroll, R. F. Casten, R. S. Chakrawarthy, D. M. Cullen, I. J. Cullen, B. Franzke, H. Geissel, J. Gerl, M. Górska, G. A. Jones, A. Kishada, R. Knöbel, C. Kozhuharov, S. A. Litvinov, Z. Liu, S. Mandal, F. Montes, G. Münzenberg, F. Nolden, T. Ohtsubo, Z. Patyk, Z. Podolyák, R. Propri, S. Rigby, N. Saito, T. Saito, C. Scheidenberger, M. Shindo, M. Steck, P. Ugorowski, P. M. Walker, S. Williams, H. Weick, M. Winkler, H.-J. Wollersheim, T. Yamaguchi, *Publisher's note: schottky mass measurement of the ^{208}Hg isotope: implication for the proton-neutron interaction strength around doubly magic ^{208}Pb*, Phys. Rev. Lett., 102(13):139904, **2009**

[CR66]   R. C. Catura, J. R. Richardson, *On the decay of ^{106}In*, Nucl. Phys., 82(2):471 – 480, **1966**

[CTT91]   J. J. Cowan, F.-K. Thielemann, J. W. Truran, *The r-process and nucleochronology*, Phys. Rep., 208(4-5):267 – 394, **1991**

[Cyb]   R. Cyburt, to be published

[DAB$^+$06]   P. Delahaye, G. Audi, K. Blaum, F. Carrel, S. George, F. Herfurth, A. Herlert, A. Kellerbauer, H.-J. Kluge, D. Lunney, L. Schweikhard, C. Yazidjian, *High-accuracy mass measurements of neutron-rich Kr isotopes*, Phys. Rev. C, 74(3):034331, **2006**

[DAB$^+$08]   M. Dworschak, G. Audi, K. Blaum, P. Delahaye, S. George, U. Hager, F. Herfurth, A. Herlert, A. Kellerbauer, H.-J. Kluge, D. Lunney, L. Schweikhard, C. Yazidjian, *Restoration of the $N = 82$ shell gap from direct mass measurements of $^{132,134}Sn$*, Phys. Rev. Lett., 100(7):072501, **2008**

[DBB$^+$06]   J. Dilling, R. Baartman, P. Bricault, M. Brodeur, L. Blomeley, F. Buchinger, J. Crawford, J. R. C. López-Urrutia, P. Delheij, M. Froese, G. P. Gwinner, Z. Ke, J. K. P. Lee, R. B. Moore, V. Ryjkov, G. Sikler, M. Smith, J. Ullrich, J. Vaz, *Mass measurements on highly charged radioactive ions, a new approach to high precision with TITAN*, Int. J. Mass Spectrom., 251(2-3):198 – 203, **2006**

[DFT84]   J. Dobaczewski, H. Flocard, J. Treiner, *Hartree-Fock-Bogolyubov description of nuclei near the neutron-drip line*, Nucl. Phys. A, 422(1):103 – 139, **1984**

[DKN83]   R. A. Dewberry, R. T. Kouzes, R. A. Naumann, *Mass of ^{104}Cd*, Phys. Rev. C, 27(2):892–893, **1983**

[DRJ63]   R. A. Damerow, R. R. Ries, W. H. Johnson, *Atomic masses from ruthenium to xenon*, Phys. Rev., 132(4):1673–1681, **1963**

[DZ95]   J. Duflo, A. P. Zuker, *Microscopic mass formulas*, Phys. Rev. C, 52(1):R23–R27, **1995**

[EEH$^+$]   V.-V. Elomaa, T. Eronen, U. Hager, J. Hakala, A. Jokinen, A. Kankainen, I. D. Moore, S. Rahaman, J. Rissanen, V. Rubchenya, C. Weber, J. Äystö, Eur. Phys. J. A, **2009**

[EMA$^+$78] H. W. Ellis, E. W. McDaniel, D. L. Albritton, L. A. Viehland, S. L. Lin, E. A. Mason, *Transport properties of gaseous ions over a wide energy range. Part II*, Atomic Data and Nuclear Data Tables, 22(3):179 – 217, **1978**

[END09]   *Evaluated Nuclear Structure Data File (ENSDF)*, **2009**

[FCS$^+$08] J. Fallis, J. A. Clark, K. S. Sharma, G. Savard, F. Buchinger, S. Caldwell, J. E. Crawford, C. M. Deibel, J. L. Fisker, S. Gulick, A. A. Hecht, D. Lascar, J. K. P. Lee, A. F. Levand, G. Li, B. F. Lundgren, A. Parikh, S. Russell, M. Scholte-van de Vorst, N. D. Scielzo, R. E. Segel, H. Sharma, S. Sinha, M. Sternberg, T. Sun, I. Tanihata, J. Van Schelt, J. C. Wang, Y. Wang, C. Wrede, Z. Zhou, *Determination of the proton separation energy of ^{93}Rh from mass measurements*, Phys. Rev. C, 78(2):022801, **2008**

[FCZ75]   W. A. Fowler, G. R. Caughlan, B. A. Zimmerman, *Thermonuclear reaction rates, II*, Ann. Rev. Astro. and Astrophys., 13(1):69–112, **1975**

[FDPA84]   B. W. Filippone, C. N. Davids, R. C. Pardo, J. Äystö, *Mass and low-lying levels of $^{106,108}In$ from the $^{106,108}Cd(p,n)\gamma$ reactions*, Phys. Rev. C, 29(6):2118–2125, **1984**

[FGM08]   B. Franzke, H. Geissel, G. Münzenberg, Mass Spectrom. Rev., 27(5):428–469, **2008**

[FHP09]   J. L. Fisker, R. D. Hoffman, J. Pruet, *On the origin of the lightest molybdenum isotopes*, Astrophys. J. Lett., 690(2):L135–L139, **2009**

[FLM$^+$06] R. B. Firestone, R. M. Lindstrom, G. L. Molnar, S. M. Mughabghab, A. V. R. Reddy, Z. Revay, V. H. Tan, C. M. Zhou, R. Paviotti-Corcuera, International Atomic Energy Agency, report, **2006**

[FMPL$^+$06] C. Fröhlich, G. Martínez-Pinedo, M. Liebendörfer, F.-K. Thielemann, E. Bravo, W. R. Hix, K. Langanke, N. T. Zinner, *Neutrino-induced nucleosynthesis of $A > 64$ nuclei: The νp process*, Phys. Rev. Lett., 96(14):142502, **2006**

[FRH$^+$05] M. A. Fehr, M. Rehkämper, A. N. Halliday, U. Wiechert, B. Hattendorf, D. Günther, S. Ono, J. L. Eigenbrode, D. Rumble, *Tellurium isotopic composition of the early solar system–A search for effects resulting from stellar nucleosynthesis, ^{126}Sn decay, and mass-independent fractionation*, Geochim. Cosmochim. Acta, 69(21):5099 – 5112, **2005**

[FZE$^+$90]   B. Fogelberg, Y. Zongyuan, B. Ekström, E. Lund, K. Aleklett, L. Sihver, *Isomerism, total decay energies, and absolute γ-ray intensities of the heavy Pd and Ag isotopes*, Z. Phys. A, 337:251–255, **1990**

[GAB$^+$05]   C. Guénaut, G. Audi, D. Beck, K. Blaum, G. Bollen, P. Delahaye, F. Herfurth, A. Kellerbauer, H.-J. Kluge, D. Lunney, S. Schwarz, L. Schweikhard, C. Yazidjian, *Mass measurements of $^{56-57}Cr$ and the question of shell reincarnation at $N = 32$*, J. Phys. G, 31(10):S1765–S1770, **2005**

[GBS$^+$07]   S. Gupta, E. F. Brown, H. Schatz, P. Möller, , K.-L. Kratz, *Heating in the accreted neutron star ccean: Implications for superburst ignition*, The Astrophysical Journal, 662(2):1188–1197, **2007**

[GCP09a]   S. Goriely, N. Chamel, J. M. Pearson, **2009**

[GCP09b]   S. Goriely, N. Chamel, J. M. Pearson, *Skyrme-Hartree-Fock-Bogoliubov nuclear mass formulas: crossing the 0.6 MeV accuracy threshold with microscopically deduced pairing*, Phys. Rev. Lett., 102(15):152503, **2009**

[GGG$^+$70]   W. Goedbloed, S. C. Goverse, C. P. Gerner, A. Brinkman, J. Blok, *An internal source scintillation spectrometer*, Nucl. Instr. Meth., 88(2):197 – 204, **1970**

[GGJ$^+$69]   G. T. Garvey, W. J. Gerace, R. L. Jaffe, I. Talmi, I. Kelson, *Set of nuclear-mass relations and a resultant mass table*, Rev. Mod. Phys., 41(4):S1–S80, **1969**

[Gho95]   P. K. Ghosh, *Ion traps*, Oxford University Press, **1995**

[GK66]   G. T. Garvey, I. Kelson, *New nuclidic mass relationship*, Phys. Rev. Lett., 16(5):197–200, **1966**

[GKT80]   G. Gräff, H. Kalinowsky, J. Traut, *A direct determination of the proton electron mass ratio*, Z. Phys. A, 297(1):35–39, **1980**

[GSH$^+$02]   S. Goriely, M. Samyn, P.-H. Heenen, J. M. Pearson, F. Tondeur, *Hartree-Fock mass formulas and extrapolation to new mass data*, Phys. Rev. C, 66(2):024326, **2002**

[GSP07]   S. Goriely, M. Samyn, J. M. Pearson, *Further explorations of Skyrme-Hartree-Fock-Bogoliubov mass formulas. VII. Simultaneous fits to masses and fission barriers*, Phys. Rev. C, 75(6):064312, **2007**

[GT07]   J. D. Gilmour, G. Turner, *Constraints on nucleosynthesis from xenon isotopes in presolar material*, Astrophys. J., 657(1):600–608, **2007**

[GZL$^+$97]   J. Guo, K. Zhao, X. Lu, Y. Cheng, T. Li, C. Fu, S. Li, Chin. J. Nucl. Phys., 19:180, **1997**

[HDK$^+$01]   F. Herfurth, J. Dilling, A. Kellerbauer, G. Bollen, S. Henry, H.-J. Kluge, E. Lamour, D. Lunney, R. B. Moore, C. Scheidenberger, S. Schwarz, G. Sikler, J. Szerypo, *A linear radiofrequency ion trap for accumulation, bunching, and emittance improvement of radioactive ion beams*, Nucl. Instr. Meth. A, 469(2):254 – 275, **2001**

[Hea09]   *Datasheet Heatwave alkali ionsources*, HeatWave Labs, Inc. ,195 Aviation Way, Suite 100, Watsonville, CA 95076-2069, USA, **2009**

[HEE$^+$07] U. Hager, V.-V. Elomaa, T. Eronen, J. Hakala, A. Jokinen, A. Kankainen, S. Rahaman, S. Rinta-Antila, A. Saastamoinen, T. Sonoda, J. Äystö, *Precision mass measurements of neutron-rich Tc, Ru, Rh, and Pd isotopes*, Phys. Rev. C, 75(6):064302, **2007**

[Her03] F. Herfurth, *Segmented linear RFQ traps for nuclear physics*, Nucl. Instrum. Meth. B, 204:587 – 591, **2003**

[Her09] F. Herfurth, *N=Z masses*, **2009**

[HWFZ76] J. A. Holmes, S. E. Woosley, W. A. Fowler, B. A. Zimmerman, *Tables of thermonuclear-reaction-rate data for neutron-induced reactions on heavy nuclei*, At. Data and Nucl. Data Tables, 18(4):305 – 412, **1976**

[IRYY62] H. Inoue, J.-Z. Ruan, S. Yasukawa, Y. Yoshizawa, *Study of the cadmium isotopes (VI): Beta and gamma ray spectroscopy of ^{112}Ag*, Nucl. Phys., 38:50 – 62, **1962**

[ISO09] *Isolde Homepage*, http://isolde.web.cern.ch/ISOLDE/, **2009**

[Jac83] J. Jackson, *Klassische Elektrodynamik*, 3rd Ed., de Gryter Verlag, Berlin, **1983**

[JCF$^+$97] Y. Jading, R. Catherall, V. N. Fedoseyev, A. Jokinen, O. C. Jonsson, T. Kautzsch, I. Klöckl, K.-L. Kratz, E. Kugler, J. Lettry, V. I. Mishin, H. L. Ravn, F. Scheerer, O. Tengblad, P. V. Duppen, W. B. Walters, A. Wöhr, *Production of radioactive Ag ion beams with a chemically selective laser ion source*, Nucl. Instrum. Meth. B, 126(1-4):76 – 80, international Conference on Electromagnetic Isotope Separators and Techniques Related to Their Applications, **1997**

[JEH$^+$06] A. Jokinen, T. Eronen, U. Hager, I. Moore, H. Penttil, S. Rinta-Antila, J. yst, *Precision experiments on exotic nuclei at IGISOL*, Int. J. Mass Spectrom., 251(2-3):204 – 211, **2006**

[JM88] J. Jänecke, P. J. Masson, *Mass predictions from the Garvey-Kelson mass relations*, At. Data Nucl. Data Tab., 39(2):265 – 271, **1988**

[Joh53] F. A. Johnson, *The decay of ^{105}Cd*, Can. J. Phys., 31(7):11361147, **1953**

[KBB$^+$03] A. Kellerbauer, K. Blaum, G. Bollen, F. Herfurth, H.-J. Kluge, M. Kuckein, E. Sauvan, C. Scheidenberger, L. Schweikhard, *From direct to absolute mass measurements: A study of the accuracy of ISOLTRAP*, Eur. Phys. J. D, 22(1):53–64, **2003**

[KBC$^+$98] M. Karny, L. Batist, D. Cano, R. Collatz, A. Gadea, M. Gierlik, R. Grzywacz, A. Guglielmetti, M. Hellström, Z. Hu, Z. Janas, R. Kirchner, F. Moroz, A. Piechaczek, A. Plochocki, E. Roeckl, B. Rubio, K. Rykaczewski, M. Shibata, J. Szerypo, J. Tain, V. Wittmann, A. Wöhr, Ann. Rep. GSI, **1998**

[KBK$^+$91] H. Keller, R. Barden, R. Kirchner, O. Klepper, E. Roeckl, D. Schardt, I. S. Grant, A. Płochocki, K. Rykaczewski, J. Szerypo, J. Zylicz, *Q_{EC} value and Gamow-Teller strength of the ^{102}Cd EC/β^+ decay*, Z. Phys. A, 339:335–361, **1991**

[KBK$^+$95] M. König, G. Bollen, H.-J. Kluge, T. Otto, J. Szerypo, *Quadrupole excitation of stored ion motion at the true cyclotron frequency*, Int. J. Mass Spectrom., 142(1-2):95 – 116, **1995**

[KEB⁺08]   A. Kankainen, V.-V. Elomaa, L. Batist, S. Eliseev, T. Eronen, U. Hager, J. Hakala, A. Jokinen, I. D. Moore, Y. N. Novikov, H. Penttilä, A. Popov, S. Rahaman, S. Rinta-Antila, J. Rissanen, A. Saastamoinen, D. M. Seliverstov, T. Sonoda, G. Vorobjev, C. Weber, J. Äystö, *Mass measurements and implications for the energy of the high-spin isomer in* ^{94}Ag, Phys. Rev. Lett., 101(14):142503, **2008**

[KFA⁺03]   U. Köster, V. N. Fedoseyev, A. N. Andreyev, U. C. Bergmann, R. Catherall, J. Cederkäll, M. Dietrich, H. D. Witte, D. V. Fedorov, L. Fraile, S. Franchoo, H. Fynbo, U. Georg, T. Giles, M. Gorska, M. Hannawald, M. Huyse, A. Joinet, O. C. Jonsson, K. L. Kratz, K. Kruglov, C. Lau, J. Lettry, V. I. Mishin, M. Oinonen, K. Partes, K. Perjrvi, B. Pfeiffer, H. L. Ravn, M. D. Seliverstov, P. Thirolf, K. V. de Vel, P. V. Duppen, J. V. Roosbroeck, L. Weissman, *On-line yields obtained with the ISOLDE RILIS*, Nucl. Instrum. Meth. B, 204:347 – 352, **2003**

[KS65]   W. Kohn, L. J. Sham, *Self-consistent equations including exchange and correlation effects*, Phys. Rev., 140(4A):A1133–A1138, **1965**

[KTUY05]   H. Koura, T. Tachibana, M. Uno, M. Yamada, *Nuclidic mass formula on a spherical basis with an improved even-odd term*, Progr. Theor. Phys, 113:305–325, **2005**

[Kug00]   E. Kugler, *The ISOLDE facility*, Hyperf. Interact., 129:23– 42, **2000**

[KUTY00]   H. Koura, M. Uno, T. Tachibana, M. Yamada, *Nuclear mass formula with shell energies calculated by a new method*, Nucl. Phys. A, 674(1-2):47 – 76, **2000**

[LA09]   D. Lunney, G. Audi, priv. Communication, **2009**

[LCD⁺97]   J. Lettry, R. Catherall, P. Drumm, P. V. Duppen, A. H. M. Evensen, G. J. Focker, A. Jokinen, O. C. Jonsson, E. Kugler, H. Ravn, *Pulse shape of the ISOLDE radioactive ion beams*, Nucl. Instrum. Meth. B, 126(1-4):130 – 134, **1997**

[LGJW62]   N. L. Lark, P. F. A. Goudsmit, J. E. J. Jansen, J. F. W.and Oberski, A. H. Wapstra, *Excited states of* ^{107}Ag, Nucl. Phys., 35:582 – 584, IN3–IN4, 585–592, **1962**

[LGR⁺05]   Y. A. Litvinov, H. Geissel, T. Radon, F. Attallah, G. Audi, K. Beckert, F. Bosch, M. Falch, B. Franzke, M. Hausmann, M. Hellstr *Mass measurement of cooled neutron-deficient bismuth projectile fragments with time-resolved Schottky mass spectrometry at the FRS-ESR facility*, Nucl. Phys. A, 756(1-2):3 – 38, **2005**

[LL79]   L. Landau, E. Lifschitz, *Lehrbuch der theoretischen Physik, Band I*, 9th Ed., Akademie Verlag, Berlin, **1979**

[Lod03]   K. Lodders, *Solar system abundances and condensation temperatures of the elements*, Astrophys. J., 591(2):1220–1247, **2003**

[LPT03]   D. Lunney, J. M. Pearson, C. Thibault, *Recent trends in the determination of nuclear masses*, Rev. Mod. Phys., 75(3):1021–1082, **2003**

[LSW65]   H. Leutz, K. Schneckenberger, H. Wenninger, *Electron capture ratios in* ^{109}Cd *and internal conversion coefficients in* $^{109}Ag^{m}$, Nucl. Phys., 63(2):263 – 272, **1965**

[MAA+07]   A. Martín, D. Ackermann, G. Audi, K. Blaum, M. Block, A. Chaudhuri, Z. Di, S. Eliseev, R. Ferrer, D. Habs, F. Herfurth, F. P. Heßberger, S. Hofmann, H.-J. Kluge, M. Mazzocco, M. Mukherjee, J. B. Neumayr, Y. Novikov, W. Plaß, S. Rahaman, C. Rauth, D. Rodrguez, C. Scheidenberger, L. Schweikhard, P. G. Thirolf, G. Vorobjev, C. Weber, *Mass measurements of neutron-deficient radionuclides near the end-point of the rp-process with SHIPTRAP*, Eur. Phys. J. A, 34(4):341–348, **2007**

[MBB+08a] M. Mukherjee, D. Beck, K. Blaum, G. Bollen, P. Delahaye, J. Dilling, S. George, C. Guénaut, F. Herfurth, A. Herlert, A. Kellerbauer, H.-J. Kluge, U. Köster, D. Lunney, S. Schwarz, L. Schweikhard, C. Yazidjian, *Mass measurements and evaluation around $A = 22$*, Eur. Phys. J. A, 35(1):31–37, **2008**

[MBB+08b] M. Mukherjee, D. Beck, K. Blaum, G. Bollen, J. Dilling, S. George, F. Herfurth, A. Herlert, A. Kellerbauer, H.-J. Kluge, S. Schwarz, L. Schweikhard, C. Yazidjian, *ISOLTRAP: An on-line Penning trap for mass spectrometry on short-lived nuclides*, Eur. Phys. J. A, 35(1):1–29, **2008**

[MGL+07]   C. Mazzocchi, R. Grzywacz, S. N. Liddick, K. P. Rykaczewski, H. Schatz, J. C. Batchelder, C. R. Bingham, C. J. Gross, J. H. Hamilton, J. K. Hwang, S. Ilyushkin, A. Korgul, W. Królas, K. Li, R. D. Page, D. Simpson, J. A. Winger, *α decay of ^{109}I and its implications for the proton decay of ^{105}Sb and the astrophysical rapid proton-capture process*, Phys. Rev. Lett., 98(21):212501, **2007**

[MGW04]   F. G. Major, V. N. Gheorghe, G. Werth, *Charged particle traps*, Springer Berlin, **2004**

[MJAB+08] M. Marie-Jeanne, J. Alonso, K. Blaum, S. Djekic, M. Dworschak, U. Hager, A. Herlert, S. Nagy, R. Savreux, L. Schweikhard, S. Stahl, C. Yazidjian, *Towards a magnetic field stabilization at ISOLTRAP for high-accuracy mass measurements on exotic nuclides*, Nucl. Instrum. Meth. A, 587(2-3):464 – 473, **2008**

[MKB+04]   M. Mukherjee, A. Kellerbauer, D. Beck, K. Blaum, G. Bollen, F. Carrel, P. Delahaye, J. Dilling, S. George, C. Guénaut, F. Herfurth, A. Herlert, H.-J. Kluge, U. Köster, D. Lunney, S. Schwarz, L. Schweikhard, C. Yazidjian, *The mass of ^{22}Mg*, Phys. Rev. Lett., 93(15):150801, **2004**

[MNMS95]   P. Moller, J. R. Nix, W. D. Myers, W. J. Swiatecki, *Nuclear Ground-state masses and deformations*, At. Data Nucl. Data Tables, 59(2):185 – 381, **1995**

[MS66]   W. D. Myers, W. J. Swiatecki, *Nuclear masses and deformations*, Nucl. Phys., 81(1):1 – 60, **1966**

[MS69]   W. D. Myers, W. J. Swiatecki, *Average nuclear properties*, Ann. Phys., 55(3):395 – 505, **1969**

[MSB+73]   J. O. Meredith, F. C. G. Southon, R. C. Barber, P. Williams, H. E. Duckworth, *Precise atomic mass differences using peak-matching by computer*, Int. J. Mass Spectrom. and Ion Phys., 10(4):359 – 370, **1973**

[MT78]   Z. Matumoto, T. Tamura, *Decay Scheme of 20 min ^{115}Ag*, J. Phys. Soc. Jap., 44(4):1070–1077, **1978**

[NAB+09]   D. Neidherr, G. Audi, D. Beck, K. Blaum, C. Böhm, M. Breitenfeldt, R. B. Cakirli, R. F. Casten, S. George, F. Herfurth, A. Herlert, A. Kellerbauer, M. Kowalska, D. Lunney, E. Minaya-Ramirez, S. Naimi, E. Noah, L. Penescu, M. Rosenbusch, S. Schwarz, L. Schweikhard, T. Stora, *Discovery of ^{229}Rn and the structure of the heaviest Rn and Ra isotopes from Penning-trap mass measurements*, Phys. Rev. Lett., 102(11):112501, **2009**

[Noz62]   M. Nozawa, *Study of the cadmium isotopes (IV) β- and $^{\gamma}$-ray spectroscopy of ^{109}In*, Nucl. Phys., 36:411 – 430, **1962**

[NWSK54]   R. H. Nussbaum, A. H. Wapstra, M. J. Sterk, R. E. W. Kropveld, *Gamma rays in the decay of ^{112}Pd and ^{112}Ag*, Physica, 21(1-5):77 – 78, **1954**

[OH73]   M. A. Oothoudt, N. M. Hintz, *The (p,t) reactions on nuclei in the rare earth region*, Nucl. Phys. A, 213(2):221 – 266, **1973**

[PHW+06]   J. Pruet, R. D. Hoffman, S. E. Woosley, H.-T. Janka, , R. Buras, *Nucleosynthesis in early supernova winds. II. The role of neutrinos*, Astrophys. J., 644(2):1028–1039, **2006**

[PKBR78]   R. C. Pardo, E. Kashy, W. Benenson, L. W. Robinson, *Mass measurement of proton-rich, medium-weight nuclei by the (^3He, ^6He) reaction*, Phys. Rev. C, 18(3):1249–1253, **1978**

[PS90]   S. Piskoř, W. Schäferlingová, *Spectroscopic information on $^{13,14}C$, ^{15}N, ^{17}O, $^{29-31}Si$, ^{33}S, ^{28}Cl and $^{111,113,115,117}Cd$ from the (d,p) reaction*, Nucl. Phys. A, 510(2):301 – 321, **1990**

[Psa04]   D. Psaltis, *Accreting Neutron Stars and Black Holes: A Decade of Discoveries*, arXiv:astro-ph/0410536v1, **2004**

[RGW+06]   W. Rapp, J. Gorres, M. Wiescher, H. Schatz, F. Kappeler, *Sensitivity of p-process nucleosynthesis to nuclear reaction rates in a 25 $M_\odot$ supernova model*, Astrophys. J., 653(1):474–489, **2006**

[RHBB+97] H. Raimbault-Hartmann, D. Beck, G. Bollen, M. König, H.-J. Kluge, E. Schark, J. Stein, S. Schwarz, J. Szerypo, *A cylindrical Penning trap for capture, mass selective cooling, and bunching of radioactive ion beams*, Nucl. Instrum. Meth. A, 126(1-4):378 – 382, **1997**

[RKA+04]   D. Rodríguez, V. S. Kolhinen, G. Audi, J. Äystö, D. Beck, K. Blaum, G. Bollen, F. Herfurth, A. Jokinen, A. Kellerbauer, H. J. Kluge, M. Oinonen, H. Schatz, E. Sauvan, S. Schwarz, *Mass measurement on the rp-process waiting point ^{72}Kr*, Phys. Rev. Lett., 93(16):161104, **2004**

[RKA+05]   D. Rodríguez, V. S. Kolhinen, G. Audi, J. Äystö, D. Beck, K. Blaum, G. Bollen, F. Herfurth, A. Jokinen, A. Kellerbauer, H.-J. Kluge, M. Oinonen, H. Schatz, E. Sauvan, S. Schwarz, *Mass measurement on the rp-process waiting point ^{72}Kr*, Eur. Phys. J. A, 25:s1.41–s1.43, **2005**

[ROB98]   S. Richter, U. Ott, F. Begemann, *Tellurium in pre-solar diamonds as an indicator for rapid separation of supernova ejecta*, Nature, 391:261–263, **1998**

[RPG$^+$89]   K. Rykaczewski, A. Płochocki, I. S. Grant, H. Gabelmann, R. Barden, D. Schardt, J. Zylicz, G. Nyman, ISOLDE, *The Gamow-Teller beta decay of ^{100}Cd*, Z. Phys. A, 332:275–284, **1989**

[RTK97]   T. Rauscher, F.-K. Thielemann, K.-L. Kratz, *Nuclear level density and the determination of thermonuclear rates for astrophysics*, Phys. Rev. C, 56(3):1613–1625, **1997**

[RTP04]   S. Rainville, J. K. Thompson, D. E. Pritchard, *An ion balance for ultra-high-precision atomic mass measurements*, Science, 303(5656):334–338, **2004**

[RVV$^+$84]   G. Rotbard, M. Vergnes, J. Vernotte, G. Berrier Ronsin, G. M. Gales, S. and. Crawley, Bulletin Am. Phys. Soc., 29:1041, **1984**

[RWMM07]   M. Redshaw, E. Wingfield, J. McDaniel, E. G. Myers, *Mass and double-beta-decay Q value of ^{136}Xe*, Phys. Rev. Lett., 98(5):053003, **2007**

[SAB$^+$01]   H. Schatz, A. Aprahamian, V. Barnard, L. Bildsten, A. Cumming, M. Ouellette, T. Rauscher, F.-K. Thielemann, M. Wiescher, *End point of the rp process on accreting neutron stars*, Phys. Rev. Lett., 86(16):3471–3474, **2001**

[SAB$^+$05]   G. Sikler, G. Audi, D. Beck, K. Blaum, G. Bollen, F. Herfurth, A. Kellerbauer, H.-J. Kluge, D. Lunney, M. Oinonen, C. Scheidenberger, S. Schwarz, J. Szerypo, *Mass measurements on neutron-deficient Sr and neutron-rich Sn isotopes with the ISOLTRAP mass spectrometer*, Nucl. Phys. A, 763:45 – 58, **2005**

[SAB$^+$06]   G. Sikler, G. Audi, D. Beck, K. Blaum, G. Bollen, F. Herfurth, A. Kellerbauer, H.-J. Kluge, D. Lunney, M. Oinonen, C. Scheidenberger, S. Schwarz, J. Szerypo, C. Weber, *Erratum to: "Mass measurements on neutron-deficient Sr and neutron-rich Sn isotopes with the ISOLTRAP mass spectrometer" [Nucl. Phys. A 763 (2005) 45]*, Nucl. Phys. A, 768(1-2):160 – 160, **2006**

[SAEF87]   L. Spanier, K. Aleklett, B. Ekström, B. Fogelberg, *The Q(β) values of the heavy Cd and In isotopes*, Nucl. Phys. A, 474(2):359 – 372, **1987**

[SAG98]   H. Schatz, A. Aprahamian, J. G *rp-process nucleosynthesis at extreme temperature and density conditions*, Phys. Rep., 294(4):167 – 263, **1998**

[Sar82]   D. G. Sargood, *Charged particle reaction cross sections and nucleosynthesis*, Physics Reports, 93(2):61 – 116, **1982**

[SB06]   L. Schweikhard, G. Bollen, *Ultra-accurate mass determination and related topics*, Bd. 251, Elsevier, int. J. Mass Spectrom., **2006**

[SBB$^+$91]   G. Savard, S. Becker, G. Bollen, H.-J. Kluge, R. Moore, T. Otto, L. Schweikhard, H. Stolzenberg, U. Wiess, *A new cooling technique for heavy-ions in a Penning trap*, Phys. Lett. A, 158(5):247–252, **1991**

[SBB$^+$07]   P. Schury, C. Bachelet, M. Block, G. Bollen, D. A. Davies, M. Facina, C. M. Folden, C. Guénaut, J. Huikari, E. Kwan, A. Kwiatkowski, D. J. Morrissey, R. Ringle, G. K. Pang, A. Prinke, J. Savory, H. Schatz, S. Schwarz, C. S. Sumithrarachchi, T. Sun, *Precision mass measurements of rare isotopes near $N = Z = 33$ produced by fast beam fragmentation*, Phys. Rev. C, 75(5):055801, **2007**

[SBL⁺03]   S. Schwarz, G. Bollen, D. Lawton, P. Lofy, D. J. Morrissey, J. Ottarson, R. Ringle, P. Schury, T. Sun, V. Varentsov, L. Weissman, *The low-energy-beam and ion-trap facility at NSCL/MSU*, Nucl. Instrum. Meth. B, 204:507 – 511, **2003**

[SCC⁺07]   M. Stoitsov, R. B. Cakirli, R. F. Casten, W. Nazarewicz, W. Satuła, *Empirical proton-neutron interactions and nuclear density functional theory: global, regional, and local comparisons*, Phys. Rev. Lett., 98(13):132502, **2007**

[Sch89]   L. Schweikhard, *Entwicklung neuer Methoden der Fouriertransformation-Ionenzyklotronresonanz-Massenspektrometrie (FT-ICR MS)*, phd thesis, **1989**

[Sch06]   H. Schatz, *The importance of nuclear masses in the astrophysical rp-process*, Int. J. Mass Spectrom., 251(2-3):293 – 299, **2006**

[SDNB06]   M. V. Stoitsov, J. Dobaczewski, W. Nazarewicz, P. Borycki, *Large-scale self-consistent nuclear mass calculations*, Int. J. Mass Spectrom., 251(2-3):243 – 251, **2006**

[SGBP04]   M. Samyn, S. Goriely, M. Bender, J. M. Pearson, *Further explorations of Skyrme-Hartree-Fock-Bogoliubov mass formulas. III. Role of particle-number projection*, Phys. Rev. C, 70(4):044309, **2004**

[SGP03]   M. Samyn, S. Goriely, J. M. Pearson, *Nuclear mass predictions within the Skyrme HFB theory*, Nucl. Phys. A, 718:653–655(3), **2003**

[Smi]   *nuclearmasses.org*

[SR92]   S. Sundell, H. Ravn, *Ion source with combined cathode and transfer line heating*, Nucl. Instrum. Meth. B, 70(1-4):160 – 164, **1992**

[SR06]   H. Schatz, K. E. Rehm, *X-ray binaries*, Nucl. Phys. A, 777:601 – 622, **2006**

[SRL78]   C. L. Smith, K. J. R. Rosman, J. R. D. Laeter, *The isotopic composition of tellurium*, Int. J. Mass Spectrom. Ion Phys., 28(1):7 – 17, **1978**

[SSFC76]   W. F. Steele, P. A. Smith, J. E. Finck, G. M. Crawley, *A survey of the (^{3}He, ^{7}Be) reaction at 70 MeV*, Nucl. Phys. A, 266(2):424 – 456, **1976**

[Str67]   V. M. Strutinsky, *Shell effects in nuclear masses and deformation energies*, Nucl. Phys. A, 95(2):420 – 442, **1967**

[Str68]   V. M. Strutinsky, *"Shells" in deformed nuclei*, Nucl. Phys. A, 122(1):1 – 33, **1968**

[TD80]   E. M. Takagui, O. Dietzsch, ^{111}In-^{109}In mass difference, Phys. Rev. C, 21(4):1667–1669, **1980**

[VRGA⁺04] J. Van Roosbroeck, C. Guénaut, G. Audi, D. Beck, K. Blaum, G. Bollen, J. Cederkall, P. Delahaye, A. De Maesschalck, H. De Witte, D. Fedorov, V. N. Fedoseyev, S. Franchoo, H. O. U. Fynbo, M. Górska, F. Herfurth, K. Heyde, M. Huyse, A. Kellerbauer, H.-J. Kluge, U. Köster, K. Kruglov, D. Lunney, V. I. Mishin, W. F. Mueller, S. Nagy, S. Schwarz, *Unambiguous identification of three β-decaying isomers in ^{70}Cu*, Phys. Rev. Lett., 92(11):112501, **2004**

[vW35]   C. F. v. Weizsäcker, *Zur Theorie der Kernmassen*, Z. Phys. A, 96:431–458, **1935**

[Wal05]   M. S. Wallace, *Experimental and theoretical challenges in understanding the rp-process on accreting neutron stars*, phd thesis, **2005**

[WAT03]   A. H. Wapstra, G. Audi, C. Thibault, *The AME2003 atomic mass evaluation (I). Evaluation of input data, adjustment procedures*, Nucl. Phys. A, 729(1):129–336, **2003**

[WBS06]   N. N. Weinberg, L. Bildsten, H. Schatz, *Exposing the nuclear burning ashes of radius expansion type I X-ray bursts*, Astrophys J., 639(2):1018–1032, **2006**

[WBS08]   C. Weber, K. Blaum, H. Schatz, *Nuclear masses in astrophysics*, PoS(NIC X)028, **2008**

[WEF⁺08]   C. Weber, V.-V. Elomaa, R. Ferrer, C. Fröhlich, D. Ackermann, J. Äystö, G. Audi, L. Batist, K. Blaum, M. Block, A. Chaudhuri, M. Dworschak, S. Eliseev, T. Eronen, U. Hager, J. Hakala, F. Herfurth, F. P. H. berger, S. Hofmann, A. Jokinen, A. Kankainen, H.-J. Kluge, K. Langanke, A. Martín, G. Martínez-Pinedo, M. Mazzocco, I. D. Moore, J. B. Neumayr, Y. N. Novikov, H. Penttilä, W. R. Plaß, A. V. Popov, S. Rahaman, T. Rauscher, C. Rauth, J. Rissanen, D. Rodríguez, A. Saastamoinen, C. Scheidenberger, L. Schweikhard, D. M. Seliverstov, T. Sonoda, F.-K. Thielemann, P. G. Thirolf, G. K. Vorobjev, *Mass measurements in the vicinity of the rp-process and the νp-process paths with the Penning trap facilities JYFLTRAP and SHIPTRAP*, Phys. Rev. C, 78(5):054310, **2008**

[WFHZ78]   S. E. Woosley, W. A. Fowler, J. A. Holmes, B. A. Zimmerman, *Semiempirical thermonuclear reaction-rate data for intermediate-mass nuclei*, At. Data and Nucl. Data Tables, 22(5):371 – 441, **1978**

[WS54]   R. D. Woods, D. S. Saxon, *Diffuse surface optical model for nucleon-nuclei scattering*, Phys. Rev., 95(2):577–578, **1954**

[WW81]   R. K. Wallace, S. E. Woosley, *Explosive hydrogen burning*, Astrophys. J. Suppl., 45:389–420, **1981**

[WZN72]   L. Westgaard, J. Żylicz, O. B. Nielsen, Proc. 4th Int. Conf. Atomic Masses and Fundamental Constants, 4, **1972**

[YBB⁺05]   C. Yazidjian, D. Beck, K. Blaum, H. Brand, F. Herfurth, S. Schwarz, *Commissioning and first on-line test of the new ISOLTRAP control system*, Eur. Phys. J. A, 25:s1.67–s1.68, **2005**

[YBF⁺06]   C. Yazidjian, K. Blaum, R. Ferrer, F. Herfurth, A. Herlert, L. Schweikhard, *A new Channeltron-detector setup for precision mass measurements at ISOLTRAP*, Hyperf. Inter., 173(2), **2006**

[ZCB89]   J.-Y. Zhang, R. F. Casten, D. S. Brenner, *Empirical proton-neutron interaction energies. Linearity and saturation phenomena*, Phys. Lett. B, 227(1):1 – 5, **1989**

[ZWYG88]   J.-Y. Zhang, C.-S. Wu, C.-H. Yu, J. D. Garrett, Contemporary Topics in Nuclear Structure Physics, Abstract Volume:109, **1988**

DANKSAGUNG

PUBLIKATIONSLISTE

accepted

Penning trap mass measurements on $^{99-109}$Cd with the ISOLTRAP mass spectrometer, and implications for the rp process
M. Breitenfeldt, G. Audi, D. Beck, K. Blaum, S. George, F. Herfurth, A. Herlert, A. Kellerbauer, H.-J. Kluge, M. Kowalska, D. Lunney, S. Naimi, D. Neidherr, H. Schatz, S. Schwarz, L. Schweikhard
Phys. Rev. C, accepted

Preparing a journey to the east of ^{208}Pb with ISOLTRAP: Isobaric purification at $A = 209$ and new masses for $^{211-213}$Fr and ^{211}Ra
M. Kowalska, S. Naimi, J. Agramunt, A. Algora, G. Audi, D. Beck, B. Blank, K. Blaum, Ch. Böhm, M. Breitenfeldt, E. Estevez, L. M. Fraile, S. George, F. Herfurth, A. Herlert, A. Kellerbauer, D. Lunney, E. Minaya-Ramirez, D. Neidherr, B. Olaizola, K. Riisager1, M. Rosenbusch, B. Rubio, S. Schwarz, L. Schweikhard, U. Warring
Eur. Phys. J. A, accepted

2009

Discovery of ^{229}Rn and the Structure of the Heaviest Rn and Ra Isotopes from Penning Trap Mass Measurements
D. Neidherr, G. Audi, D. Beck, K. Blaum, Ch. Böhm, M. Breitenfeldt, R. B. Cakirli, R. F. Casten, S. George, F. Herfurth, A. Herlert, A. Kellerbauer, M. Kowalska, D. Lunney, E. Minaya-Ramirez, S. Naimi, E. Noah, L. Penescu, M. Rosenbusch, S. Schwarz, L. Schweikhard, T. Stora
Phys. Rev. Lett. 102, 112501 (2009)

Investigation of Space-Charge Phenomena in Gas-Filled Penning Traps
S. Sturm, K. Blaum, M. Breitenfeldt, P. Delahaye, A. Herlert, L. Schweikhard, F. Wenander
AIP conf. Proc. 1114, 185-190 (2009)

2008

The elliptical Penning trap: Experimental investigations and simulations
M. Breitenfeldt, S. Baruah, K. Blaum, A. Herlert, M. Kretzschmar, F. Martinez, G. Marx, L. Schweikhard, N. Walsh
Int. J. Mass Spectrom. 275, 34-44 (2008)

Time-separated oscillatory fields for high-precision mass measurements on short-lived Al and Ca nuclides

S. George, G. Audi, B. Blank, K. Blaum, M. Breitenfeldt, U. Hager, F. Herfurth, A. Herlert, A. Kellerbauer, H.-J. Kluge, M. Kretzschmar, D. Lunney, R. Savreux, S. Schwarz, L. Schweikhard, C. Yazidjian,
Europhys. Lett. 82, 50005 (2008)

2007
Ramsey Method of Separated Oscillatory Fields for High-Precision Penning Trap Mass Spectrometry
S. George, S. Baruah, B. Blank, K. Blaum, M. Breitenfeldt, U. Hager, F. Herfurth, A. Herlert, A. Kellerbauer, H.J. Kluge, M. Kretzschmar, D. Lunney, R. Savreux, S. Schwarz, L. Schweikhard, C. Yazidjian
Phys. Rev. Lett. 98, 162501 (2007)

Simultaneous Monitoring of the the Radial Modes of the Ion Motion and their Manipulation in Penning Traps by FT-ICR Mass Spectrometry
M. Breitenfeldt, F. Ziegler, A. Herlert, G. Marx, L. Schweikhard
Int. J. Mass Spectrom. 263, 94-100 (2007)

2006
Penning trap mass spectrometry for nuclear structure studies
K. Blaum, D. Beck, M. Breitenfeldt, S. George, F. Herfurth, A. Herlert, A. Kellerbauer, H.-J. Kluge, D. Lunney, R. Savreux, S. Schwarz, L. Schweikhard, C. Yazidjian
Hyperfine Interact. 171, 83-91 (2006)

Trap-based Cluster Research and Cluster-based Investigations on Ion Storage at ClusterTrap
L. Schweikhard, M. Breitenfeldt, A. Herlert, F. Martinez, G. Marx, N. Walsh
in NON-NEUTRAL PLASMA PHYSICS VI, eds.: M. Drewsen, U.I. Uggerhoj, H. Knudsen, AIP Conf. Proc. 862, p. 264-273,ISBN 978-0-7354-0360-4, (2006)

High-precision mass measurements for reliable nuclear astrophysics calculations
A. Herlert, S. Baruah, K. Blaum, M. Breitenfeldt, P. Delahaye, M. Dworschak, S. George, C. Guénaut, U. Hager, F. Herfurth, A. Kellerbauer, H.-J. Kluge, D. Lunney, M. Marie-Jeanne, R. Savreux, L. Schweikhard, C. Yazidjian
Proc. of the Int. Symposium on Nuclear Astrophysics Nuclei in the Cosmos IX, CERN, Geneva, Switzerland, June 2006, Proceedings of Science PoS(NIC-IX)051, (2006)

The ion-catcher device for SHIPTRAP
J. B. Neumayr, L. Beck, D. Habs, S. Heinz, J. Szerypo, P. G. Thirolf, V. Varentsov, F. Voit, D. Ackermann, D. Beck, M. Block, Z. Di, S. Eliseev, H. Geissel, F. Herfurth, F. P. Heßberger, S.vHofmann, H.-J. Kluge, M. Mukherjee, G. Münzenberg, M. Petrick, W. Quint, S. Rahaman, C. Rauth, D. Rodrguez, C. Scheidenberger, G. Sikler, Z. Wang, C. Weber, W. Plass, M. Breitenfeldt, A. Chaudhuri, G. Marx, L. Schweikhard, A. F. Dodonov, Y. Novkov, M. Suhonen
Nucl. Instr. Meth. B, (2006)

2005

The ion trap facility SHIPTRAP, Status and perspectives
M. Block, D. Ackermann, D. Beck, K. Blaum, M. Breitenfeldt, A. Chauduri, A. Doemer, S. Eliseev,
D. Habs, S. Heinz, F. Herfurth, F. P. Heßberger, S. Hofmann, H. Geissel, H.-J. Kluge, V. Kolhinen,
G. Marx, J. B. Neumayr, M. Mukherjee, M. Petrick, W. Plass, W. Quint, S. Rahaman, C. Rauth,
D. Rodriguez, C. Scheidenberger, L. Schweikhard, M. Suhonen, P. G. Thirolf, Z. Wang, C. Weber,
and the SHIPTRAP collaboration
Eur. Phys. J. A 25, s01, 49-50 (2005)

CURRICULUM VITAE

Personal Data

Name   Martin Breitenfeldt

Place of Birth   Berlin, Germany

Date of Birth   December 15, 1980

Marriage Status   unmarried

Nationality   German

School Education

1987-1993   Primary School in Greifswald, Germany

1993-1999   Grammar School in Greifswald, Germany

1999   Abitur

Military Service

10/1999-09/2000   Basic military service at the German Navy

Study and Diploma

10/2000-09/2005   Study of physics at the University of Greifswald

09/2005   Diploma thesis in physics
                  Topic: "Anregungs- und Nachweismethoden
                  von Ionenbewegungen in Penningfallen"

Study and Diploma

10/2005-2009   PhD student at the Institute for Physics, University of Greifswald

08/2006-12/2008   Working at ISOLTRAP, CERN

Greifswald, August 28, 2009